



Advanced Batteries, Accumulators and Fuel Cells

INTERNATIONAL CONFERENCE

August 31st- September 3rd, 2025

Organised by:

Department of Electrical and Electronic Technology, Faculty of Electrical Engineering and Communication, Brno University of Technology

Organizing committee:

Tomáš Kazda Marie Sedlaříková

Honourary Scientific Committee:

- Petr Vanýsek, Northern Illinois University, DeKalb, Illinois, USA
- Arnaldo Visintin, INIFTA, La Plata, Argentina
- Günter Fafilek, TU Wien, Vienna, Austria
- Elena Shembel, USCTU, Dnipro, Ukraine
- Vito Di Noto, University of Padova, Padova, Italy
- Harry Hoster, Universität Duisburg-Essen, Duisburg, Germany
- Boris Markovsky, Bar-Ilan University, Tel Aviv, Israel
- Philipp Adelhelm, Friedrich Schiller University, Jena, Germany
- Laurence Hardwick, University of Liverpool, Liverpool, UK
- Renata Oriňáková, UPJŠ, Košice, Slovakia
- Andrea Fedorková-Straková, UPJŠ, Košice, Slovakia
- Grzegorz Lota, Poznan University of Technology, Poznan, Poland

Organisation Committee:

- Marie Sedlaříková, FEEC BUT, Brno, Czech Republic
- Tomáš Kazda, FEEC BUT, Brno, Czech Republic
- František Klein, Brno, Czech Republic
- Libuše Trnková, FEEC BUT, Brno, Czech Republic
- Miroslav Zatloukal, FEEC BUT, Brno, Czech Republic
- Jiří Libich, FEEC BUT, Brno, Czech Republic
- Tomáš Binar, FEEC BUT, Brno, Czech Republic
- Jiří Švarc, University of Defence, Brno, Czech Republic
- Pavlína Sedlaříková, Brno, Czech Republic

Program Committee:

- Marie Sedlaříková, FEEC BUT, Brno, Czech Republic
- Arnaldo Visintin, INIFTA, La Plata, Argentina
- Mariela Ortiz, INIFTA, La Plata, Argentina
- Petr Vanýsek, Northern Illinois University, DeKalb, Illinois, USA
- Günter Fafilek, TU Wien, Vienna, Austria
- Boris Markovsky, Bar-Ilan University, Tel Aviv, Israel
- Harry Hoster, *Universität Duisburg-Essen*, *Duisburg*, *Germany*
- Gavin Harper, University of Birmingham, Birmingham, United Kingdom
- Dominika Capková, University of Limerick, Limerick, Ireland
- Grzegorz Lota, Poznan University of Technology, Poznan, Poland
- Marta Kasprzyk, Warsaw University of Technology, Warsaw, Poland
- Murat Ceylan, Gebze Teknik Üniversitesi, Kocaeli, Turkey
- Ondřej Čech, FEEC BUT, Brno, Czech Republic
- Jiří Vaněk, FEEC BUT, Brno, Czech Republic
- Vítězslav Novák, FEEC BUT, Brno, Czech Republic
- Petr Bača, FEEC BUT, Brno, Czech Republic
- Tomáš Kazda, FEEC BUT, Brno, Czech Republic
- Helena Polsterová, FEEC BUT, Brno, Czech Republic
- Miroslav Zatloukal, FEEC BUT, Brno, Czech Republic
- Kristýna Jandová, FEEC BUT, Brno, Czech Republic
- Andrea Fedorková-Straková, UPJŠ, Košice, Slovakia
- Jiří Libich, FEEC BUT, Brno, Czech Republic
- Tomáš Binar, FEEC BUT, Brno, Czech Republic

Main Sponsors:

SKODA



CHROMSPEC

Other Sponsors:















Co-Sponsored by



 $\underline{\mathring{2}}$ Springer

Monatshefte für Chemie - Chemical Monthly

We would like to express our thanks to the Brno University of Technology, Faculty of Electrical Engineering and Communication for support and help with organising 26thABAF conference

Contents

Lithium Batteries and Related Systems

G. Abbas Structural Insights for Transition Metal Sulfide/Carbon Composite Electrode for Li-ion Batteries: In-situ/Ex-Situ Characterizations
W. Al-Shatty, D. Deganello, O. Ogunbanjo, P. Anderson, J. Baker Investigation of Decomposition Methods of Mixed Carbonaceous Materials to Enable New Thermal Methods for Graphite Recovery from Battery Manufacturing Scrap9
J. Báňa, J. Zhu, T. Kazda Effect of Negative Electrode Calandering to Performance of Recycled Graphite12
M. Bilek Influence of Primary Electron Beam-Induced Material Heating15
P. Čudek, K. Jaššo, D. Capková Preparation and Analysis of Organic Carbon for Electrochemical Power Sources
H. Fei, N. Joseph, P. Sáha Lithium Iron Oxide as the Prelithiation Additive for Lithium Iron Phosphate Battery
H. Hálová, L. Preisler, M. Kunz, L. Chladil Effect of Iron Precursor Selection on Spray Drying Synthesis of LiFePO ₄ Cathodes
J. Hokkanen, S. Montes, S. Passerini Compatibility of High-Voltage Cathodes with Ionic Liquids in Lithium-Metal Batteries
A. Hölzlhammer, G. Fafilek, S. Montes, S. Passerini Quasi-Solid-State Electrolytes: Enhancing the Future of Lithium-Ion Batteries
K. Jaššo, D. Biolek Electrochemical Impedance Spectroscopy of Li-ion Batteries: Techniques, Challenges, and Solutions
M. Kasprzyk, M. Dzierżawska, A. Zalewska Study on New Non-Crystallizing Solvents and Electrolytes for Li-Ion Batteries
O. Klvač, D. Trochta, T. Kazda, L. Novák Operando SEM Workflow for Characterization of Li-ion Batteries
J. Kramář, Z. Nováček, D. Trochta, O. Klvač, T. Kazda, J. Neuman Cathode Particle Contact Loss Degradation Analysis Using SPM-in-SEM
M. Broszkiewicz, L. Niedzicki LiTDI-PC-Based Electrolytes for a Wider Li-Ion Batteries Operation Temperature Range41
I. M. Shcherbatiuk, T. V. Lisnycha, K. D. Pershina, S. O.Solopan The Reasons Capacity Loss in Li-ion Battery with Anatase/Rutile Anode under the Cycling

O. V. Markevych, Yu. V. Polishchuk, V. V. Zinin, K. M. Sukhyi Reserve Lithium Power Sources with Enhanced Specific Energy Based on Innovative MnO ₂ +MoO ₃ Cathodes
M. Šedina, J. Amici, T.Kazda Evaluating the Response of Various Li-ion Chemistries to Nail Penetration
E. Sedláčková, J. Kasper, T. Finsterle, K. Dušek, V. Knap Investigation of Electrical and Acoustic Impedance with Volumetric Deformation of a Li-ion Cell Under Varying State of Charge
Yu. V. Shmatok, N. I. Globa, I. V. Romanova Single Cation Doped LiMexMn ₂ -xO ₄ as Cathode Materials for Lithium-Ion Batteries
Yu. V. Shmatok, N. I. Globa, I. V. Romanova Effect of Ni and La Dual Doping on Electrochemical Characteristics of LiMn ₂ O ₄ in Lithium-Ion Systems
P. Souček, T. Rada, T. Pitoňáková, J. Seidenglanz, P. Vašina Feasibility Study of Magnetron Sputtering Prepared High Entropy Oxide Thin Films as Anodes for Lithium and Sodium ion Batteries
D. Trochta, O. Klvač, L. Novák, T. Kazda Multiscale Structural Evolution in Lithium-ion Batteries Investigated by Operando Scanning Electron Microscopy
D. Li, J. Zhu The Application of Synchrotron-based XRD and X-ray Tomography in Battery Research
Supercapacitors
B. Mladenova, M. Dimitrova, G. Ivanova, A. Stoyanova Enhanced Natural Clay Materials for Supercapacitor Energy Technologies
L. Soserov, V. Bachvarov, R. Rashkov, M. Arnaudova, E. Lefterova, A. Stoyanova Electrochemically Deposited Nickel-Molybdenum Layers on Nickel Substrates for Hybrid Supercapacitors
Fuel Cells
G. Borisov, E. Petkucheva, B. Mladenova, E. Slavcheva Multilayered Nickel-Based Gas Diffusion Electrodes for Water Electrolysis in Zero-Gap Configuration
D. Budáč, V. Miloš, M. Carda, M. Paidar, K. Bouzek The Effect of Electrolyte Structure on the ORR and OER Kinetics in Solid Oxide Cells

M. O. Danilov, G. I. Dovbeshko, S. S. Fomanyuk, O. P. Gnatyuk, V. Boilko, O. Bezkrovnyi, B. M. Romanyuk, T. Sabov, I. A Rusetskyi, G.Ya. Kolbasov Synthesis the Non-Agglomerated Unzipped Multi-Walled Carbon Nanotubes as Electrode Materials for Fuel Cells	. 77
E. Petkucheva, G. Borisov, N.Borisov, E. Slavcheva DDM Activated Stainless Steel Electrodes for Alkaline Electrolysis	. 80
Aqueous Batteries	
N. I. Globa, Yu. V Shmatok Effect of Tetraglyme on Electrochemical Characteristics of LiMn ₂ O ₄ -AC System in Aqueous Electrolyte Li ₂ SO ₄ - H ₂ O-TG	. 82
Y. He, J. Červenka Organic/Water Mixed Electrolyte for Aqueous Dual-Ion Batteries	. 84
L. Kavan Zn/Li Dual-Ion Batteries with Water-in-Salt Electrolytes	. 85
J. Kršek, M. Marek, A. Taccori, P. Mazúr Microemulsion Redox Flow Batteries for Cheap Stationary Energy Storage	. 86
P. Křivík Temperature Changes During Repeated Cooling of a Lead-Acid Battery	. 88
H. K. Machhi, S. S. Soni, J. Červenka Hierarchically Porous Metal-Organic Gel Hosting Catholyte for Limiting Iodine Diffusion and Self-Discharge Control in Sustainable Aqueous Zinc-I ₂ Batteries	. 91
New Systems of Batteries	
D. Capkova, D. McNulty, T. Kazda, K. M. Ryan Direct Contact Prelithiation of Silicon/Graphite Anodes for Lithium-Ion Batteries	. 92
M.Ceylan Entropy Profile for Sodium-ion Batteries	. 95
T. Finsterle, J. Kasper, V. Knap, P. Hrzina Suitability of Sodium-Ion Based Battery Pack as a Cold-Start Alternative to a Conventional 12V/15Ah Lead Acid Starter Battery	. 96
J. Kasper, J. Kočí, K. Nováková, T. Finsterle, P. Hrzina, V. Knap Low-Temperature Discharging Performance Comparison of Sodium-Ion and Lithium-Ion Cylindrical Batteries	. 99
S. Narayanan, B. Rajagopalaa, D. Ezhumalai, J. Reiter, M. Valtiner Evaluation of Cycling Performance and Degradation Mechanisms in Commercial Sodium-ion Batteries	102

L. Niedzicki, K. Rogala, M. Kasprzyk, M. Broszkiewicz Solid Polymer Electrolytes for Li-ion and Post-Li-ion Batteries Based on Novel Salts and Plasticizers
A. Šimek, T. Kazda and O. Čech Hard Carbon-Tin Composite as High-Capacity Anodes for Sodium-ion Batteries
M. Zukalová, T. Supiňková, L. Kavan Macroporous Carbon Additive Enhancing the Cycling Stability of Li-sulfur Batteries
Photovoltaics
S. V. Chivikov, I. A.Rusetskyi, A.M.Davydov Performance and Stability of a CdSe Photoanode in a Photoelectrochemical Cell
J. Vaněk, J. Jandová, P. Vanýsek, P. Maule, M. Čepil FT-IR and GC-MS Analysis of the Chemical Recycling Products of the PV Module
Corrosion, Applications and Simulations
M. Fridrich, E. Sedláčková, J. Weinzettel Environmental Impacts of Alternative Fuels in Public Transportation
N. Klusoňová, F. Kekula, J. Kasper, J. Zemen, J. Sadil, V. Knap Impact of Particle Size Distribution on the Behavior of Lithium-ion Batteries Under Dynamic Operation
G. Kratošová, G. S. Martynková, S. Holešová, and L. Plesník Assessing Battery Separator Integrity: Microstructure, Phase, and Safety Analysis
M. Rae, M. Ottaviani, M. Singh Development of an Effective Second-Life Protocol for Rechargeable Batteries for Medical Electronic Devices
R. Balasubramaniyan, E. Duraisamy, N. Swathy,b, J. Reiter Advancing High-Energy Battery Technologies: Scaling High-Si and High-Ni NMC9055 Cells to Mass Production
M. Sedlařík, P. Vyroubal, P. Tomíček, M. Mačák, M. Šedina, T. Kazda Comprehensive Digital Twin for Stationary Battery Energy Storage
L. Trnková Advanced Application of Elimination Voltammetry with Linear Scan in Electroanalysis and Electrotechnology
P. Vyroubal, M. Sedlařík, M. Mačák, M. Šedina, T. Kazda Reduced Modeling of Lilon Battery Thermal Abuse

Structural Insights for Transition Metal Sulfide/Carbon Composite Electrode for Li-ion Batteries: In-situ/Ex-Situ Characterizations

G. Abbasa

^aDepartment of Chemistry, University of Saskatchewan, Saskatoon, Canada

The surging energy demand requires new sustainable and more efficient energy storage systems that integrate materials with elemental abundance, low toxicity, and scalability. Despite the commercial scalability of Li-ion batteries (LIBs), the safety concerns, low energy density, and limited cyclic stability hinder their application in EVs. In this context, engineering the architecture of electrode materials by incorporating carbon into the material for composite formation could resolve the issues of low current density and cyclic stability. We employed transition metal sulfides encapsulated in carbon as a composite electrode material for LIBs. The profound increase in specific capacity was observed during galvanostatic charge/discharge cycling, which could be attributed to structural transitions occurring in the electrode material during the charge/discharge process. The ex-situ characterizations (XRD, SEM) were performed to confirm the structural transitions that occurred during the charge/discharge process. Furthermore, to explore the reversibility of the charge storage process and structural modifications, in-situ Raman spectroelectrochemistry analysis was conducted in a homemade cell. Moreover, to demonstrate the ionic intercalation into the electrode material and discriminate the contribution of diffusion and surface process, electrochemical kinetic analysis was performed. This research can set a direction to figure out the functional electrode material for next-generation Li and beyond Li-ion batteries.

Investigation of Decomposition Methods of Mixed Carbonaceous Materials to Enable New Thermal Methods for Graphite Recovery from Battery Manufacturing Scrap

W.Al-Shatty^a, D.Deganello^b, O.Ogunbanjo^c, P.Anderson^c, J.Baker^a

^aFaculty of Engineering and Design, University of Bath, BA2 7AY, UK

^bFaculty of Science and Engineering, Swansea University, SA1 8EN, UK

^cSchool of Chemistry, University of Birmingham, B15 2TT, UK

The purpose of this research, led by the University of Bath in collaboration with the University of Birmingham and Swansea University, is to investigate the decomposition methods of mixed carbonaceous materials, enabling new thermal methods for graphite recovery from battery manufacturing scrap. The significance of the thermal recovery effect lies in its ability to reveal the behavior of graphite after thermal treatment. The result indicates that removing organic binders from the slurry accrued at 450 and 470 °C for 2 and 1 hours, respectively, and under near infrared radiation at 100 % (intensity) and for 12 seconds (residence time).

Introduction

Graphite is considered a critical raw material in the USA, China, and Europe (1). It is the most commonly used anode material in lithium-ion batteries (LIBs) due to its stability and high capacity, which can be maintained over numerous charge cycles (2, 3). It enables fast and efficient charging while supporting long-cycle lives. Additionally, graphite is relatively inexpensive, non-toxic, an excellent conductor of electricity, stable at high temperatures, low in reactivity, and has a low thermal expansion coefficient (4, 5). These properties make graphite ideally suited for batteries in electrified transportation, electronic devices, and grid-based storage.

To assess how effectively this novel thermal removal principle can separate active materials from the graphite slurry, we investigated the efficiency of novel near-infrared radiation compared with conventional furnaces. The active materials are to be separated from conductive carbon black (CB) and organic binders (CMC and SBR). We initially discuss the characteristics of the thermal treatment, including the decomposition temperatures of the binder, CB, and graphite, which significantly influence the material recovery and highlight the challenges within the suggested process. Next, we present the experimental results, in which heat temperatures, treatment time (conventional furnace) intensity, and radiation exposure (NIR treatment) are varied, thereby altering the temperature achieved by the sample. This work investigates how different thermal treatments affect the physical properties, structure, and morphology of the graphite and

CB, followed by electrochemical characterization of both the thermally recovered materials in a battery cell.

Materials, Slurry Preparation, and Thermal Treatments

Graphite anode powder (Sigma-Aldrich- 907154), Carboxymethyl Cellulose (CMC, 9004-32-4), Styrene Butadiene Rubber (SBR, MTI), and Carbon Black (CB, Imerys) have been used directly to prepare graphite anode slurry. Making the graphite slurry was by using a formulation of (95:5:2:2) of (graphite, CB, SBR, CMC) (6). After drying (0.2 g) of dry slurry was thermally treated by two methods: conventional furnace and NIR.

To assess the decomposition temperature of materials, along with the surface morphology and specific surface area of the starting materials before and after thermal treatment, the following analytical methods were utilized: thermogravimetric analysis (TGA), scanning electron microscopy (SEM), and evaluation of electrochemical performance.

Results and Discussions

Two thermal treatment methods were employed in this study: a conventional furnace and near-infrared (NIR) radiation, each under varying conditions. Both approaches proved effective in the removal of organic binders, CMC, and SBR_from the graphite anode. Specifically, complete binder decomposition was achieved in the conventional furnace at 470 °C for 1 hour and at 450 °C for 2 hours. Similarly, exposure to NIR at 100% intensity for just 12 seconds also facilitated efficient binder removal, as illustrated in Figure 1(a–c). Furthermore, the XRD patterns presented in Figure 1(d–e) confirm the structural integrity of the graphite anode following thermal treatment, indicating that the applied conditions effectively eliminated the binders without significantly altering the crystalline structure.

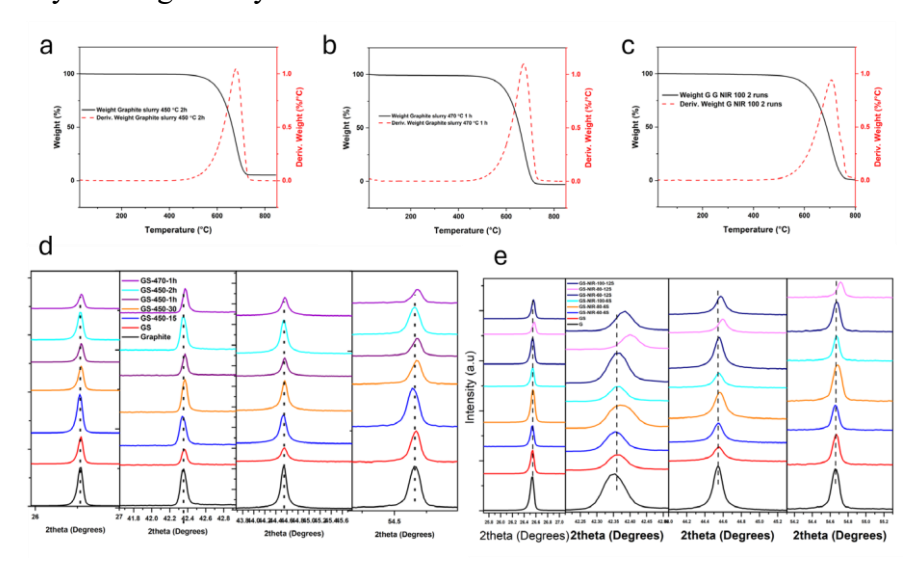


Figure 1. The TGA profile was obtained under conditions involving the removal of organic binders (CMC and SBR) in a conventional furnace at 470 °C for 1 hour and at 450 °C for 2 hours, followed by exposure to NIR at 100% intensity for 12 seconds (designated as a, b, and c, respectively). In addition, the XRD patterns are provided for both pre- and post-thermal treatment conditions, as illustrated in panels (d) for the conventional furnace and (e) for the NIR method.

Figure 2 (a). A comparison of the performance of different thermally treated graphite using CMC/SBR as binder. The result reveals a significant capacity loss for both NIR and furnace-treated graphite with increasing charging current. Meanwhile on comparing the performance of the graphite with CMC/SBR binder and graphite PVDF

binder (figure 2), the results indicate that graphite with CMC/SBR binder experiences significant capacity loss as charging current increases, whereas graphite with PVDF binder demonstrates more stable capacity despite an initial irreversible capacity reduction caused by rapid SEI formation. Overall, graphite with PVDF binder maintains better performance under higher charging currents, while graphite with CMC/SBR shows notable performance degradation.

The remaining SBR in the graphite anode powder is illustrated in Figure 2 (b and c). The figure indicates that all organic binders have been eliminated following thermal treatment in a conventional furnace at 470 °C for 1 hour and 450 °C for 2 hours, respectively. Additionally, exposure to NIR at 100% intensity for 12 seconds also contributed to this removal.

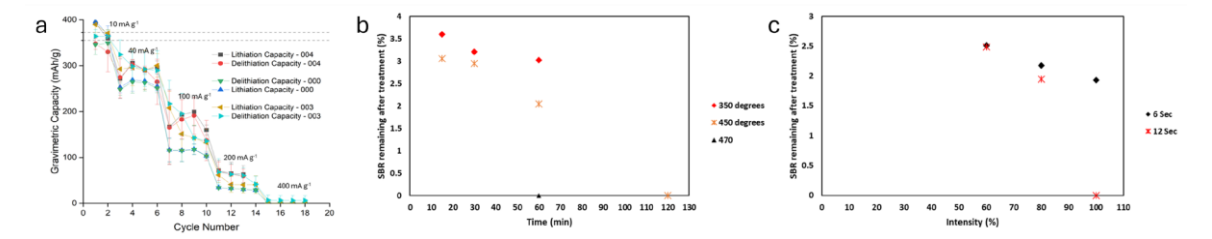


Figure 2. Performance of different thermally treated graphite using CMC/SBR as binder (a), and the remaining SBR after thermal treatments: conventional furnace (b), NIR (c).

Acknowledgments

We gratefully acknowledge funding from the EPSRC ECR Fellowship NoRESt EP/S03711X/1 and TReFCo EP/W019167/1. The authors would like to thank the access to characterisation equipment to Swansea University Advanced Imaging of Materials (AIM) facility, which was funded in part by the EPSRC (EP/M028267/1) and the European Regional Development Fund through the Welsh Government (80708).

- 1. N. Cao, Y. Zhang, L. Chen, W. Chu, Y. Huang, Y. Jia, and M. Wang, J. Power Sources, 483, 229163 (2021).
- 2. Y. Gao, J. Zhang, H. Jin, G. Liang, L. Ma, Y. Chen, and C. Wang, Carbon, 194, 362 (2022).
- 3. R. Golmohammadzadeh, Z. Dimachki, W. Bryant, J. Zhang, P. Biniaz, M. M. Banaszak Holl, C. Pozo-Gonzalo, and P. Chakraborty Banerjee, J. Environ. Manage., 343, 118205 (2023).
- 4. K. He, Z.Y. Zhang, and F.S. Zhang, J. Hazard. Mater., 386, 121633 (2020).
- 5. X. Ma, M. Chen, B. Chen, Z. Meng, and Y. Wang, ACS Sustain. Chem. Eng., 7, 19732 (2019).
- 6. J. Li, G. Wang, and Z. Xu, Waste Manag., 52, 221 (2016).

Effect of Negative Electrode Calandering to Performance of Recycled Graphite

J. Báňa^a, J. Zhu^a, T. Kazda^a

^aDepartment Of Electrical and Electronic Technology, University of Technology Brno, Czech Republic

^bDepartment of Chemistry - Ångström Laboratory; Structural Chemistry, Uppsala University, Sweden

The escalating demand for lithium-ion batteries (LIBs) necessitates not only efficient recycling but also optimized manufacturing processes. While graphite anodes are cost-effective and abundant, their full potential in LIBs is often untapped due to sub-optimal production methods. This study focuses on calendering (pressing) as a crucial step to significantly enhance graphite anode properties. We investigate how precise control over the calendering process directly impacts the anode's electrochemical performance. Our findings demonstrate that strategic compression levels can lead to substantial improvements in the capacity and cycling stability of graphite anodes, ultimately contributing to the development of more efficient and durable LIBs.

Introduction

Graphite is a cornerstone of the commercial lithium-ion battery (LIB) market, prized for its excellent electrochemical properties and abundant availability. However, its performance gradually degrades with each charge and discharge cycle. The goal of graphite recycling is to effectively remove impurities and metal residues, ultimately restoring its crystal structure. Fortunately, continuous advancements are leading to more efficient and sustainable recycling methods. These innovations allow graphite from used LIBs to be effectively returned to the battery production cycle, bolstering the circular economy and significantly reducing the environmental impact of battery manufacturing.

The initial and crucial step in reconditioning used graphite involves meticulously removing impurities. These can include residues from the solid electrolyte interphase (SEI), polymer binders, conductive additives, general dirt, and metal deposits originating from cathode materials or current collectors. To achieve this necessary cleanliness, various methods are employed, most commonly heat treatment, chemical treatment or combination of these methods. [1][2].

Pressing anodes for LIBs is a critical process step that significantly affects electrochemical performance. Proper compression increases the density of the active material, resulting in higher volumetric energy density of the battery. However, excessive pressing can reduce electrode porosity, limiting lithium-ion transport rates and potentially leading to reduced performance at high discharge currents and impaired cycle stability. Optimal pressing of electrode is therefore essential to achieve a balance between energy density and ion transport kinetics, thereby extending battery life.[3][4]

Experiment

This study builds upon previous research published in *Monatshefte für Chemie - Chemical Monthly* [5]. We focused on a commercial Motoma LFP 18650 battery (1500 mAh) that had undergone 500 cycles at a 1C-rate to simulate aging. This cycling resulted in an 8.4% capacity drop, leaving the battery with 1375 mAh.

Upon dismantling the aged battery, the graphite anode was extracted and weighed 6.156 g. Subsequent electrochemical testing of the extracted graphite revealed a capacity exceeding 300 mAh/g.

The extracted graphite underwent calcination in an inert nitrogen atmosphere for 10 hours at 1000°C. A slurry was then prepared by mixing 80% graphite, 10% PVDF, and 10% SupP carbon black using a magnetic stirrer, with NMP as the solvent. This slurry was coated onto a copper current collector to form electrodes, which were then dried at 60 °C for 24 hours.

To investigate the effect of compression, the active material in the samples was calendered to achieve approximate compression levels of -10%, -20%, -30%, and -40%. These graphite anode samples were then dried in vacuum and assembled into 2025 coin cells using Celgard polymer separator and 1M LiPF₆ in EC:DMC and Li counter electrode. Formed coin cells were electrochemically cycled using a Neware BTS cycler. The capacities obtained from these tested samples are presented in Figure 1.

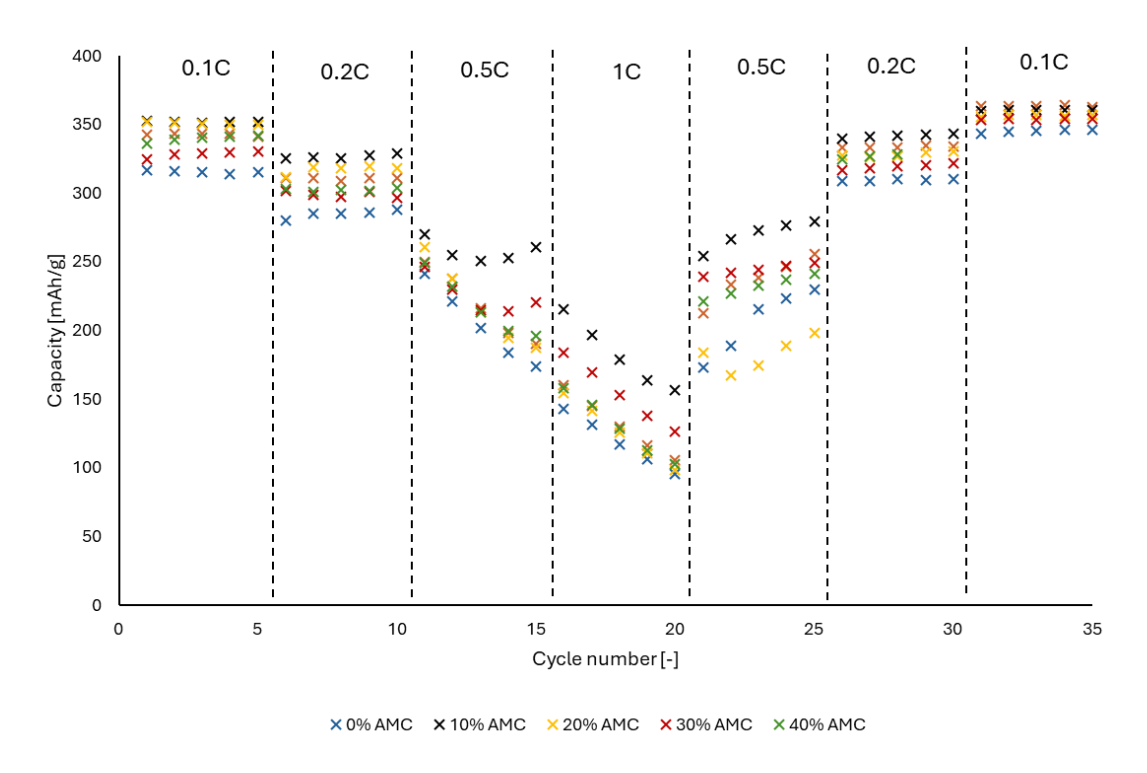


Figure 1: Cycling at different C-rate of recycled graphite anodes (*AMC – active mass compression)

Figure 1 shows that the unpressed sample achieves approximately 315 mAh/g during the initial 0.1C cycles. As the current load increases, the capacity drops to below 100 mAh/g by the 20th cycle at 1C. Subsequently, the capacity recovers as the current load decreases, reaching around 345 mAh/g in the final cycle.

Notably, all compressed samples consistently outperform the uncompressed sample at every current load. The best performance is observed in the sample with a

10% thickness reduction. This sample's capacity starts at around 350 mAh/g in the initial 0.1C cycles. With increasing current load, its capacity decreases to 156 mAh/g by the 20th cycle at 1C. Afterward, the capacity increases as the current load decreases, reaching 356 mAh/g in the final cycle. Capacity of calendered sample is about 11% increased in first cycles of 0.1C and difference in last cycle of 1C is about 60%.

Conclusion

This study demonstrates that recycling graphite from end-of-life LIBs offers a promising path for sustainable battery production. A key finding is how calendering recycled graphite anodes significantly impacts their electrochemical properties. We found that optimal compression substantially increases the resulting electrode capacity and stability, which is crucial for the efficient reuse of the material.

Our results indicate that meticulous control over the pressing of electgrode is critical for achieving stable and high capacity in recycled graphite anodes. Optimizing this step can significantly contribute to making graphite recycling more economically and environmentally attractive, thereby supporting the circular economy in the LIB sector.

Acknowledgments

This work was supported by the specific research programme (project No. FEKT-S-23-8286).

- 1. LU, Yingqi, Kaiyuan PENG a Lingen ZHANG.. ACS ES&T Engineering 2022, 2022-04-08, 2(4), 586-605
- 2. WU, Jiawei, Mengting ZHENG, Tiefeng LIU, et al. Energy Storage Materials 2023, 54, 120-134
- 3. HASELRIEDER, Wolfgang, Stoyan IVANOV, Daniel Klaus CHRISTEN, Henrike BOCKHOLT a Arno KWADE. ECS Transactions. The Electrochemical Society, 2013, 2013-4-1, 50(26), 59-70
- 4. MEYER, Chris, Henrike BOCKHOLT, Wolfgang HASELRIEDER a Arno KWADE. Journal of Materials Processing Technology [online]. Elsevier BV, 2017, 249, 172-178
- 5. BÁŇA, Jiří, Pavel ČUDEK, Martin ŠEDINA, Antonín ŠIMEK a Tomáš KAZDA. Monatshefte für Chemie Chemical Monthly 2024, 155(3-4), 253-259

Influence of Primary Electron Beam-Induced Material Heating

M. Bílek^a

^aDepartment of Electrical and Electronic Technology, Brno University of Technology, Technická 10, 616 00 Brno, Czech Republic

The manuscript addresses the issue of localized heating of the investigated LiFePO₄ material due to the primary electron beam in Environmental Scanning Electron Microscope observation. Mathematical-physics analyses of two beam power variants were performed using Ansys Fluent system: one with very low energy load on the material and the other with relatively high power. The localized heating state of the material was monitored, with particular attention to the cooling time required for the heated spot to return to its initial temperature, thereby preventing heat accumulation.

Introduction

At the Department of Electrical and Electronic Technology, Faculty of Electrical Engineering and Communication Technologies, Brno University of Technology, research is conducted on electrochemical power sources, including lithium-ion and post-lithium-ion battery systems, as well as aspects related to lithium systems (recycling, extraction) [1][2]. This research also encompasses electrochemical measurements and the synthesis of electrode materials for positive electrodes in Li-ion accumulators and post-lithium systems [3]. Concurrently, research in Environmental Scanning Electron Microscopy (ESEM) is being performed in collaboration with the Institute of Scientific Instruments of the Czech Academy of Sciences [4][5][6]. This paper addresses the impact of the incident beam energy in ESEM on the local temperature increase of the sample.

Materials and Methods

This manuscript presents a mathematical-physics analysis of material heating caused by electron beam impact. These analyses were performed using Ansys Fluent as a 2D axisymmetric, transient problem. The study focused on LiFePO₄ as a cathode material, with a thermal conductivity of 1.79 W.m⁻¹K⁻¹, a density of 3.6 g.cm⁻³, and Heat capacity of 1000 J. kg⁻¹K⁻¹. Two scenarios were calculated: a commonly used variant with a voltage U_{k1} = 5kV and I_1 = 4pA, and a second extreme variant with U_{k2} = 20kV and I_2 = 2nA. For both scenarios, a dwell time of 100 µs/pixel was selected. The boundary conditions for these simulations are depicted in Fig. 1, where the green region represents a cutout of the overall sample, the blue region is the surrounding gas above the sample moist air), the yellow region is the volume of the first pixel, and the red region is the volume of the second pixel, simplified as a ring encompassing the first pixel and having the same volume.

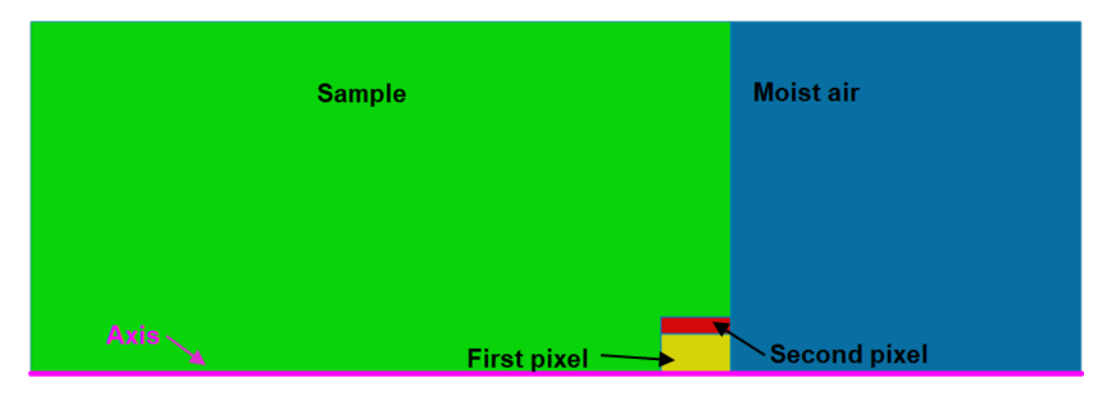


Fig. 1. Boundary conditions.

The pixel size was determined based on the beam current and analysis type, utilizing the Kanaya-Okayama relation [1].

$$R = \frac{2.76 \times 10^{-2} A E_0^{1.67}}{\rho Z^{0.89}}$$
 [1]

where: R is the electron range, A is the average atomic mass, E_0 denotes the initial electron beam energy, ϱ represents the material density, and Z is the atomic number.

Results

Fig. 2 illustrates the temporal temperature profile within the volume of the first pixel. It is evident that for the lower power variant (Fig. 2a), the temperature increase was negligible, only in the order of hundredths of degrees Celsius, with a return to the initial temperature occurring within milliseconds. In contrast, the high-power variant (Fig. 2b) showed a temperature increase of 4 °C, followed by a more gradual cooling. A critical aspect of these analyses is ensuring that, in the case of repeated scanning of a given location, the temperature returns to its initial state before the beam revisits the same spot, thereby preventing heat accumulation.

In future studies, additional materials relevant to this field will be analyzed, focusing on distinct properties crucial for the given heating and cooling problem. These properties primarily include density, heat capacity, and thermal conductivity of the materials.

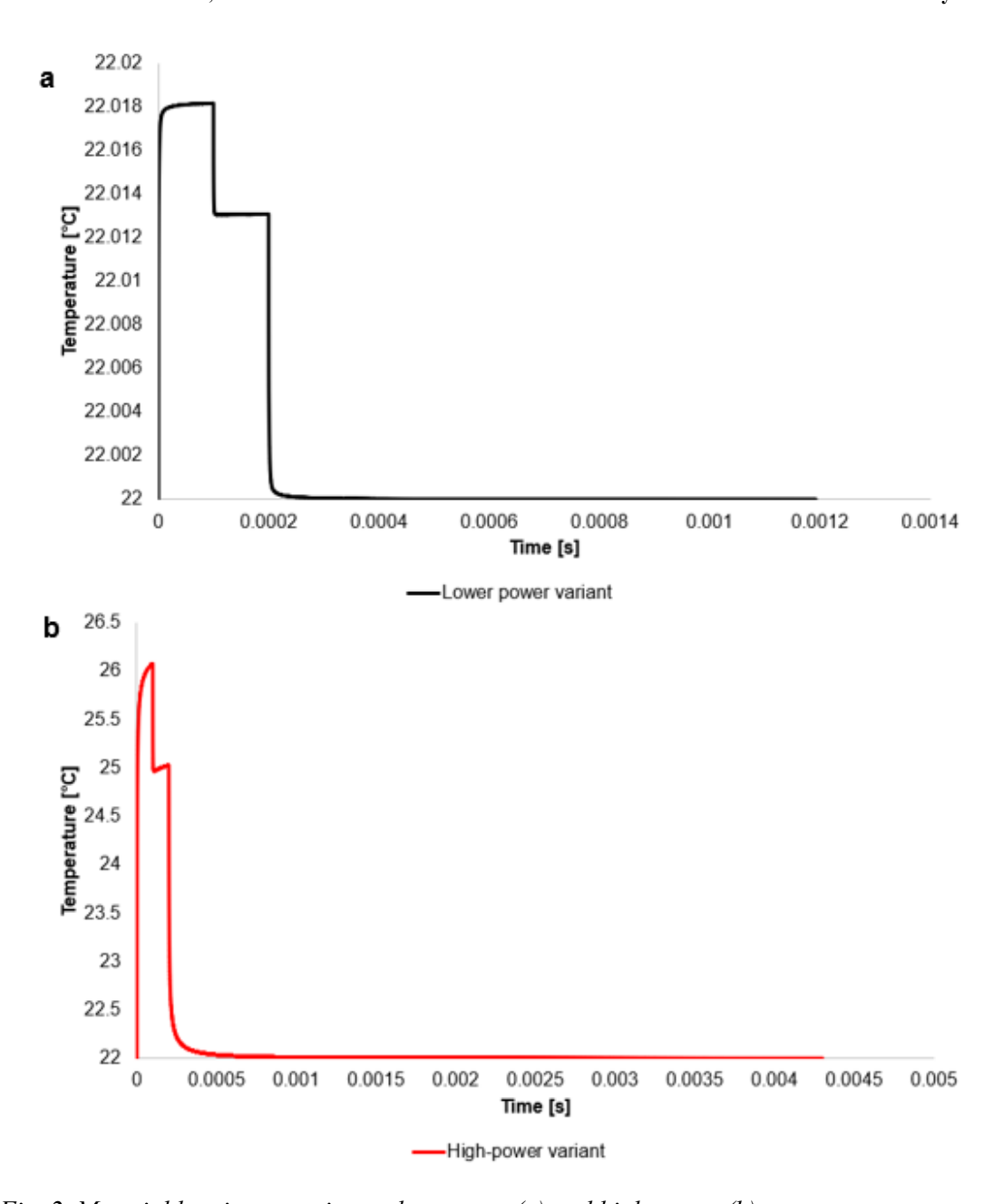


Fig. 2. Material heating over time at low power (a) and high power (b).

Conclusion

Analyses were conducted on the heating effects of LiFePO₄ material induced by the primary electron beam during observation in an ESEM. Two extreme variants of the applied beam power were examined, considering the cooling time required for the heated spot to return to its initial temperature to prevent heat accumulation. These findings will inform subsequent analyses for other types of materials used in lithiumion batteries, which possess different properties influencing the thermal balance and various operational electron beam power modes.

- 1. Vyroubal, P.; Kazda, T. Finite Element Model Of Nail Penetration Into Lithium Ion Battery. Journal of Energy Storage 2018, 20 (1), 451-458. doi: 10.1016/j.est.2018.10.008
- 2. Kazda, T.; Čudek, P.; Vondrák, J.; Sedlaříková, M.; Tichý, J.; Slávik, M.; Fafilek, G.; Čech, O. Lithium-Sulphur Batteries Based On Biological 3D Structures. Journal of Solid State Electrochemistry 2018, 22 (2), 537-546. doi: 10.1007/s10008-017-3791-0
- 3. Syrový, T.; Kazda, T.; Akrman, J.; Syrová, L. Towards Roll-To-Roll Printed Batteries Based On Organic Electrodes For Printed Electronics Applications. Journal of Energy Storage 2021, 40 (1), 1-9. doi: 10.1016/j.est.2021.102680
- 4. Dordevic, B.; Neděla, V.; Tihlaříková, E.; Trojan, V.; Havel, L. Effects Of Copper And Arsenic Stress On The Development Of Norway Spruce Somatic Embryos And Their Visualization With The Environmental Scanning Electron Microscope. New Biotechnology 2019, 48 (1), 35-43. doi: 10.1016/j.nbt.2018.05.005
- 5. Tihlaříková, E.; Neděla, V.; Dordevic, B. In-Situ Preparation Of Plant Samples In Esem For Energy Dispersive X-Ray Microanalysis And Repetitive Observation In Sem And Esem. Scientific Reports 2019, 9 (1), 1-8. doi: 10.1038/s41598-019-38835-w
- 6. Neděla, V.; Konvalina, I.; Lencová, B.; Zlámal, J. Comparison Of Calculated, Simulated And Measured Signal Amplification In A Variable Pressure Sem. Nuclear instruments & methods in physics research section a-accelerators spectrometers detectors and associated equipment 2011, 645 (1), 79-84. doi: 10.1016/j.nima.2010.12.200

Preparation and Analysis of Organic Carbon for Electrochemical Power Sources

P. Čudek^a, K. Jaššo^{a,b}, D. Capková^{a,c}

^aDepartment of Electrical and Electronic Technology, Brno University of Technology, Technická 10, 616 00 Brno, Czech Republic

^bDepartment of Electrical Engineering, Faculty of Military Technology, University of Defence, Kounicova 65, 662 10 Brno, Czech Republic

^cDepartment of Chemical Sciences and Bernal Institute, University of Limerick, V94 T9PX Limerick, Ireland

Porous carbons synthesized from carbon-rich precursors are widely employed in various advanced applications, including energy storage systems. Their unique hierarchical structure and the incorporation of functional heteroatoms make them promising materials for addressing key limitations of lithium—sulphur batteries, such as low electrical conductivity and the dissolution of long-chain polysulfides. This paper focuses on the synthesis of porous carbon derived from spent coffee grounds through the process of hydrothermal carbonization. The resulting material exhibits high purity and a low sulphur content, making it a suitable candidate for electrochemical applications. The use of waste biomass as a sustainable carbon source not only adds value to agricultural byproducts but also contributes to the development of environmentally friendly energy storage materials.

Introduction

Lithium-sulphur (Li-S) electrochemical power sources are considered a promising alternative to lithium-ion (Li-ion) accumulators in certain applications due to their exceptionally high theoretical energy density. Developing Li-S batteries using biowaste derived materials offers a sustainable pathway for next generation energy storage technologies. Porous carbon with a hierarchical structure and embedded functional heteroatoms can effectively infiltrate the sulphur cathode and address key challenges faced by Li-S systems specifically, the low electrical conductivity of sulphur and the dissolution of long chain polysulfides. [1]

Incorporating sulphur into porous carbon yields a high initial discharge capacity with minimal capacity fading over time. Its robust carbon framework accommodates the volumetric expansion during sulphur redox reactions, while its unoccupied pores serve as polysulfide reservoirs. This helps mitigate the shuttle effect and enhances electrochemical stability. Furthermore, the interconnected pore network promotes efficient electron and ion transport, resulting in superior rate capabilities compared to cathodes containing pristine sulphur. These findings highlight the potential of renewable and ecological carbon sources in advancing high performance Li-S batteries.

Beyond battery applications, porous carbon materials owing to their diverse surface morphologies are also suitable for use in supercapacitor electrodes and hydrogen storage adsorbents. [2][3] This versatility has driven extensive research into synthesizing porous carbon from various biogenic precursors. [4]

Carbon can be readily produced from biological waste. In selecting a suitable biowaste source, key criteria included particle size, availability, and elemental purity favouring materials composed primarily of carbon, hydrogen, and oxygen, while minimizing other elemental contaminants. Spent coffee grounds represent a promising candidate. Rich in organic compounds with negligible amounts of nitrogen and trace elements, coffee grounds have already undergone partial thermal treatment during brewing, reducing the presence of volatile organic acids and hydrocarbons. Their natural particle size, typically on the order of tens of micrometres, further supports their suitability for direct conversion.

This article details the production of carbon from spent coffee grounds by hydrothermal carbonization (HC), along with an assessment of residual elemental content using energy dispersive X-ray spectroscopy (EDS). A known limitation of HC is the retention of sulphur within the resulting carbon material. However, if this residual sulphur can be sufficiently minimized, it may not hinder performance particularly in light of the material's intended application in Li-S battery cathodes. [5]

Experiments

Spent coffee grounds from espresso preparation were used as the precursor for the synthesis of organic carbon. At each stage of the carbon production process, surface morphology was examined using scanning electron microscopy (SEM), and elemental composition was analysed by energy dispersive X-ray spectroscopy (EDS) at accelerating voltages of $5 \, kV$ and $20 \, kV$.

An accelerating voltage of $5\,kV$ was selected to achieve improved spectral resolution in the low atomic number (light element) region. However, at this lower voltage, X-ray generation is limited to a shallow interaction volume approximately $300\,nm$ for carbon and even less for elements with higher atomic densities making the analysis more surface sensitive. In contrast, a voltage of $20\,kV$ enables X-ray generation from a greater depth, up to approximately $3.8\,\mu m$ for carbon, thus providing more bulk representative information. The use of both accelerating voltages enabled a comparative analysis, where similar results under optimal conditions suggest a homogeneous distribution of elements throughout the samples near surface region.

The original coffee grounds mixture consisted primarily of carbon and oxygen, with approximately 3.5 wt% of nitrogen. The coffee grounds were then mixed with demineralized water and boiled at $100 \, ^{\circ}C$ with constant stirring until the mixture was dried. EDS showed no significant changes when analysed at an accelerating voltage of $5 \, kV$. However, at $20 \, kV$ allowing detection from greater depths an increase of about $10 \, \%$ in oxygen content was observed, accompanied by a corresponding decrease in carbon. This notable reduction in detected carbon may be attributed to the evaporation of residual aromatic hydrocarbons remaining in the coffee grounds after espresso brewing. The nitrogen content remained nearly unchanged.

Next, the dried coffee grounds underwent hydrothermal carbonization (HC). 20 g of coffee were soaked in 50 ml of 30 % H₂SO₄ and heated at 180 °C for 18 hours. EDS analysis performed after HC showed up to a 30 % increase of sulphur on the surface of the mixture, with approximately 20 % sulfur content in the bulk.

The resulting HC mixture was then filtered with one litre of deionized water, followed by another EDS analysis. Results indicated a significant reduction in surface

sulphur content from 30% to 2%, while the overall sulphur content in the mixture was 6%.

Subsequent repeated filtrations with deionized water were carried out until the filtrate reached neutral pH, using a total of 3 liters of deionized water. This washing further decreased the sulphur content to below 4 %. Given the neutral pH of the filtrate, it is assumed that additional washing would not further reduce the sulphur content.

The resulting mixture was then combined with KOH in a 1:1 ratio and activated under a nitrogen atmosphere at temperatures of 500 °C, 750 °C, and 1000 °C. After activation, the mixture was filtered again, and elemental analysis was conducted.

TABLE I. Results of EDS of coffee grounds performed at accelerating voltages of 5 kV

Procedure	C [wt.%]	N [wt.%]	O [wt.%]	S [wt.%]
Fresh coffee grounds	67.48	2.81	29.71	0.00
Dried coffee grounds	69.00	2.61	28.40	0.00
After HC	39.97	0.00	28.36	31.67
11 filtration	77.84	0.00	20.01	2.15
Final filtration	81.64	0.00	17.37	0.99

TABLE II. Results of EDS of coffee grounds performed at accelerating voltages of 20 kV

Procedure	C [wt.%]	N [wt.%]	O [wt.%]	S [wt.%]
Fresh coffee grounds	69.86	4.27	25.86	0.00
Dried coffee grounds	59.96	4.01	36.03	0.00
After HC	47.87	0.00	31.44	20.69
11 filtration	73.13	0.00	20.36	6.51
Final filtration	75.07	0.00	21.15	3.78

TABLE III. Results of EDS of coffee grounds performed at accelerating voltages of 5 kV

Procedure	C [wt.%]	O [wt.%]	S [wt.%]	K [wt.%]
Mixed with KOH before Activation	36.30	28.40	11.50	23.80
Activated on 500 °C	18.8	23.2	11.1	46.9
Filtered after activation on 500 °C	57	19.6	16.9	6.5
Activated on 750 °C	7.9	24	13	55.1
Filtered after activation on 750 °C	85.7	8.3	3.7	2.3
Activated on 1000 °C	41.3	18.4	9.9	30.4
Filtered after activation on 1000°C	84.9	10.3	4.8	0

TABLE IV. Results of EDS of coffee grounds performed at accelerating voltages of 20 kV

TABLE 17. Results of EDS of coffee grounds performed at accelerating voltages of 20 KV					
Procedure	C [wt.%]	O [wt.%]	S [wt.%]	K [wt.%]	
Mixed with KOH before Activation	34.7	31.2	7.8	26.3	
Activated on 500 °C	27.7	29.6	9.6	33.1	
Filtered after activation on 500 °C	64.6	21.7	10.3	3.4	
Activated on 750 °C	14.7	33.9	9.2	42.2	
Filtered after activation on 750 °C	87.8	7.3	4	0.9	
Activated on 1000 °C	50.7	20.2	8.1	21	
Filtered after activation on 1000°C	88.6	7.4	3.7	0.3	

Conclusion

The experimental results suggest that spent coffee grounds represent a promising precursor for the synthesis of porous carbon suitable for application in Li-S batteries. Thus far, the material has undergone hydrothermal carbonization, followed by washing, chemical activation with KOH at various temperatures, and a subsequent washing step.

EDS analysis reveals that HC effectively removes nitrogen, however, it introduces sulphur contamination into the carbon structure. Despite thorough washing with deionized water, complete removal of sulphur was not achieved. Similarly, KOH activation led to residual potassium content that could not be eliminated entirely. However, through activation at 1000 °C and subsequent washing, the potassium content was reduced to 0.3 wt% (see Table IV) or completely eliminated from the surface (see Table III). The presence of these impurities may be negligible in terms of their impact on the intended applications.

Future work will focus on evaluating the electrical conductivity and porosity of the prepared carbon, prior to its incorporation into cathode materials for lithium-sulphur batteries.

Acknowledgments

This work was supported by the specific graduate research of the Brno University of Technology No. FEKT-S-23-8286, by institutional support from the Ministry of Defence of the Czech Republic and D.C. acknowledges the EU Horizon 2023 research and innovation program under the Marie Sklodowska-Curie Postdoctoral Fellowship Grant no. 101152715 (SALSA Project).

- 1. Sandeep and A.V. Ravindra, *Diamond and Related Materials*, **146**, 111158 (2024)
- 2. K. Nema and K. Mohanty, R. Thangavel, *Journal of Industrial and Engineering Chemistry*, **121**, 235 (2023).
- 3. A.Turkyilmaz, K. Isinkaralar, M. Dogan, B. K. Kizilduman and Z. Bicil, Sustainable Chemistry and Pharmacy, 40, 101634 (2024)
- 4. X. Zhang, G. He, H. Sun, W. Cui, H. Song, J. Li and J.Zheng, *International Journal of Electrochemical Science*, **19**, 100617 (2024)
- 5. A. Santanatoglia, S. Angeloni, G. Caprioli, L. Fioretti, M. Ricciutelli, S. Vittori and L. Alessandroni, *Food Chemistry*, **454**, 139717 (2024)

Lithium Iron Oxide as the Prelithiation Additive for Lithium Iron Phosphate Battery

H. Fei^a, N. Joseph^a, P. Sáha^b

^aCentre of Polymer Systems, Tomas Bata University in Zlín, Zlín 76001 Czech Republic

^bUniversity Institute, Tomas Bata University in Zlín, Zlín 76001 Czech Republic

Lithium iron phosphate (LFP) batteries have emerged as a dominant solution for stationary energy storage systems due to their inherent safety, low cost, and long cycle life. Their widespread adoption addresses the instability of power grids caused by the integration of intermittent renewable energy sources, such as solar and wind. To further enhance the energy density and cycling performance of LFP batteries, prelithiation has been identified as a critical strategy. Among various prelithiation methods, cathode prelithiation stands out for its simplicity and practicality. In this context, lithium-rich lithium iron oxide (LFO) has gained attention as an ideal prelithiation additive for LFP batteries, owing to its cost-effectiveness and high specific capacity during the initial charging process.

In this study, we employed LFO as a cathode additive to enable prelithiation in a single-unit LFP pouch cell. During the formation charging process, LFO released excess lithium ions to compensate for irreversible lithium loss due to SEI formation (Fig. 1a). After formation, degassing, and electrolyte replenishment, the LFO-modified cell demonstrated a higher initial capacity (Fig. 1b) and superior capacity retention. This strategy not only mitigates lithium inventory loss but also enhances the overall electrochemical performance of the LFP battery. However, LFO is highly moisture sensitive, and the residual after its delithiation could increase cathode resistance. Thus, further optimization of LFO's stability and compatibility is necessary.

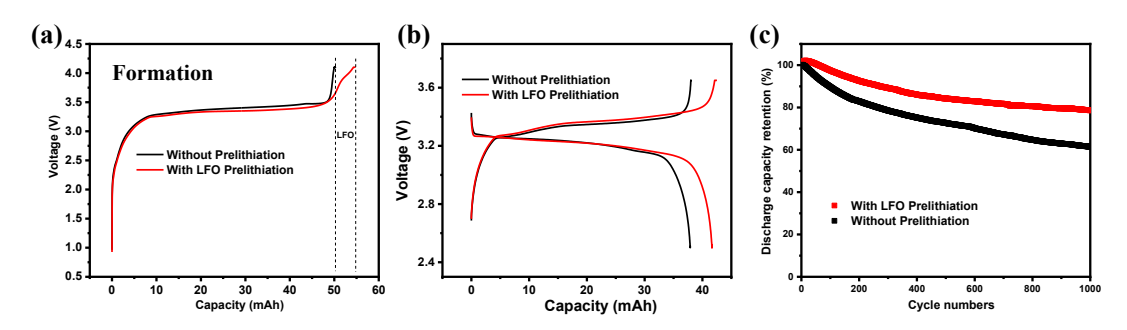


Fig.1 (a) The formation, (b) initial charge/discharge at 0.25C, and (c) cycling stability of the LFP full cells with and without LFO prelithiation.

Acknowledgments

This work is supported by the Technology Agency of the Czech Republic (TK05020019) and the Ministry of Education, Youth and Sports of the Czech Republic–DKRVO (RP/CPS/2024-28/005).

Effect of Iron Precursor Selection on Spray Drying Synthesis of LiFePO₄ Cathodes

H. Hálová^a, L. Preisler^b, M. Kunz^a, L. Chladil^a

^a Department of Electrical and Electronic Technology, BUT, 616 00 Brno, CR

^b Department of Power Engineering, BUT, 616 69 Brno, CR

Lithium iron phosphate was synthesized via spray drying synthesis to compare the effect of two different iron precursors: ferric citrate and ferric acetylacetonate. The synthesized powder was subsequently calcinated at 650 °C under a nitrogen atmosphere. SEM analysis revealed spherical particles below 2 µm for both routes, while EDS showed complete absence of phosphorus in the samples prepared with ferric citrate. TGA indicated significantly lower residual mass for this precursor. On the other hand, the results for the sample with ferric acetylacetonate show corresponding ratio between iron and phosphorus and, at the same time, according to XRD, the formation of a corresponding LiFePO₄ phase.

Introduction

Lithium iron phosphate (LiFePO₄) is a widely used cathode material for lithiumion batteries thanks to its thermal stability, long cycle life, safety and low cost. However, pure LFP demonstrates low electronic and ionic conductivity. Its electrochemical performance depends strongly on particle size, morphology, and phase purity, all of which are influenced by the synthesis route and subsequent processing. [1][2]

Spray drying synthesis offers fast scalable method to produce homogeneous submicron powder. For this reason, it is an attractive alternative to traditional synthesis methods. This technique is widely used in diverse industries, but laboratory usage, especially for cathode materials, require further investigation. For successful spray drying synthesis, all precursors must be fully dissolved in the chosen medium (typically water), which makes finding suitable and affordable liquid challenging. [3][4]

Experimental

Precursor solutions for LiFePO₄ synthesis were prepared using stoichiometric amounts of lithium dihydrogen phosphate combined with two different iron sources to investigate the effect of precursor chemistry. In the first solution, ferric citrate was used as the iron source (solution LFP20), while in the second solution ferric acetylacetonate was added (solution LFP19). Citric acid was added to both solutions as a chelating agent and carbon source. The concentrations of the solutions were 0,05 M and 0,015 M respectively.

Both solutions were atomized in a spray dryer with an inlet temperature of $200\,^{\circ}$ C. The dried particles were collected by electrostatic precipitator. The length of the individual experiments was from 3 to 7 hours. Selected samples were subsequently calcinated at $650\,^{\circ}$ C for 2.5 hours under a nitrogen atmosphere.

Results and discussion

As shown in Figure 1, the spray-dried LFP powders had a spherical morphology. For the sample prepared from solution LFP19, the particle diameter ranged from 0.2 μm to 1.2 μm , while the material from solution LFP20 showed a slightly wider distribution between 0.3 μm and 1.8 μm . The analysis confirmed the uniform distribution of elements in the synthesized powders, except for the zero phosphorus content in LFP20 sample. The detailed elemental composition is summarized in Table 1.

For the LFP19 material, EDS analysis indicated consistent stoichiometry in several samples, demonstrating the reproducibility of the synthesis. The measured Fe:P atomic ratio was close to 1:1, indicating that the desired stoichiometry was achieved. In contrast, the absence of phosphorus in LFP20 confirms that this precursor route did not lead to the formation of the desired phase, despite comparable particle morphology.

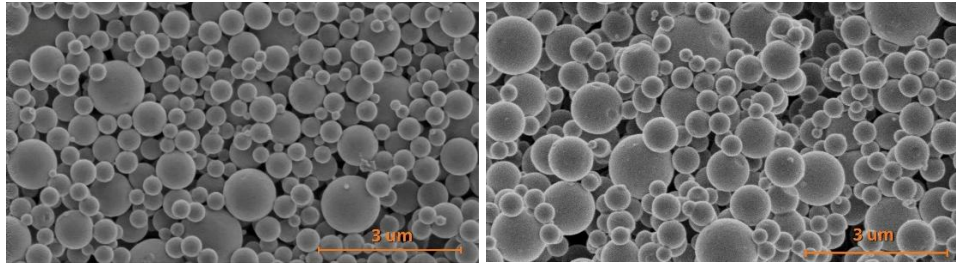


Figure 1. SEM picture of synthesized powder – solution LFP19 (left) and solution LFP20 (right).

Table 1.	EDS analysis of	f synthesized	powder for	solution .	LFP19	and LFP20.

	Element	Atomic Ratio (%)	Atomic Ratio Error (%)
	C	23.2	0.1
LFP19	0	64.2	0.3
LFF19	P	6.2	0.0
	Fe	6.4	0.0
	C	42.7	0.2
LFP20	0	49.9	0.3
	P	0.0	0.0
	Fe	7.4	0.1

The difference in chemical composition is further investigated by thermogravimetric analysis. TGA revealed a major mass loss near 200 °C associated with water evaporation. At this temperature, LFP20 precursor exhibited a noticeably higher mass drop compared to LFP19, suggesting that the ferric citrate solution probably retained a greater amount of bound water during spray drying. The LFP19 precursor reached mass stabilization above 500 °C with a total mass loss of ~50 %, while LFP20 sample continued decomposing up to 800 °C, retaining only ~15 % of its initial weight (Figure 2).

Based on these results, the route with usage of ferric citrate was excluded from further experiments, and only the LFP19 precursor was subjected to XRD analysis. The XRD spectra of the LFP19 sample can be seen in Figure 3. The analysis confirmed the presence of a single olivine LiFePO₄ phase without detectable secondary impurities, indicating complete phase formation after spray drying and thermal treatment.

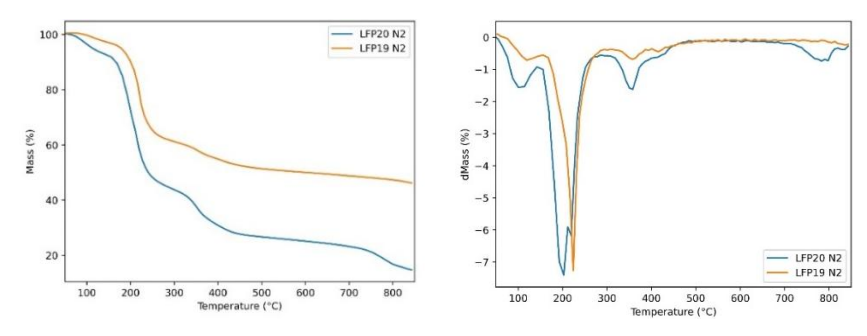


Figure 2. TGA analysis of LFP material – solution LFP19 and LFP20.

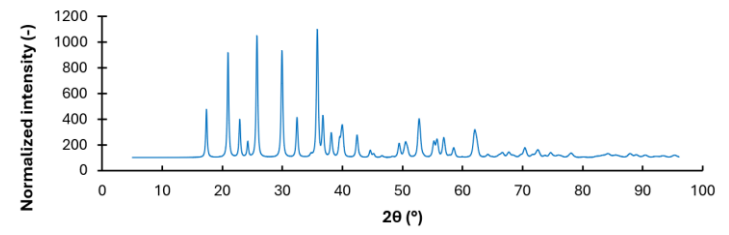


Figure 3. XRD analysis of LFP19, temperature of calcination 650 °C.

Conclusion

Spray drying has been successfully used for the synthesis of LiFePO₄ precursors on a laboratory scale, proving that this method is also applicable outside industrial applications. A comparison of two iron sources highlighted the key role of the chemical composition of precursors: when ferric citrate (LFP20) was used, spherical particles were formed, but phosphorus was not incorporated, while when ferric acetylacetonate (LFP19) was used, submicron particles with the 1:1 Fe:P ratio and a stable olivine phase after calcination were formed. These results confirm that spray drying can produce active LFP material under controlled laboratory conditions and underscore the importance of selecting suitable precursors.

Acknowledgments

This work was supported by the specific graduate research of the Brno University of Technology No. FEKT-S-23-8286 and No. FEKT/FSI-J-24-8579.

- 1. E. Styuf and M. Othman et al, J. Of Power Sources, **642**, 236951 (2025).
- 2. A. Nekahi and A.K. Kumar et al, Materials Science and Engineering, **159**, 100797 (2024)
- 3. S. Kaushik and G. Kumar et al, *J. of Energy Storage*, **97**, 112818 (2024).
- 4. T. Zhengwang and Z. Li, *J. of Energy Storage*, **98**, 113085 (2024).

Compatibility of High-Voltage Cathodes with Ionic Liquids in Lithium-Metal Batteries

J.Hokkanen^{a,b}, S. Montes^a, S. Passerini^a

^aBattery Technologies, AIT Austrian Institute of Technology GmbH, Vienna, Austria

^bUniversity of Oulu, Oulu, Finland

The ever-growing popularity of electric vehicles creates a demand for safe, high-performance batteries. Lithium-metal batteries (LMBs) with high-voltage cathodes are one of the most promising and researched solutions due to their high energy density and good performance. However, the use of volatile organic-based electrolytes makes them a possible safety hazard. To improve the safety of LMBs new types of electrolytes are being developed and researched. One promising type of electrolyte for LMBs are quasi-solid-state electrolytes consisting of a porous ceramic framework impregnated with an ionic liquid.

In this work LMBs with an ionic liquid as electrolyte are assembled and compared to ones with a conventional, organic carbonate-based liquid electrolyte. Cells are assembled in coin cell casings with Li metal anodes and a range of different commercial cathode active materials are being tested, including LNMOs as well as uncoated and coated NMCs. Due to the viscose nature of ionic liquids, they are facing challenges in wetting the separator which affects their performance and stability negatively. An alternative method used in this work is to introduce ionic liquids to LMBs by mixing them in the slurry used to make the high-voltage cathodes.

The results of this work show the comparison of electrochemical performance and stability of coin cells with ionic liquid and conventional, organic carbonate-based liquid electrolytes. Results of cyclic voltammetry, potentiostatic electrochemical impedance spectroscopy and galvanostatic cycling at various C-rates are presented.

Quasi-Solid-State Electrolytes: Enhancing the Future of Lithium-Ion Batteries

A. Hölzlhammer, G. Fafilek, S. Montes, S. Passerini

Batteries are a cornerstone of the energy transition and the European Green Deal, enabling renewable energy integration and the decarbonization of transport and energy storage. However, safety concerns, such as thermal runaway from liquid electrolytes, and the energy density limitations of lithium-ion batteries present significant challenges. Solid-state electrolytes such as LLZO, LATP, and LAGP are promising alternatives, particularly when combined with energy-dense lithium-metal anodes, but they still exhibit lower ionic conductivity than conventional liquid electrolytes. To address this a non-flammable ionic liquid can be added to the solid-state electrolyte.

Herein, the investigation of quasi-solid-state electrolytes comprising solid-state electrolytes, such as LLZO, LATP and LAGP infused with the ionic liquid Pyr₁₄FSI and LiTFSI salt is presented. This hybrid approach can significantly enhance the ion mobility and thus improving the ionic conductivity compared to the all-solid-state electrolytes. The study further examines fabrication methods for the solid-state electrolytes, focusing on pore formation using polymethyl methacrylate (PMMA) as a pore-forming agent in varying sizes and concentrations, and characterizing the resulting porosity via SEM and gas adsorption techniques.

The ionic liquid is introduced into the porous structure using vacuum infiltration to ensure uniform distribution. Additionally, impedance spectroscopy and cyclic voltammetry are employed to investigate ion transport mechanisms and the structural compatibility between the ceramic framework and the ionic liquid. Our results highlight the improved ionic conductivity of quasi-solid-state systems relative to conventional liquid electrolytes and underline their potential as safer, high-performance alternatives for next-generation lithium-ion and lithium-metal batteries.

Electrochemical Impedance Spectroscopy of Li-ion Batteries: Techniques, Challenges, and Solutions

K. Jaššo^{a,b}, D. Biolek^b

^aDepartment of Electrical Engineering, University of Defence, 662 10 Brno, Czech Republic

^bDepartment of Electrical and Electronic Technology, Brno University of Technology, 616 00 Brno, Czech Republic

Electrochemical Impedance Spectroscopy (EIS) has emerged as a powerful diagnostic tool for investigating the dynamic behavior and degradation mechanisms of lithium-ion (Li-ion) batteries. This technique enables the separation and quantification of various electrochemical processes across a wide frequency range, offering valuable insights into charge transfer, diffusion, and interfacial phenomena. Despite its potential, the practical application of EIS in battery research and industry faces significant challenges, including complex data interpretation, non-linear system behavior, and sensitivity to experimental conditions. This paper reviews the fundamental principles of EIS, explores state-of-the-art measurement techniques, and discusses common pitfalls in data analysis.

Introduction

Lithium-ion (Li-ion) batteries have become the cornerstone of modern energy storage systems, powering everything from portable electronics to electric vehicles and grid-scale storage. As the demand for higher energy density, longer cycle life, and improved safety continues to grow, the need for advanced diagnostic tools to monitor and understand battery behavior becomes increasingly critical. Among these tools, Electrochemical Impedance Spectroscopy (EIS) stands out for its ability to non-invasively probe the internal electrochemical processes of batteries across a wide frequency spectrum.

EIS is a non-destructive and highly sensitive technique that has gained considerable attention for characterizing the internal states of batteries. The method provides qualitative and quantitative information, making it an invaluable tool for fundamental research and practical diagnostics. By applying a small AC voltage (or current) perturbation over a broad frequency range, EIS enables the deconvolution of overlapping processes such as charge transfer resistance, solid electrolyte interphase (SEI) formation, ionic diffusion, and electrode degradation [1]. These parameters are essential for evaluating battery health, predicting performance degradation, and optimizing battery management systems (BMS). However, the practical application of EIS is often hindered by challenges including complex data interpretation, sensitivity to measurement conditions, and the need for accurate equivalent circuit modeling. This paper aims to provide a comprehensive overview of EIS techniques applied to Li-ion batteries, highlighting both theoretical foundations and practical considerations. We discuss current challenges in EIS implementation and interpretation, and explore emerging solutions.

Quality of the measurement system

The accuracy and reliability of EIS measurements depend heavily on the quality and configuration of the measurement system, including the potentiostat, cables, and the measured system. Improper measurement conditions can introduce artifacts or systematic errors, leading to incorrect interpretation of impedance data.

A key tool for assessing the performance of a potentiostat in EIS applications is the contour plot, which maps the instrument's accuracy across a frequency-resistance (or frequency-impedance) domain. The accuracy contour plot is a log-log plot, fashioned as a Bode-type plot, where the magnitude of the impedance is plotted versus frequency. These plots, often provided by potentiostat manufacturers, illustrate regions of reliable measurement accuracy. Operating outside these boundaries can result in degraded data quality, particularly at high frequencies or with low-impedance and high-impedance systems [2].

Another critical factor in measurement quality is the connection method between the potentiostat and the electrochemical cell. Four-point (4-wire) setups, which separate current-carrying and voltage-sensing electrodes, offer significant advantages over two-point (2-wire) setups, especially in low-impedance systems or when long cables are used. In a 2-point configuration, the measured voltage includes the resistance of the cables and contact points, which can distort high-frequency measurements. In contrast, a 4-point configuration eliminates this error by measuring voltage directly at the cell terminals, thereby ensuring more accurate impedance readings across the entire frequency spectrum [3].

In addition, the length and shielding of cables play a non-negligible role, particularly at high frequencies. Poor shielding or excessive cable length can introduce inductive artifacts or electromagnetic interference, further distorting the EIS spectrum. Therefore, it is recommended to minimize cable length, use twisted and shielded cables, and ensure proper grounding during measurements [4].

Ensuring high-quality impedance measurements thus requires careful attention not only to the electrochemical system but also to the configuration and limitations of the measurement hardware. Proper calibration, contour plot validation, and appropriate connection techniques are essential for acquiring trustworthy EIS data.

Quality of the measured data

While EIS is theoretically based on the assumption that the system under investigation is linear, time-invariant, and causal (LTI), real-world systems such as lithium-ion batteries often deviate from these ideal conditions. In practice, batteries can exhibit nonlinear time-invariant (NLTI) or even nonlinear time-variant (NLTV) behavior due to several factors, including state-of-charge (SoC) drift, hysteresis effects, temperature fluctuations, and internal relaxation dynamics during the measurement itself [5].

These deviations from linear time-invariant behavior can introduce significant distortions into the measured impedance spectrum, particularly at low frequencies where prolonged measurement times increase the likelihood of system drift or state changes. Consequently, the resulting data may exhibit poor repeatability, frequency-dependent non-causal phase shifts, or spectral artifacts that do not correspond to any physically meaningful electrochemical process.

Quality indicators

To aid in the assessment of data reliability, some modern potentiostats, such as those from BioLogic incorporate built-in quality indicators. These include Total Harmonic Distortion (THD), Non-Stationary Distortion (NSD), and Noise-to-Signal Ratio (NSR), each quantifying a distinct aspect of measurement validity (5):

- **THD** evaluates the linearity of the system by measuring the presence of higher-order harmonics in the response signal. A low THD (typically <5%) indicates that the system behaves linearly under the applied perturbation amplitude.
- **NSD** quantifies time-dependent changes in the system by detecting spectral energy at frequencies adjacent to the fundamental. Elevated NSD values are a clear indication of system drift or dynamic transitions during measurement.
- **NSR** expresses the ratio of extraneous spectral content (noise) to the fundamental signal. It ensures that the response amplitude is sufficiently high relative to the noise level.

These diagnostic tools enable real-time identification of data segments corrupted by nonlinearity, non-stationarity, or excessive noise. Based on the output of these indicators, researchers can either reject unreliable data or adapt the experimental protocol accordingly—for example, by lowering the perturbation amplitude, shortening the acquisition window, or narrowing the frequency range to exclude unstable regions.

Data interpretation and equivalent circuit modeling

The core strength of EIS lies in its ability to deconvolute complex electrochemical processes through frequency-resolved analysis. However, extracting physically meaningful parameters from impedance spectra requires proper data interpretation, typically achieved via equivalent circuit modeling (ECM). In this approach, the measured impedance is fitted to a network of idealized electrical components that represent underlying electrochemical phenomena.

For Li-ion batteries, commonly used models include variants of the Randles circuit, consisting of a solution resistance (R_s), charge transfer resistance (R_{ct}), and a constant phase element (CPE) or double-layer capacitor (C_{dl}), often in series with a Warburg element to represent diffusion processes. In more advanced representations, additional elements may be introduced to account for SEI resistance, porous electrode behavior, or electrode/electrolyte non-idealities.

Despite their utility, ECMs are inherently non-unique, meaning multiple circuit topologies may fit the same data set equally well. This leads to the risk of overparameterization and poor physical interpretability. To mitigate this, circuit selection should be guided by prior electrochemical knowledge, literature benchmarks, and, where possible, complementary characterization methods.

Model fitting is typically performed using nonlinear least-squares algorithms. To ensure reliability, goodness-of-fit metrics such as chi-squared values, residual analysis, and Kramers–Kronig validation should be applied. Additionally, sensitivity to initial guesses and parameter confidence intervals must be evaluated, especially in systems with overlapping time constants or broad dispersions.

Recent developments include automated model selection tools and machine-learning-assisted fitting, which aim to reduce user bias and accelerate the analysis.

Nonetheless, human expertise remains essential to prevent misinterpretation of data and to ensure that the selected model reflects the actual physical processes in the battery.

Effective equivalent circuit modeling not only provides insights into battery kinetics and degradation mechanisms but also enables quantitative tracking of internal parameters, such as R_{ct} and diffusion resistance, across aging cycles or operational conditions.

Conclusion

Electrochemical Impedance Spectroscopy remains a powerful, non-destructive tool for probing the internal dynamics of lithium-ion batteries. Its ability to distinguish between charge transfer, diffusion, and interfacial processes makes it invaluable for both fundamental research and practical diagnostics. However, obtaining high-quality, interpretable data requires rigorous attention to the entire measurement chain ranging from the potentiostat and cable configuration to system linearity and stability. Advanced features such as contour plots, 4-point cell connections, and real-time quality indicators (THD, NSD, NSR) enhance the reliability of EIS measurements and help researchers avoid common pitfalls associated with nonlinear and non-stationary behavior. When properly applied, these tools enable precise monitoring of electrochemical parameters and support the development of robust battery management and prognostic systems. Continued progress in model validation, data interpretation, and real-time integration of EIS into battery systems will be key to fully unlocking its potential in next-generation energy storage technologies.

Acknowledgments

This work was supported by the Czech Science Foundation under grant No. 24-12982S and specific graduate research of the Brno University of Technology No. FEKT-S-23-8286 and by institutional support from the Ministry of Defence of the Czech Republic.

- 1. Ch. Lazanas and M. I. Prodromidis, ACS Meas. Sci. Au, 3, 162 (2023).
- 2. BioLogic Science Instruments, *Application Note 54: How to Read EIS Accuracy Contour Plots*, BioLogic, Seyssinet-Pariset, France (2015).
- 3. BioLogic Science Instruments, *Why 4-Point Measurements?*, BioLogic, Seyssinet-Pariset, France (2024).
- 4. Gamry Instruments, *How Cabling and Signal Amplitudes Affect EIS Results*, Gamry Instruments, Warminster, PA (2020).
- 5. BioLogic Science Instruments, *Application Note 64: EIS Quality Indicators: THD, NSD and NSR*, BioLogic, Seyssinet-Pariset, France (2018).

Study on New Non-Crystallizing Solvents and Electrolytes for Li-Ion Batteries

M. Kasprzyk^a, M. Dzierżawska^a, A. Zalewska^a

^aFaculty of Chemistry, Warsaw University of Technology, Noakowskiego 3, Warsaw 00-664, Poland

New non-crystallizing solvent mixtures are developed based on one of the organic carbonates, ethylene carbonate (EC) or propylene carbonate (PC), mixed with poly(propylene glycol) PPG with an average molar mass of 425 g.mol⁻¹. In the presented work, new electrolytes will be shown. The basic parameters of the electrolytes have been measured: conductivity, lithium transference number, and voltammetry. Differential scanning calorimetry (DSC) has been performed to define the non-crystallizing region in these systems.

Introduction

The development of the modern world is based on the development of new energy sources and methods for storing energy. That is why Li-ion batteries are one of the energy sources that are still developing very fast.

The lack of crystal formation during temperature drop may be crucial for the better health of the Li-ion battery and make it more resistant to temperature changes. The volume changes rapidly during crystallization, so that electrodes might be damaged afterwards. This may lead to fatal battery failure. That is why the non-crystallizing solvents may solve that important issue.

In the presented work, we would like to show new non-crystallizing electrolytes based on non-crystallizing solvent mixtures. It is already known that such systems may appear when organic carbonates are mixed with poly(ethylene glycol). In the work presented herein, we would like to show mixtures based on chosen organic solvents (ethylene carbonate or propylene carbonate) with poly(propylene glycol). These systems also show non-crystallizing regions.

Two salts have been chosen for that investigation: LiPF₆ (lithium hexafluorophosphate) and LiTDI (lithium 4,5-dicyano-2-(trifluoromethyl)imidazolide)

Experimental and results

In this study, liquid solvent mixtures and liquid electrolytes will be presented. All of them have been measured using DSC. Some of the systems showed glass temperature below -100°C.

These liquid electrolytes exhibit relatively high conductivity (above 1 mS.cm⁻¹ at 20°C). The lithium transference numbers are higher in the case of LiTDI systems than in LiPF₆ electrolytes. These electrolytes' high electrochemical stability window is also observed, up to 4.7 V vs. Li.

- 1. M.C. Smart, B.V. Ratnakumar, S. Surampudi, *J. Electrochem. Soc.*, **149(4)**, A361 (2002).
- 2. M. Kasprzyk, A. Zalewska, L. Niedzicki, A. Bitner, M. Marcinek, W. Wieczorek, *Solid State Ionics*, **308**, 22 (2017).
- 3. M. Kasprzyk, A. Zalewska, W. Wieczorek, J. Phys. Chem. C., 124(9), 5046 (2020).
- 4. M. Kasprzyk, M. Tymejczyk, A. Zalewska, M. Broszkiewicz, M. Pyzik, *J. Mol. Liq.*, **434**, 127949 (2025)

Operando SEM Workflow for Characterization of Li-ion Batteries

O. Klvač^{a,b}, D. Trochta^{a,b}, T. Kazda^a, L. Novák^b

^aDepartment of Electrical and Electronic Technology, Faculty of Electrical Engineering and Communication, BUT, Technická 10, 616 00 Brno, Czech Republic

^bThermo Fisher Scientific Brno, Vlastimila Pecha 12, 627 00, Brno, Czech Republic

We present an operando SEM workflow for real-time monitoring of structural changes in Li-ion batteries, demonstrated on an NMC111/LTO cell with ionic liquid electrolyte. The method enables high-resolution imaging during cycling. This approach valuable insights into electrode provides degradation advanced mechanisms and supports battery material development.

Introduction

Real-time observation of structural changes in lithium-ion battery (LIB) electrodes is crucial for understanding degradation mechanisms and optimizing material performance [1][2][3]. We present a comprehensive operando scanning electron microscopy (SEM) workflow that enables direct visualization of microstructural evolution during electrochemical cycling. The study focuses on an LiNi_{0.33}Mn_{0.33}Co_{0.33}O₂ (NMC111) cathode paired with a Li₄Ti₅O₁₂ (LTO) anode and employs an ionic liquid electrolyte. This approach provides valuable insights into electrode behavior and opens pathways for the design of more robust battery systems.

Experimental Setup

The investigated system consisted of an NMC111-based cathode and an LTO anode. As electrolyte, a 1 M solution of lithium hexafluorophosphate (LiPF₆) in N-Propyl-N-methylpyrrolidinium bis(fluorosulfonyl)imide was used, absorbed into a Whatman glass-fiber separator. Prior to assembly, a region of the NMC electrode was cross-sectioned using argon ions in a broad ion beam (BIB) system (CleanMill, Thermo Fisher Scientific), exposing the internal microstructure for SEM analysis.

All battery components were handled under an inert argon atmosphere. After polishing, the electrodes were transferred into an Ar-filled glovebox, where the full cell was assembled into a custom-designed SEM-compatible holder (Figure 1-a). This holder allowed electrochemical operation inside the SEM vacuum chamber and was connected externally to a potentiostat (Biologic SP 200). To ensure full environmental control, all transfers between systems (CleanMill, glovebox, SEM) were performed using the CleanConnect gas-tight transfer module.

The cell was cycled in constant current mode at 0.1C within a voltage range of 1.3–2.8 V. During cycling, SEM imaging was performed using the ETD and CBS detectors of a Thermo Scientific Quattro SEM. This setup enabled simultaneous acquisition of high-resolution SEM images and electrochemical data.

Results and Discussion

Sequential SEM imaging revealed progressive volume changes and crack formation in the NMC111 particles during cycling. These observations were correlated with specific stages of the charge/discharge curves, allowing identification of microstructural events tied to lithiation and delithiation processes (Figure 1-b,c). The imaging data provided clear evidence of particle expansion and mechanical stress accumulation, highlighting the utility of this approach for failure analysis and material optimization.

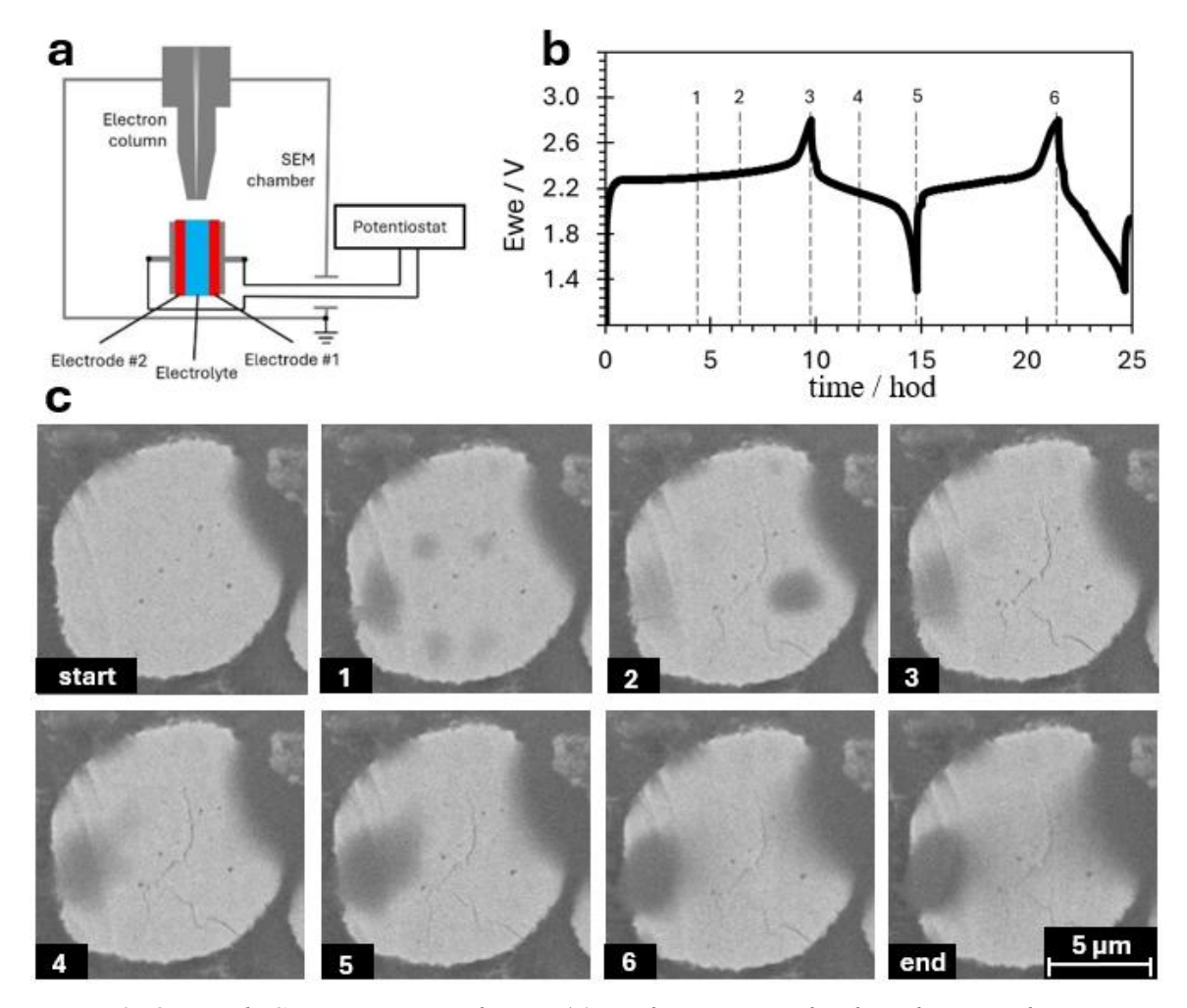


Figure 2. Operando SEM experimental setup (a); cycling curve with selected points where SEM images were taken (b); taken SEM images (c)

Conclusion

This work demonstrates a robust operando SEM methodology for tracking electrode changes in real time during battery operation. The approach relies on prepolishing by broad ion beam milling and maintenance of an inert environment throughout all stages. The method is not limited to the liquid-electrolyte system used here; it is broadly applicable to battery chemistries such as Li, Na based that are compatible with vacuum conditions, including solid-state configurations.

Acknowledgments

This work was supported by the specific graduate research of the Brno University of Technology FEKT-S-23-8286. The work was developed in cooperation with Thermo Fisher Scientific Brno.

- 1. Y. Liang, C. Z. Zhao, H. Yuan, Y. Chen, W. Zhang, J. Q. Huang, D. Yu, Y. Liu, M. M. Titirici, Y. L. Chueh, H. Yu, Q. Zhang, A review of rechargeable batteries for portable electronic devices, Infomat. 1 (2019) 6-32.
- 2. W. Y. Lee, H. Lee, S. Ha, C. Lee, J. H. Bae, In Man Kang, K. Kim, J. Jang, Effect of Mg Doping on the Electrical Performance of a Sol-Gel-Processed SnO2 Thin-Film Transistor, Electronics. 9 (2020) 523-523.
- 3. D. Liu, Z. Shadike, R. Lin, K. Qian, H. Li, K. Li, S. Wang, Q. Yu, M. Liu, S. Ganapathy, X. Qin, Q. H. Yang, M. Wagemaker, F. Kang, X. Q. Yang, B. Li, Review of Recent Development of In Situ/Operando Characterization Techniques for Lithium Battery Research, Advanced Materials. 31 (2019).

Cathode Particle Contact Loss Degradation Analysis Using SPM-in-SEM

J. Kramář^{a,b}, Z. Nováček^b, D. Trochta^{c,d}, O. Klvač^{c,d}, T. Kazda^c, J. Neuman^a

^aNenoVision s.r.o, Purkyňova 127, 612 00 Brno-Medlánky, Czech Republic ^bBrno University of Technology, Institute of Physical Engineering, Technická 2896, 616 69 Brno, Czech Republic

^cBrno University of Technology, Department of Electrical and Electronic Technology, Technicka 3058/10, 616 00 Brno, Czech Republic ^dThermo Fisher Scientific Brno, Vlastimila Pecha 12, Brno 627 00, Czech Republic

Advances in battery technology demand characterization tools that link microstructure with electrochemical performance. Conventional electrochemical methods lack nanoscale resolution, while electron microscopy cannot directly probe electrical properties. Atomic Force Microscopy enables local topographical and electrical mapping, yet its separate operation from electron microscopy limits direct correlation. Integrating complementary techniques is essential for revealing degradation mechanisms and guiding next-generation battery design.

Introduction

The growing demand for safer, more efficient, and higher-capacity energy storage systems is driving the advancement of battery technologies. In recent years, battery production capacity has expanded significantly, a trend expected to continue. The simultaneous reduction in battery cell costs and the expansion of global manufacturing highlight their crucial role in future energy storage [1][2].

Current research explores a variety of electrode and separator materials, each with unique advantages and challenges. However, new materials often introduce complexities in understanding their microstructure. Traditional electrochemical methods lack the lateral resolution needed for local electrical property analysis. While Scanning Electron Microscopy (SEM) - based techniques provide insights into structural, chemical, and crystallographic properties, they cannot directly image electrical properties [3][4].

A promising approach is Atomic Force Microscopy (AFM), where a sharp tip interacts with the sample surface to acquire various data maps of topography for height and roughness analysis. Additionally, applying a bias to the tip enables electronic property investigation [5][6].

Conventionally, SEM and AFM operate as separate devices under different conditions, making direct correlations difficult. Our approach integrates AFM within an SEM platform (AFM-in-SEM) using the LiteScope microscope. This setup enables simultaneous in-situ nanoscale electrical measurements alongside SEM-based structural and chemical insights. Such correlative characterization is essential for understanding chemical, structural, and electronic interactions in batteries [7][8].

One critical challenge in battery performance is particle contact loss in the cathode. This occurs when particles lose connection with the conductive matrix, leading

to trapped electrons and reduced energy density. Some particles remain in charged or partially charged states, limiting active material utilization and degrading battery performance. Addressing this issue is key to improving energy capacity and cycle life [9][10].

Experimental

Our project employs nanoscale characterization to investigate particle contact loss and its impact on battery efficiency. Conductive AFM (CAFM) probes local conductivity at the cathode level, identifying contact loss areas. We identify key degradation factors by analyzing particle size distribution, state of charge, and contact behavior.

This methodology is demonstrated on an ion beam-polished NMC cathode (Fig.1), where a) SEM image, b) local conductivity, and c) topography of the same region are shown. In the conductivity map, contrast variations indicate different electrical contacts among cathode particles.

Integrating these techniques within an AFM-in-SEM platform enables correlative in-situ characterization, combining electrical, structural, and chemical data. This comprehensive approach provides deeper insights into degradation mechanisms, helping optimize battery design and advance next-generation energy storage solutions.

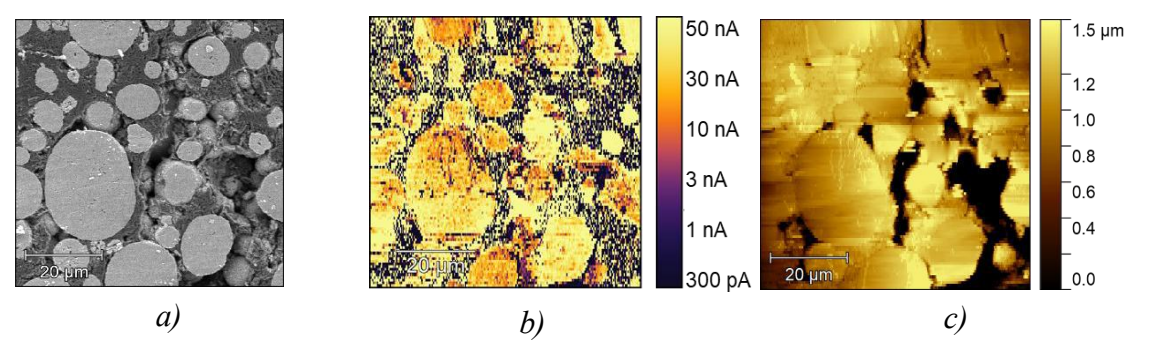


Figure 1. a) SEM image, b) local conductivity map, and c) topography of Argon ion beam polished cross-section of NMC cathode.

- 1. Freeing Energy. Energy Fact. Online. Available from: https://www.freeingenergy.com/facts/learning-lithium-ion-batteries-economies-price-decline-g202/. [cit. 2024-09-22].
- 2. Goodenough, J.B., Park, K.S. The Li-ion rechargeable battery: a perspective. J. Electrochem. Soc.
- 3. 164.1 (2013): A5019. https://doi.org/10.1149/2.0251701jes.
- 4. Schmaltz, T., Wicke, T., Weymann, L., Voß, P., Neef, C., & Thielmann, A. (2022). Solid-state battery roadmap 2035+
- 5. Powering Advanced Battery Technology and Research with TESCAN Solutions. Online.
- 6. Kramář, J. Optimization and microstructure analysis of solid-state batteries. Brno University of Technology, 2024.
- 7. Otoyama, Misae, et al. "Visualizing local electrical properties of composite electrodes in sulfide all-solid-state batteries by scanning probe microscopy." The Journal of Physical Chemistry C 125.5 (2021): 2841-2849.

- 8. Dao, R., Neuman, J. Innovative In-Situ AFM-in-SEM Characterization Workflow of Cathode Components. Microscopy. Microscopy and Microanalysis, 30(Supplement 1), (2024).
- 9. Novotná, V., Horák, J., Konečný, M., Hegrova, V., Novotný, O., Nováček, Z., Neuman, J. AFM- in-SEM as a Tool for Comprehensive Sample Surface Analysis. Microscopy Today, 28.3 (2020): 38–46.
- 10. Janek, J., Zeier, W.G. Challenges in speeding up solid-state battery development. Nat Energy 8, 230–240 (2023).
- 11. Janek, J., Zeier, W. A solid future for battery development. Nat Energy 1, 16141 (2016).

LiTDI-PC-Based Electrolytes for a Wider Li-Ion Batteries Operation Temperature Range

M. Broszkiewicz^a, L. Niedzicki^a

^aFaculty of Chemistry, Warsaw University of Technology, Noakowskiego 3, Warsaw 00-664, Poland

LiTDI- and PC-based electrolytes were developed for a wider Liion battery operation temperature range. The basic parameters of the electrolytes have been measured: conductivity, lithium cation transference number, thermal properties and electrochemical stability window. Subsequently, the electrolytes with the highest application potential were tested in full cells exhibiting performance similar or superior (particularly at lower and higher temperatures) to the commercial systems.

The aim of this work was to investigate the feasibility of electrolytes for lithiumion cells based on lithium 4,5-dicyano-2-(trifluoromethyl)imidazolate (LiTDI) and propylene carbonate (PC). Propylene carbonate is a solvent of much lower melting point compared to the typically used ethylene carbonate, potentially widening the temperature range of electrolyte operation by far. However, it displays problems with compatibility with graphite anodes. At the beginning of the work, the LiTDI-based electrolytes were optimized in terms of ionic conductivity. Those electrolytes were prepared with PC and its mixtures with linear carbonates: dimethyl carbonate (DMC), ethyl-methyl carbonate (EMC) or diethyl carbonate (DEC). The highest conductivity of 6.3 mS·cm⁻¹ was obtained for the electrolyte containing 0.61 mol·kg⁻¹ of LiTDI in the mixture of 45PC-55DMC (n/n). Considering the lithium cation transference number, this electrolyte also showed the highest cationic conductivity. Based on DSC tests, this electrolyte remains liquid down to -60°C. Further research investigated the compatibility of this electrolyte with electrodes: graphite anode, Si/C composite anode and lithium-cobalt-manganese-nickel oxide (NMC) cathode. Tests included cycling of half-cells and full cells. The capacity retention and rate capability were investigated and compared with the performance of commercial electrolyte. The investigated electrolyte proved to be compatible with the electrodes when standard additives (FEC and VC) were used. It also provided similar or superior performance compared to reference electrolytes.

The Rasons Capacity Loss in Li-ion Battery with Anatase/Rutile Anode under the Cycling

I.M. Shcherbatiuk^a, T.V. Lisnycha^a, K.D. Pershina^{a,b}, S.O.Solopan^a

^aV.I. Vernadsky Institute of General and Inorganic Chemistry, National Academy of Sciences of Ukraine, Palladin Ave., 32/34, Kyiv, 03142, Ukraine

^bNational Technical University of Ukraine "Igor Sikorsky Kyiv Polytechnic Institute", Berestejskyi Ave.,37, Kyiv, 03056, Ukraine

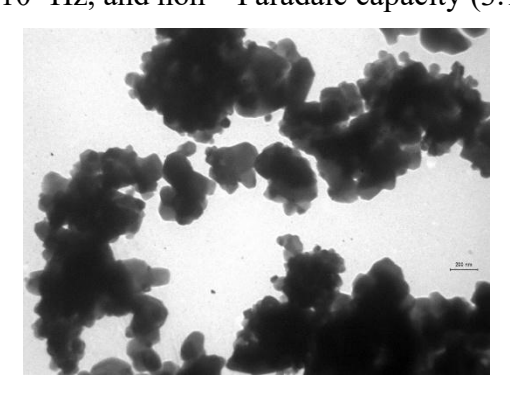
> The X-ray powder diffraction analysis, scanning electron microscopy (SEM), energy dispersive spectroscopy (EDS), transmission Electron microscopy (TEM), Emmet-Teller method, and galvanostatic cycling were used for investigating phase content and morphology impact on capacity loss in Li-ion battery with anatase \rutile anode. Pore radii distributions were obtained from isotherms in terms of the density functional theory. The XRD - patterns and TEM images detected presence the two mixed TiO₂ phases (anatase and rutile) with a cube-like particle morphology and quasi core-shell structure. The presence of two polymorphs of TiO₂ increases the crystallite size of anatase and rutile relatively single phases of anatase and rutile, average pore size, and decreases the surface area of rutile. Experimental results demonstrate a correlation between crystallite size and oxygen vacancies and capacity loss in Li-ion battery with anatase \rutile anode under the galvanostatic cycling.

Introduction

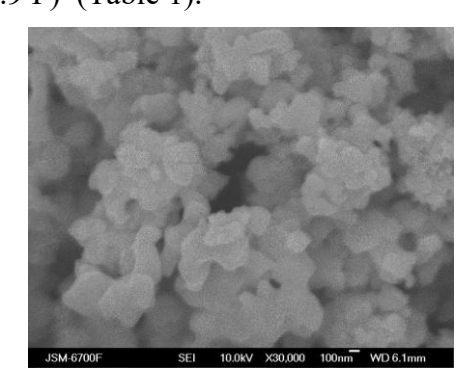
TiO₂-based materials are the possible candidates for replacing graphite in negative electrodes for Li-ion batteries due there safety, low cost, and ability to deliver high specific power. The wide use of such materials is restrained because of the differences in the solid electrolyte phase (SEI) formation on the surface of the various Titanium polymorphs [1]. Although Li-ion intercalation/deintercalation in TiO₂ occurs within the stability window of the electrolyte, there are some reports about the formation of SEI observed on the surface of TiO2 above 1.5 V vs. Li/Li+. However, it is still questionable whether an SEI may be formed on the surface of TiO2 phases similarly to the one formed on the surface of other materials for negative electrodes or it's formation has other steps and features connected with phase content and size distribution of particles. From the electrochemical and morphological analysis, it appears that, upon cycling to more cathodic cut-off potentials, the anataseTiO₂ nanoparticles are becoming less active with the fast fading of the specific charge and by the increase in the overpotential for the intercalation/deintercalation process [2]. The reason, this effect is not fully identified. So, in this work, the main target was to identify the reasons a capacity loss in the Li-ion battery with anatase \rutile anode under the galvanostatic cycling connected with the inner structure and morphology of anatase/rutile mixed-phase TiO₂ nanoparticles.

Experimental and discussion of results

Anatase/rutile samples (with size 90-230 nm) were synthesized using alkaline hydrolysis of TiCl₄ solutions [3]. The samples were dried at 150 °C for 10 h with further thermal treatment at 350-470 °C in the air for 45 hours. The structural investigation and X-ray powder diffraction analysis were performed on a (Cu-Ka radiation (1 \(\frac{1}{4} \) 0.15418 nm) and a Bragg 20 configuration. The phase content and crystallite size estimations were performed use Match 3.0 software. SEM images and EDX data obtained on a JEOL F-6301 scanning electron microscope. A high resolution TEM images were obtained on a JEM 2010 microscope. Specific surface areas and pore size distributions for the synthesized samples were calculated from nitrogen adsorption/desorption curves (NOVA 2200e, Quantachrome, USA) using the Nova Win 2.0 software. The total surface area of the materials S_{total} was calculated by the Brunauer-Emmet-Teller method (BET). Pore radii distributions were obtained from isotherms in terms of the density functional theory (DFT). Charge-discharge measurements of the TiO₂ contained anode in Li-ion element were performed on an electrochemical module Autolab 30 PGSTAT301N Metrohm Autolab in a two-electrode cell (disk cell). In order to investigate the processes affecting the overall specific capacity loss during anatase rutile cycling, lower potential limits have been applied, namely 1 V vs. Li/Li⁺. The Xray powder diffraction analysis detected the main TiO₂ polymorphs phases (Anatase and Rutile) in all samples prepared via alkaline hydrolysis of the ortho-titanic acid. The both phases (Anatase and Rutile) have a tetragonal crystal system with space groupe I 41/a m d (141) for anatase, and P 42/m n m for rutile. The unit cell for anatase is 3,7842 Å, and for rutile - 4,5922 Å. The morphology of the TiO₂ nanoparticles was characterized by TEM, as shown in Figure 1 a is a mixture of anatase and rutile phase, which has a cube-like particle morphology with a size about 75–225 nm in length and 80-130 nm in width. A cuboid particle morphology with a size about 20-50 nm in length and 20-40 nm in width, and some irregularly shaped particles with quasi coreshell structure. The surface of such mixed phases has morphology like a conglomerate with various pore radiuses and the average size of particles up to micrometer (Fig. 1 b). The presence of two polymorphs of TiO2 increases the crystallite size of anatase and rutile relatively single phases of anatase and rutile, average pore size, and decreases the surface area of rutile (Table 1). The close anatase-rutile contact creates opportunities to change the quantity the surface oxygen vacancies, and additional surface defects for better Li-ion intercalation due to high capacity $(0.68\pm0.03 \text{ F})$ in the frequency range 10^3 $\div 10^5$ Hz, and non – Faradaic capacity (3.17 ± 0.9 F) (Table 1).



a



b

Fig. 1. SEM and TEM images of the anatase/rutile samples

As TiO_2 is an intercalation anode, it follows a basic mechanism of Li^+ insertion and extraction during the charge/discharge cycle: $TiO_2 + xLi^+ + xe = Li_xTiO_2$

 $(1 \le x \le 0)$ (1). The theoretical capacity of anatase TiO₂ is 336 mAh.g⁻¹ equivalent to x = 1.

TABLE I.	Mornhological a	ind canacitance data d	of anatase/rutile samples
	midi piididzicai a	ina capacitance uata v	oi aiiatase/i atiit saiiipies

111DEE 1. 11101 photogram and capacitance data of difference 1 defice samples								
Sample	Crystallite	Average	Surface area (m ² g ⁻¹)		C, F $(10^3 \div$	$C, F (10^{-2})$		
	size* (nm)	pore			10^5Hz)	$\div 10^1 \mathrm{Hz}$		
		size, nm	This	Literature				
			work					
1	91,46 (R).	1,75; 30	8,51	-	0.68 ± 0.03	3.17 ± 0.9		
	376,05 (A)							
Anatase	16,3 (A)	1,7	6,09	5,90 [3]				
Rutile	42,7 (R)	5,5	31,41	50				

^{*}Calculated from XRD data using Eq. (1). A denotes anatase and R denotes rutile

It was detected a stable loss of capacity during galvanostatic cycling of the Li/TiO₂ system (Fig.2). According to EDS analysis the quantity of oxygen on the surface more into times relatively stechiometric amount in TiO₂. It may be the reason for decreasing the capacity because of increasing the surface oxygen content competed with Li ions:

$$nTiO_2 + V_O + xLi^+ + xe \rightarrow Li_xTi_nO_{2n-1} (4.1 \le 2n-1 \le 4.7)$$
 (2)

V₀- oxygen vacancy

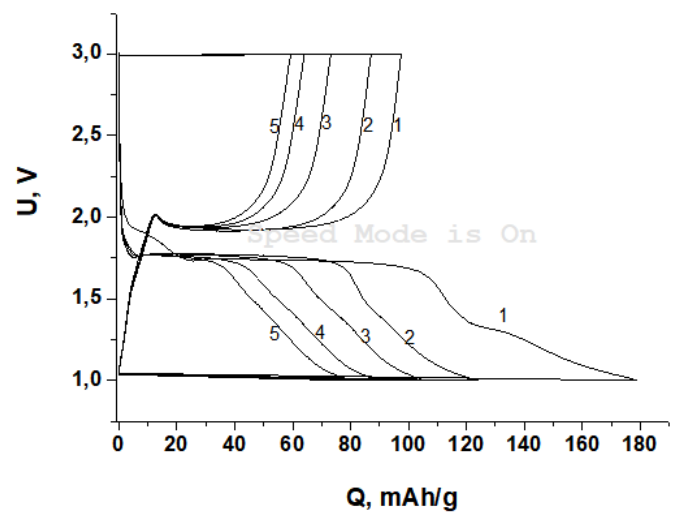


Fig. 2. Charge-discharge voltage profile of the Li/TiO₂ (anatase-rutile) system

Hence, a direct relationship between the condition of anatase -rutile surface, oxygen vacancies, galvanostatic cycling period, pore distribution, crystallites size, and capacity loss is found. It can be stated that crystallites size and surface amount of the oxygen vacancies are the main reasons for capacity loss in Li-ion battery with anatase \rutile anode under the cycling for the first five cycles.

Acknowledgments

The authors would like to express their deep appreciation to the National Academy of Sciences of Ukraine (NASU) for the financial support our work (SR N^0 0122U200365).

- 1. Madej, E., Ventosa, E., Klink, S., Schuhmann, W., & La Mantia, F. *Physical Chemistry Chemical Physics*, 16(17), 7939-7945. (2014).
- 2. Paul, S., Rahman, M. A., Islam, M. S., Islam, M. R., & Siddiqui, S. E. T. *Battery Energy*, *1*(4), 20220018. (2022).
- 3. Shcherbatiuk, I. M., Lisnycha, T. V., & Pershina, K. D. Chemistry, Physics & Technology of Surface/Khimiya, Fizyka ta Tekhnologiya Poverhni, 16(1). (2025).

Reserve Lithium Power Sources with Enhanced Specific Energy Based on Innovative MnO₂+MoO₃ Cathodes

O. V. Markevych^a, Yu. V. Polishchuk^a, V. V. Zinin^a, K. M. Sukhyi^a

^aUkrainian State University of Science and Technologies, Dnipro, 49010, Ukraine

An innovative technology has been proposed for producing cathodes for backup power sources based on advanced composite MnO₂+MoO₃ cathodes with the use of graphene. The main advantages of such cathodes include high electrode mass density and a high content (96%) of electrochemically active materials, which enables achieving a high energy content in the battery. The technology has been implemented in 2325 coin cell. The optimal graphene content and the optimal MnO₂: MoO₃ ratio in the cathodes have been determined.

Introduction

Reserve batteries are one of the key components in powering critical infrastructure for both military and civilian applications. In the military sector, they ensure the operation of communication, control, and navigation systems under emergency conditions [1]. In the civilian sector, lithium batteries are used as emergency power sources for medical equipment, data centers, telecommunications, emergency lighting systems, banks, airports, subways, railways, and building life-support systems – particularly as primary power sources in UPS systems for data centers and hospitals [2][3].

Currently, among the various available options, lithium-based sources dominate as backup batteries. This is due to their low self-discharge rate (~1% per year), which is enabled by a passivating film on metallic lithium in aprotic electrolytes.

The cathode materials of lithium reserve batteries include solid-phase oxides (MnO₂, MoO₃, V₂O₅), fluorides (CF_x), and sulfides (FeS₂). MnO₂ is one of the most widely used materials for primary and next-generation batteries [4]. Hybrid MnO₂–CF_x cathodes demonstrate increased energy value, stable voltage, and are used in commercial batteries produced by Ultralife [5][6].

MoO₃ has attracted attention due to its ability to form non-stoichiometric molybdenum oxide bronzes during lithium intercalation, which enhances electrical conductivity during discharge [7]. These properties are exhibited by ballast-free MoO₃ thin-film cathodes [8][9] and electrodes with added carbon nanotubes [10]. However, the high cost of production remains a barrier to commercialization.

Experiment

Experiments were conducted in an electrolyte composed of PC: DME (3:1) with 1 M LiClO₄. Lithium was used as the anode, with its surface modified by a lithium–aluminum alloy. The anode thickness was 580 µm, and its weight ranged from 80 to 85 mg. Composite MnO₂+MoO₃ cathodes were prepared by pre-mixing MnO₂ with a carbon-based material (graphene), followed by the addition of MoO₃. A fluoropolymer suspension was used as the binder component. The content of the fluoropolymer binder

in the cathode mass was 1%. The prepared cathodes were heat-treated at 250 ± 5 °C for 4 hours. Galvanostatic discharge of 2325-type coin cells was performed at 1 mA until a cutoff voltage of 2.0 V (in some cases, down to 1.8 V). The experiments were conducted at a temperature of +25 °C.

Results and discussion

To determine the optimal graphene content in the cathode composition, a MnO₂: MoO₃ ratio of 50:50 was applied. The average discharge voltage of cells with 1% graphene relative to the MnO₂ content is relatively low, measuring 2.1 V (Fig. 1, curve 1). Clearly, this amount of graphene does not ensure effective reduction of interfacial resistance between manganese and molybdenum oxide phases across the entire composite contact surface.

It should be noted that the discharge profile of the composite cathode is characterized by a single plateau, despite the fact that the electrochemical reduction processes of MnO₂ and MoO₃ during lithium-ion intercalation occur at different potentials. The capacity of cells with 1% graphene content is approximately 270 mAh/g of cathode material. The Faradaic efficiency of active materials approaches 90% [11].

Increasing the graphene content in the cathode mass to 3% relative to the MnO₂ quantity results in a dramatic change in the cathode profile (Fig. 1, curve 2) and a rise in discharge voltage to 2.4 V. Discharge curve 2 exhibits three voltage plateaus, corresponding sequentially to the electrochemical reduction of MnO₂ (2.9 V) and MoO₃ at 2.5 and 2.25 V. The contribution of capacity associated with the latter two plateaus indicates the establishment of a compromise voltage defined by the simultaneous reduction of both oxides.

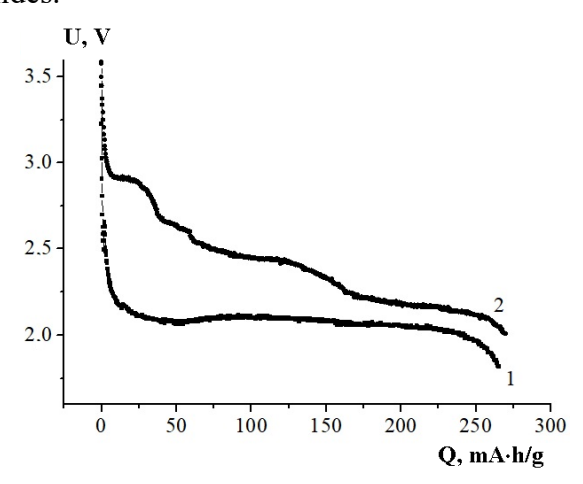


Figure 1. Discharge characteristics of 2325 coin cells with composite MnO_2 : MnO_3 (50:50) cathodes. Discharge current: 1 mA. Graphene content relative to MnO_2 : curve 1-1%; curve 2-3%. Electrolyte: PC, DME (3:1), 1 M LiClO₄. The weight of the cathode mass is 1.05 ± 0.005 g.

Figure 2 shows galvanostatic discharge curves of cells with cathodes containing different MnO₂ to MoO₃ ratios in the cathode composition. Increasing the MoO₃ content in the cathode mass from 10% to 30% leads to changes in both the profile of the galvanostatic discharge curve and the capacity of the power sources. As the amount of MnO₂ in the cathode mass decreases, the plateau at 2.9 V shortens. However, the discharge capacity of the cathodes and the cells as a whole increase to nearly 270 mAh. Further increasing the MoO₃ content and decreasing MnO₂ in the cathode does not enhance the electrochemical capacity but results in a shortening of the upper plateau at

2.8–2.9 V. Notably, once the MnO₂ content in the cathode drops below 70%, the capacity no longer increases significantly, remaining at around 280 mAh/g. Based on the obtained data, a dependence graph was constructed showing the energy value of coin power sources as a function of the MnO₂ to MoO₃ ratio in the cathode composition. This dependence is presented in Figure 3.

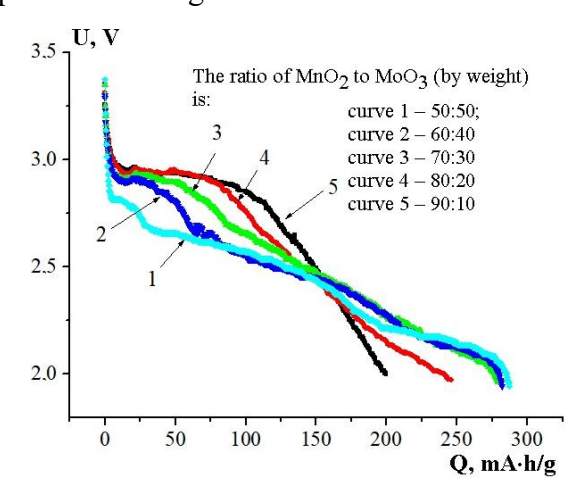


Figure 2. Discharge characteristics of 2325 coin cells with composite cathodes containing various ratios of the electrochemical components MnO_2 and MoO_3 in the cathode mass. Graphene content: 3% relative to MnO_2 . Electrolyte: PC, DME (3:1), 1 M LiClO₄. The weight of the cathode mass is 1.05 ± 0.005 g.

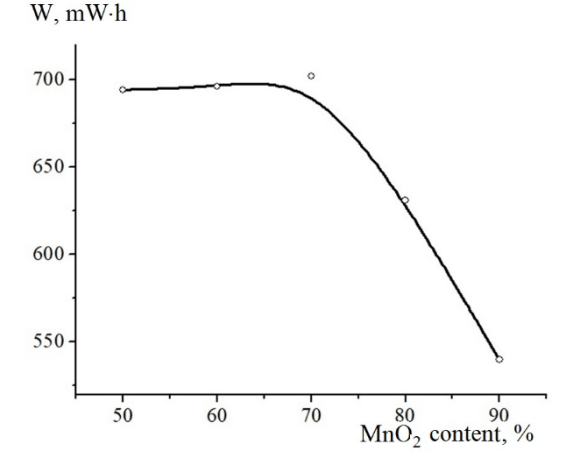


Figure 3. Effect of MnO_2 content (MnO_2 : MoO_3 ratio) in the cathode on the energy of coin cell with composite cathodes. Graphene content: 3% relative to MnO_2 . Electrolyte: PC, DME (3:1), 1 M LiClO_4 . The weight of the cathode mass is 1.05 ± 0.005 g. Discharge current: 1 mA. Temperature: $+25 \, ^{\circ}\text{C}$.

Based on the Fig. 3 data, the highest coin cell energy value is observed for a MnO₂: MoO₃ ratio ranging from 50:50 to 70:30 by weight. This level reaches approximately 700 mWh per coin cell. To determine the optimal MnO₂: MoO₃ ratio in the cathode composition is important to consider not only the energy value but also economic efficiency. MoO₃ is known to be significantly more expensive than MnO₂. Therefore, from an economic standpoint, the most favorable cathode composition is one that provides the highest energy value while containing a minimal amount of the more costly component. Thus, the recommended MnO₂: MoO₃ ratio in the cathode composition of composite cathode-based power sources is 70:30.

Conclusions

The optimal graphene content in composite $MnO_2 + MoO_3$ cathodes is 3% relative to MnO_2 . Optimizing the graphene content increased the discharge voltage by an average of 0.4 V at a discharge current of 1 mA.

The optimal MnO₂: MoO₃ ratio in the composite cathode has been identified in terms of achieving maximum energy performance in reserve 2325 coin cell. Taking economic factors into account, the recommended ratio is 70:30.

The energy value of the 2325 coin cell prototypes at the optimal oxide ratio in the cathode averages 700 mWh.

- 1. G. Ritchie, Military Applications of Reserve Batteries, (1996).
- 2. S. Coccato, K. Barhmi, I. Lampropoulos, S. Golroodbari, and W. van Sark, Batteries, 11, 179 (2025). https://doi.org/10.3390/batteries11050179
- 3. S.-M. Jung, B. Ricci, and G. Chung, 2015 IEEE 15th International Conference on Environment and Electrical Engineering (EEEIC), 7165294 (2015). https://doi.org/10.1109/EEEIC.2015.7165294.
- 4. Z. Cao, Q. Xiao, G. Lei, and Z. Li, SN Appl. Sci., 1, 1530 (2019). https://doi.org/10.1007/s42452-019-1585-y
- 5. Z. Luo, J. Wan, W. Lei, Y. Zhao, Y. Pan, and Z. Ma, Mater. Technol., **35** (13–14), 836–842 (2019). https://doi.org/10.1080/10667857.2019.1701255
- 6. J.-H. Cho, E. Yoo, J.-S. Yeo, Y. Hyunki, and Y. Choi, ECS Meet. Abstr., MA2022-02, 153 (2022). https://doi.org/10.1149/MA2022-022153mtgabs.
- 7. P. G. Dickens and P. G. Wiseman, J. Solid State Chem., 10 (3), 211–215 (1975).
- a. V. Markevich and E. M. Shembel, Vopr. Khimii i Khim. Tekhnol., 3, 171–175 (2005).
- 8. H. N. Sumedha, M. Shashank, B. M. Praveen, and G. Nagaraju, Results Chem., 4, 100493 (2022). https://doi.org/10.1016/j.rechem.2022.100493
- 9. H. Sheng, Y. Lin, D. Wei, L. Li, Q. Zhang, L. Sun, et al., Nanomaterials, **13** (15), 2272 (2023). https://doi.org/10.3390/nano13152272.
- 10. O. V. Markevych, Y. V. Polishchuk, V. V. Zinin, K. I. Vavilon, and K. M. Sukhyy, Vopr. Khimii i Khim. Tekhnol., **157** (6), 89 (2024). https://doi.org/10.32434/0321-4095-2024-157-6-89-94

Evaluating the Response of Various Li-ion Chemistries to Nail Penetration

M. Šedina^a, J. Amici^b and T.Kazda^a

^a Department of Electrotechnology, Brno University of Technology, Brno 61600, Czech Republic

^b Electrochemistry Group Department of Applied Science and Technology – Politecnico di Torino – Corso Duca degli Abruzzi 24, 10129 Torino -Italy

The safety of lithium-ion batteries under mechanical abuse, such as nail penetration, depends strongly on cell chemistry and state of charge (SoC). Chemistries like LFP and LTO offer high thermal stability and low risk of thermal runaway, while NMC, NCA, and LCO are more reactive, especially at high SoC. This paper compares the thermal behavior of common Li-ion chemistries based on their material properties and published studies, highlighting their safety characteristics for use in electric vehicles and energy storage systems.

Introduction

Lithium-ion (Li-ion) batteries are widely used due to their high energy density and long cycle life. In large battery applications, such as electric vehicles and energy storage, safety is a primary concern. The safety response of a Li-ion cell is strongly influenced by its chemistry. Differences in cathode materials, electrolyte formulations, and internal design affect the severity of thermal runaway and gas generation. This study compares the behavior of selected Li-ion chemistries under nail penetration conditions.

Cathode materials and its thermal stability

As was mentioned above, the safety performance of Li-ion batteries under abuse conditions is strongly dependent on the chemistry of their electrodes. Parameters of each chemistry can be seen in Figure 1.

Lithium iron phosphate (LFP) provides excellent thermal stability due its strong internal structure, which means that the risk of thermal runaway is reduced even under extreme conditions, like high mechanical stress or high external temperatures.

Lithium cobalt oxide (LCO) is the most unstable cathode material used in commercial batteries. It is more sensitive to thermal runaway and oxygen release at high temperatures, which can lead to a risk of fire and explosion [1].

Nickel-rich materials, such as NMC (LiNi_xMn_yCo_{1-x-y}O₂) and NCA (LiNi_xAl_yCo_{1-x-y}O₂), offer high energy density with increased stability compared to LCO, but still can't get the stability of the LFP, the instability of the material grows with a high state of charge (SoC)[2][3].

Typically, Li-ion batteries are produced with graphite anodes. There is another commercially used type of anode. Lithium titanate (LTO) has achieved excellent safety

due to its high structural stability and lower operating voltage. This material is nearly immune to thermal runway or explosion [4].

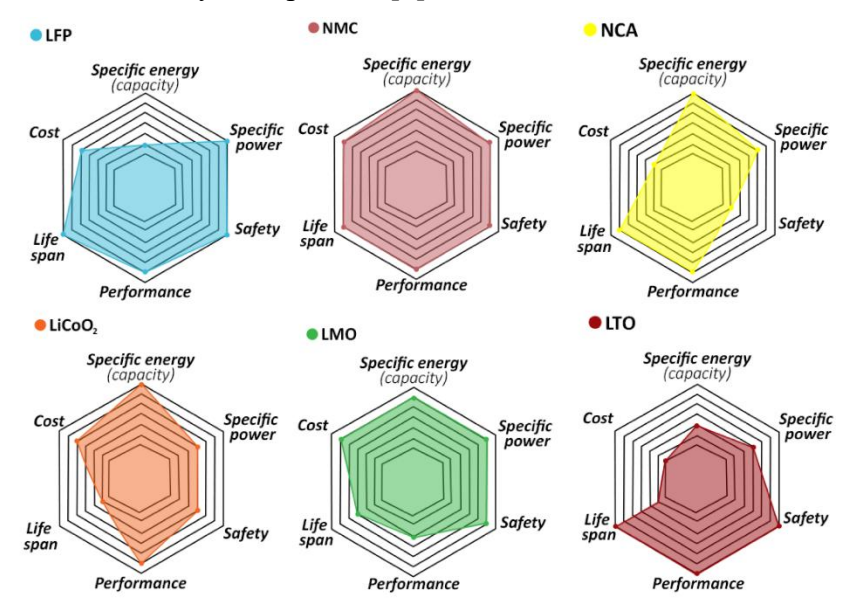


Figure 1. Battery chemistry parameters [5]

Penetration testing

There are several types of penetration tests for Li-ion batteries. Most common is the nail test, in which a battery is penetrated with a defined nail, which causes an internal short circuit.

Results from other studies

L. Zhang and his colleagues monitored the progression of thermal runaway during penetration testing of Li-ion batteries. Their study focused on the influence of the battery's SoC as well as the thickness and material of the penetrating nail. The tests were conducted using 18650 cells with a capacity of 3500 mAh and NCA cathodes. The results showed that with increasing SoC, both the maximum temperature and the rate of temperature rise increased, leading to a more severe thermal runaway event. Furthermore, thicker nails were found to reduce both the peak temperature and its rate of increase, as they conducted more heat away from the cell. Regarding the material of the penetrating object, it was observed that at high SoC, more conductive nails enhanced thermal propagation within the cell, while at lower SoC, they helped to mitigate it by conducting heat away more effectively. In contrast, non-conductive nails exhibited the opposite behavior [6].

In a separate experiment, H. Wang and his team attempted to induce thermal runaway by applying localized pressure on the battery instead of piercing it, aiming to create an internal short circuit between the electrodes. Two types of pouch cells with identical external dimensions—representative of those used in electric vehicles—were tested: LFP cells (18 Ah) and NMC cells (25 Ah). LFP cells were tested at 90% and 100% SoC, while NMC cells were tested at 50%, 60%, 80%, and 92% SoC. None of the LFP samples experienced thermal runaway and were considered safe by the authors. The same applied to the NMC samples at 50% SoC. However, at 60% SoC, safety was reduced and half of the tested NMC cells exhibited thermal runaway. At 80% and 92% SoC, all tested NMC cells underwent thermal runaway, classifying them as unsafe

under mechanical stress. These results suggest that LFP cells are significantly safer than NMC cells under similar conditions [7].

Results from other studies

For our experiment, we tested both large-format and cylindrical Li-ion cells. As a testing device was use battery performance calorimeter equipped with nail actuator THT ARC EV+. The large-format group included an NMC pouch cell with a capacity of 5,000 mAh, an LCO pouch cell with a capacity of 16,000 mAh, and an LFP prismatic cell with a capacity of 10,000 mAh. Penetration tests were conducted on fresh cells at 0% and 100% SoC, as well as on cycled cells, which made 10 full charge–discharge cycles at 60 °C at 0,5C and one cycle at 80°C with 1C.

The cylindrical cell included five chemistries: NMC (3300 mAh), NCA (3200 mAh), LFP (1500 mAh), LTO (1300 mAh), and LCO (2500 mAh). For all cylindrical cells, penetration tests were performed on fresh samples at 0% and 100% SoC.

Acknowledgments

This work was supported by the specific graduate research of the Brno University of Technology No. FEKT-S-23-8286.

- 1. SPOTNITZ, R. a J. FRANKLIN, *Journal of Power Sources*. Elsevier BV, **113**(1), 81-100 (2003).
- 2. BAK, Seong-Min, Myeongjun SONG, Zulipiya SHADIKE, et al., *Nano Energy*. Elsevier BV, **126**, (2024)
- 3. XIA, Heyi, Cheng LIU, Lu SHEN, Jing YU, Baohua LI, Feiyu KANG a Yan-Bing HE, 2020. *Journal of Power Sources*. Elsevier BV, **450**, (2020)
- 4. HALL, Florian, Jonas TOUZRI, Sabine WUSSLER, Hilmi BUQA a Wolfgang G. *Journal of Energy Storage*. Elsevier BV, 17, (2018)
- 5. SALGADO, Rui Martim, Federico DANZI, Joana Espain OLIVEIRA, Anter EL-AZAB, Pedro Ponces CAMANHO a Maria Helena BRAGA. *Molecules*, **26**(11) (2021)
- 6. WANG, Hsin, Edgar LARA-CURZIO, Evan T. RULE a Clinton S. WINCHESTER. *Journal of Power Sources*. Elsevier BV, **342** (2017)
- 7. MAO, Binbin, Haodong CHEN, Zhixian CUI, Tangqin WU a Qingsong WANG. *International Journal of Heat and Mass Transfer*, Elsevier BV, **122** (2018)

Investigation of Electrical and Acoustic Impedance with Volumetric Deformation of a Li-ion Cell Under Varying State of Charge

E. Sedláčková^a, J. Kasper^a, T. Finsterle^a, K. Dušek^a, and V. Knap^a

^a Dept. of Electrotechnology, Faculty of Electrical Engineering, Czech Technical University, Praha, Czech Republic

With the growing use of lithium-ion batteries, the need for efficient diagnostic methods is increasing. This work aims to explore the potential of acoustic impedance as a fast and non-invasive method for monitoring the state of a battery cell. Ultrasound diagnostics are relatively new in the field of batteries but show promising potential due to their speed and simplicity. For comparison, standard methods such as electrochemical impedance spectroscopy (EIS) and strain measurement were employed to monitor mechanical changes during charging and discharging cycles. The study involves experimental monitoring of changes in electrical and acoustic impedance along with volumetric deformation of the cell under varying states of charge. The goal is to identify the correlations between the different methods and evaluate the feasibility of using acoustic diagnostics as a rapid alternative to conventional techniques.

Introduction

The use of lithium-ion batteries (LIBs) has significantly increased over the past decades and has become the subject of extensive research. Every year, billions of cells are produced worldwide, finding applications in mobile phones, portable computers, power tools, and hybrid or electric vehicles. Despite the many advantages of LIB technology, there are still numerous material and engineering challenges to overcome [1][2].

Battery monitoring and diagnostics are becoming increasingly important with the growing demand for reliable and long-lasting energy storage. Understanding a battery's condition is essential for safe operation and informed decisions about its further use or recycling.

Since the internal states of batteries cannot be measured directly, their state is usually estimated using model-based approaches based on externally measurable quantities such as voltage, current, or temperature. Recently, there has been an increased interest in more complex diagnostic approaches that include methods utilizing quantities other than just electrical, such as acoustic or mechanical, and that open possibilities for advanced real-time diagnostics [3][4].

Overview of diagnostics and monitoring methods

Electrochemical Impedance Spectroscopy

Electrochemical Impedance Spectroscopy (EIS) is a non-invasive diagnostic method that provides detailed information about the internal state of a battery. The

principle involves applying a small alternating current or voltage and measuring the resulting voltage response at different frequencies. This allows an impedance characteristic to be obtained that reflects the electrochemical processes taking place inside the cell. Due to its sensitivity to changes in the battery's internal structure, EIS has become a popular laboratory tool for diagnosing the battery's state of health (SOH), with testing able to be performed without interfering with normal operation [5][6].

Innovative Battery Diagnostic Techniques

The first of these innovative methods involves using strain gauges to monitor internal stress. During charging, lithium-ion intercalates into the graphite anode, causing the battery's volume to increase. During discharging, the opposite occurs. These cyclical changes in electrode volume generate internal mechanical stresses due to the limitations imposed by the battery construction. Research shows that monitoring deformation using strain gauges, in addition to electrical signals, can improve the accuracy with which the state of charge (SOC) is estimated. Furthermore, the maximum strain measured can be used to predict battery capacity degradation [7][8]. Another method is diagnosis by ultrasound. Ultrasonic waves are propagated through the object under test, allowing for accurate real-time monitoring of material properties, internal damage, and structural integrity. With this capability, ultrasonic inspection can be used to detect changes in the internal material properties within a battery, and thus, early detection of incipient failure or degradation [9][10].

Experiment

In this experiment, the response of a lithium-ion battery is investigated during step charging with increments of 5% SOC at a constant current of 0.1 C and a temperature of 25 °C. After each step, three different measurements are performed: mechanical response using a strain gauge connected to an Arduino, acoustic analysis of internal changes using an EPOCH650 ultrasonic flaw detector, and EIS. The aim is to observe possible structural and electrochemical changes inside the cell at various SOC. Figure 1 shows the reflected ultrasonic wave at 50% SOC.

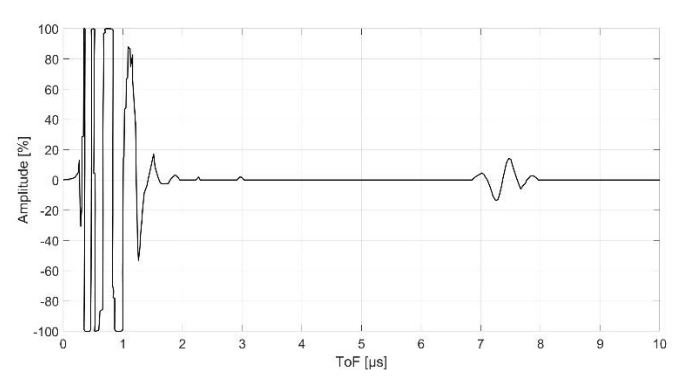


Figure 1. Reflected ultrasonic wave at 50% SOC at 25°C.

Conclusions

In recent years, there has been a growing interest in developing new, faster and more accurate diagnostic techniques for monitoring the health of lithium-ion batteries, especially in the context of their massive deployment in mobile electronics, transportation and energy storage. The aim of these methods is not only to detect

degradation or failures early, but also to support decision-making processes regarding the reuse or recycling of batteries. This work focuses on finding the links between traditional electrochemical diagnostic methods, such as EIS, and newly investigated physical approaches - specifically, monitoring mechanical changes in battery cells using strain gauging and detecting internal structural changes using ultrasonic methods. The main objective is to assess whether these alternative non-invasive techniques can serve as a reliable and sufficiently sensitive tool for real-time battery health monitoring across different cell types and formats.

Acknowledgments

This work was supported by the Grant Agency of the Czech Technical University in Prague, grant No. SGS24/136/OHK3/3T/13, and the project "The Energy Conversion and Storage", funded as project No. CZ.02.01.01/00/22_008/0004617 by Programme Johannes Amos Comenius, call Excellent Research. The research leading to these results has also received funding from European Union's Horizon Europe Programme under the BatteReverse project, grant agreement n°101103706. Views and opinions expressed are however those of the author(s) only and do not necessarily reflect those of the European Commission. Neither the European Union nor the granting authority can be held responsible for them.

- 1. K. Rhodes, N. Dudney, E. Lara-Curzio, and C. Daniel, *J Electrochem Soc*, **157**, A1354 (2010).
- 2. B. Scrosati and J. Garche, *J Power Sources*, **195**, 2419–2430 (2010).
- 3. A. G. Hsieh et al., *Energy Environ Sci*, **8**, 1569–1577 (2015).
- 4. J. Y. Kim, Z. L. Wang, S. M. Lee, and J. W. Byeon, *Microelectronics Reliability*, **100–101** (2019).
- 5. Z. Wang et al., Sustainable Energy Technologies and Assessments, **60** (2023).
- 6. L. A. Middlemiss, A. J. R. Rennie, R. Sayers, and A. R. West, in *Energy Reports*, vol. 6, p. 232–241, Elsevier Ltd (2020).
- 7. D. Vidal et al., *J Power Sources*, **514**, 230552 (2021) https://www.sciencedirect.com/science/article/pii/S0378775321010508.
- 8. J. Song et al., *Energy Technology*, **12** (2024).
- 9. Y. Wu, Y. Wang, W. K. C. Yung, and M. Pecht, *Electronics (Basel)*, **8**, 751 (2019).
- 10. L. Gold et al., *J Power Sources*, **343**, 536–544 (2017).

Single Cation Doped LiMe_xMn_{2-x}O₄ as Cathode Materials for Lithium-Ion Batteries

Yu. V. Shmatok^a, N. I. Globa^a, I. V. Romanova^{a,b}

^a V.I. Vernadsky Institute of General and Inorganic Chemistry of the NAS of Ukraine, 32/34 Palladina Ave., Kyiv 03142, Ukraine

^b Institute for Sorption and Problems of Endoecology of the NAS of Ukraine,

Kyiv 03164, Ukraine

Improving the energy performance of lithium-ion batteries, reducing their production costs, and enhancing environmental safety necessitate innovative approaches and solutions in the development and study of advanced electrode materials and electrolytes [1]. In this context, the optimization and investigation of lithium-manganese spinels (LiMn₂O₄) as cathode materials in various electrolyte systems align closely with current research trends. Doping LiMn₂O₄ with cations of different types is an effective way to improve its electrochemical characteristics [2].

In this work, the physicochemical and electrochemical characteristics of modified spinels, of the general formula LiMe_xMn_{2-x}O₄, where Me is Fe, Ni, Ce and La, synthesized by thermal decomposition of citrate precursors, is discussed. The influence of the metal cation nature on the structural and surface properties of spinels is established by X-ray diffraction (XRD), scanning (SEM) and transmission (TEM) electron microscopy. It is shown that Fe and Ni cations, which are close in size to Mn ions, are incorporated into the LiMn₂O₄ structure with corresponding changes in the crystal lattice parameters. The rare earth cations Ce and La, which are larger in size, mainly form separate phases in the form of CeO₂ oxide and LaMnO₃ perovskite, respectively. For all cations, a decrease in the size of spinels particles compared to pure LiMn₂O₄ is observed.

The specific, cyclic and kinetic characteristics of the synthesized spinels in systems with aprotic and aqueous electrolytes have been determined by galvanostatic and cyclic voltammetry methods. It is shown that in aprotic electrolyte, the studied spinels demonstrate excellent stability of specific capacity during long-term cycling and are capable of retaining about 25% of the capacity at discharge current densities up to 50 C. In aqueous electrolytes, at similar current densities, the specific capacity is preserved at the level of ~90%, but the cycling stability is worse compared to the aprotic system. It is shown that optimization of the composition of the aqueous electrolyte contributes to the improvement of the cyclic characteristics of spinels. Differences in the electrochemical behavior of spinels doped with different cations in aprotic and aqueous electrochemical systems are discussed.

- 1. M. Armand, P. Axmann, D. Bresser, M. Copley, K. Edström, C. Ekberg, D. Guyomard, B. Lestriez, P. Novák, M. Petranikova, W. Porcher, S. Trabesinger, M. Wohlfahrt-Mehrens, H. Zhang, *J. Power Sources*, **479**, 228708 (2020).
- 2. X. Hou, X. Liu, H. Wang, X. Zhang, J. Zhou, M. Wang, *Energy Storage Mater.*, **57**, 577 (2023).

Effect of Ni and La Dual Doping on Electrochemical Characteristics of LiMn₂O₄ in Lithium-Ion Systems

Yu. V. Shmatok^a, N. I. Globa^a, I. V. Romanova^{a,b}

^a V.I. Vernadsky Institute of General and Inorganic Chemistry of the NAS of Ukraine, 32/34 Palladina Ave., Kyiv 03142, Ukraine

^b Institute for Sorption and Problems of Endoecology of the NAS of Ukraine, Kyiv 03164, Ukraine

Structural and surface modification of lithium manganese spinel LiMn₂O₄ are essential strategies for enhancing its electrochemical performance as a cathode material in various lithium-ion systems. This study considers the effect of dual doping of spinel LiMn₂O₄ with nickel and lanthanum ions on its capacitive, cyclic, and kinetic characteristics in electrochemical systems with aprotic and aqueous electrolytes.

Introduction

Lithium manganese spinel LiMn₂O₄ is a cathode material whose study remains relevant, considering the requirements of modern lithium-ion batteries [1]. Improvement of the electrochemical characteristics of spinel can be achieved by optimizing its crystal structure and surface modification. This allows to reduce the negative impact of side processes, such as the Jahn-Teller effect and disproportionation reaction, on the specific and kinetic characteristics of LiMn₂O₄ during the charge/discharge. This work presents the results of a study of the effect of dual doping of LiMn₂O₄ spinel with Ni and La ions on the physicochemical characteristics and electrochemical behavior in systems with aprotic and aqueous electrolytes.

Experimental

Spinels of the composition LiNi_{0.03}La_{0.02}Mn_{1.95}O₄, LiNi_{0.05}La_{0.02}Mn_{1.93}O₄, LiNi_{0.05}La_{0.05}Mn_{1.9}O₄ and pure LiMn₂O₄ were synthesized by thermal annealing of citrate precursors, as described in Ref. [2]. The influence of Ni and La ions on the structure and surface properties of the synthesized compounds was analyzed using X-ray diffraction (XRD), scanning electron microscopy (SEM) and transmission electron microscopy (TEM) methods.

Electrochemical characteristics of the synthesized samples in aprotic and aqueous electrolytes were investigated by cyclic voltammetry, galvanostatic cycling and electrochemical impedance spectroscopy methods. Studies with aprotic electrolyte (1 M LiPF₆ EC:DMC:DEC, LP-71) were carried out in CR2016 coin cells with a Li metal electrode. Studies with aqueous electrolyte (5 M solution LiNO₃ in H₂O) were carried out in teflon cells with an activated carbon counter electrode (Kausorb-212 activated carbon) and an Ag/AgCl reference electrode.

Results and Discussion

It is established by XRD method that as a result of the synthesis, Ni ions, whose radius is close to that of Mn, are completely incorporated into the spinel structure, replacing Mn³⁺ in the 16d octahedral positions. The incorporation of nickel ions leads to a slight compaction of the crystal lattice and strengthening of the spinel structure due to a stronger Ni-O bond. Unlike Ni ions, La ions form a separate crystalline phase LaMnO₃ with a perovskite structure on the spinel surface. SEM and TEM showed that all doped spinels have smaller particle sizes compared to pure LiMn₂O₄, which are 100-150 nm and 200-300 nm, respectively. For all spinels, the particles have the shape of a truncated octahedron with developed (110) and (100) faces, which contribute to reducing the solubility of manganese and have open channels that facilitate the diffusion of lithium ions.

The obtained spinel samples are investigated as cathode materials in electrochemical systems with aprotic and aqueous electrolytes. The initial specific capacity of spinels in the aprotic system is 121, 99, 98 and 85 mAh/g for the samples LiMn₂O₄, LiNi_{0.03}La_{0.02}Mn_{1.95}O₄, LiNi_{0.05}La_{0.02}Mn_{1.93}O₄ and LiNi_{0.05}La_{0.05}Mn_{1.9}O₄, respectively. For the aqueous system, the dependence of the initial specific capacity on the composition of the spinels is preserved, but the corresponding values are several percent lower than for the aprotic system. Thus, the type of electrolyte has practically no effect on the initial specific capacity, but significantly affects the cycling stability. The corresponding dependences of the specific capacity on the cycle number during cycling in aprotic and aqueous electrolytes are shown in Fig. 1. In an aprotic electrolyte, all doped spinels demonstrate excellent cycling stability with a capacity retention of 92-95% after 800 cycles at 5 C at 25°C and 89-96% after 150 cycles at 1 C at 55°C (similar values for pure LiMn₂O₄ are 77 and 72%, respectively). In an aqueous system, the specific capacity during cycling is less stable, but even in this case, doped spinels demonstrate a better result. After 400 charge/discharge cycles at current densities of 3/1.5C, the capacity retention for the LiNi_{0.03}La_{0.02}Mn_{1.95}O₄, LiNi_{0.05}La_{0.02}Mn_{1.93}O₄ and LiNi_{0.05}La_{0.05}Mn_{1.9}O₄ and LiMn₂O₄ samples was 54, 51, 67 and 21%, respectively.

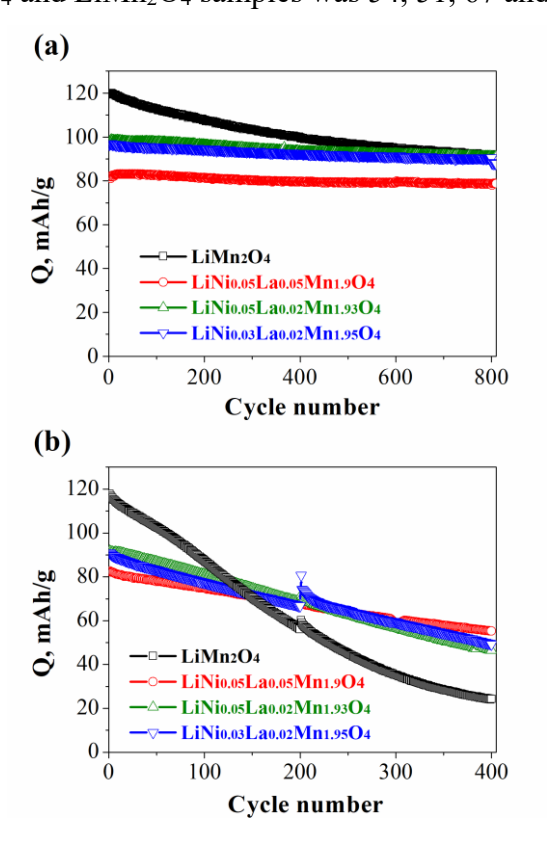


Figure 1. Dependences of discharge specific capacity on cycle number during cycling at 25 °C (a) in aprotic system at charge/discharge current densities of 1/5 C and (b) in aqueous system at charge/discharge current densities of 3/1.5 C.

The high specific conductivity of the 5 M LiNO₃ solution in H₂O, compared to the aprotic electrolyte LP-71 (154 and ~10 mS cm⁻¹, respectively), is the main factor contributing to obtaining high specific capacitance at high current densities. Thus, in the LP-71 electrolyte, the capacity retention at a current density of 50 C is 27-40%, depending on the spinel sample, and in an aqueous solution this value is about 90%. The diffusion coefficients of lithium ions ($D_{\text{Li+}}$) and the controlling mechanisms of charge transfer have been calculated from voltammograms obtained at scan rates of 0.1–1 mV/s [3]. The calculated values of $D_{\text{Li+}}$ for both systems are within 2.3×10⁻¹⁰ - 2.6×10⁻⁹ cm²/s. The values of the coefficient b, which allow to establish the predominant charge transfer mechanism (b = 0.5 corresponds to the diffusion mechanism, and b = 1 corresponds to the capacitive mechanism), were calculated from the slope of the linear logarithmic dependence log (I) – log (v). The obtained values of parameter b significantly exceed 0.5, which indicates a mixed diffusion-capacitive charge transfer in the aprotic system and a predominantly capacitive mechanism in the aqueous system.

- 1. J. Ma, T. Liu, J. Ma, C. Zhang, J. Yang, Adv. Sci., 11(2), 2304938 (2024).
- 2. Y.V. Shmatok, N.I. Globa, V.A. Sirosh, I.V. Romanova, S.A. Kirillov, *Monatsh. Chem.* **155**, 281 (2024).
- 3. T. Kim, W. Choi, H. C. Shin, J. Y. Choi, J. M. Kim, M. S. Park, W. S. Yoon, *J. Electrochem. Sci. Technol.*, **11**(1), 14 (2020).

Feasibility Study of Magnetron Sputtering Prepared High Entropy Oxide Thin Films as Anodes for Lithium and Sodium ion Batteries

P. Souček^a, T. Rada^a, T. Pitoňáková^a, J. Seidenglanz^a, and P. Vašina^a

^aDepartment of Plasma Physics and Technology, Faculty of Science, Masaryk University, Brno, Czech Republic

This contribution explores the possibilities of the use of magnetron sputtering for the preparation of high entropy oxides as novel materials for Li- and Na-ion battery anodes. It is shown that the method provides a good platform due to its ease of preparation of the said materials and provides a wide tuning area regarding their chemistry and microstructure.

Introduction

Lithium-ion (Li-ion) batteries have now been on the market for three decades and have evolved to present so far unmatchable combination of high energy and power densities, long cycle life and affordable costs [1]. Cathode materials in Li-ion batteries have significantly evolved since the first battery in 1991. However, graphite still has a 98% market share, with 2% of the market being taken by Li₄Ti₅O₁₂. Nevertheless, graphite's performance is limited by its lithium storage mechanism – intercalation and de-intercalation of Li-ions and the formation of graphite intercalation products. A revolution on the anode side of the battery is needed to push the performance of future Li-ion batteries significantly. The concept of high entropy oxides (HEOs) was first proposed in 2015. HEOs form a single-phase crystal structure and are composed of at least five element cations in the metallic sublattice with a concentration between 5 and 35%. The absence of principal elements in high-entropy materials can disrupt the formation of a dominant coordination environment, instead creating a diverse ensemble of local environments. This can reduce the short-range order that can harm the electrochemical performance, enabling the high entropy oxides to exhibit enhanced capacity and rate capability [2].

So far, the battery HEOs are produced as bulk materials by solid-state or wetchemical processes [3]. Solid-state processes are fairly simple, but they require high temperatures and high energy consumption and even then, they might not form the nanostructures that are required. On the other hand, wet-chemical processes are more complicated, lead to better elemental mixing and nanostructure formation, but they often require harmful chemicals, and there's the need to remove the solvents and other reagents. The common drawback of both methods is that bulk materials are created. As only the surface of the material undergoes the chemical reaction, any bulk "volume" is unnecessary, only increasing the price and raw material use. The solution would be to produce the anode in the form of a thin film, possibly even exploiting graphite-HEO nanoparticle interactions [1,4]. Magnetron sputtering is a plasma-based thin-film deposition method working in a thermal non-equilibrium state and is often used to produce high entropy alloys in the form of coatings [5]. High entropy oxide coatings can be easily deposited using reactive magnetron sputtering under an argon/oxygen atmosphere [6]. During non-reactive as well as reactive magnetron sputtering, the energy onto the growing coating is provided by energetic particles bombarding the growing coating. Each impacting particle delivers a high amount of energy to a very localized volume of the growing coating. These impacts cause local thermal spikes,

leading to a localized temperature increase, and the affected coating volume then rapidly cools and undergoes rapid quenching. The high entropy materials may undergo various phase transformations that cannot happen in bulk. This way, metastable phases can be prepared by magnetron sputtering. Moreover, a rapid cooling rate can restrict the diffusion of elements and further restrain the nucleation and growth of the intermetallic compounds, favouring the formation of solid-solution phases.

First, we will focus on the rock salt system. Copper, cobalt, magnesium, nickel and zinc are all divalent and readily form a (MgCoNiCuZn)O phase [7]. Zn and Co are the electrochemically active elements providing the main capacity of the anode from the first lithiation process. Mg²⁺ is electrochemically inert in the potential range available in a battery and cannot be reduced by Li. It stabilises the oxide phase that accommodates Li+ in the discharged state and hosts Co²⁺ and Zn²⁺ in the charged state. Cu and Ni do not participate in the redox reaction after the first lithiation cycle. Instead, they form the backbone of the nanoscale 3D metallic network, providing excellent electron conductivity. Secondly, spinel structure provides more levy for the elements and allows us to limit the use of critical elements and raw materials. We can omit cobalt and magnesium, as chromium, copper, iron, manganese, and nickel readily form a (CrMnFeNiCu)₃O₄ spinel phase [8]. In this case, the lithiation/de-lithiation mechanism is even more complex, as the long-range ordering of the material was lost after the first few discharge cycles, and only short-range ordering was preserved. Nevertheless, it was observed that the spinel structure was changed to rock salt in and that not all the elements are fully electrochemically active. Nevertheless, very good battery parameters were achieved [8].

Experimental

The coatings were deposited by reactive DC magnetron sputtering from segmented elemental targets or from a compound target under oxygen and argon flow. The HVM Flexilab (HVM Plasma s.r.o., Czech Republic) deposition device has three magnetron heads in a confocal configuration. The powers on the magnetrons were varied to obtain the desired compositions. The depositions were performed on 2 (100) silicon pieces 2 x 1 cm in size and 1 R-plane sapphire substrate 1x 1 cm in size. Substrates were ultrasonically cleaned in acetone and then in isopropanol for 180 seconds before placement in the centre of the substrate holder. The base pressure before the deposition of 10⁻⁴ Pa was reached by an oil-free scroll vacuum pump and a Hipace 300 turbomolecular pump. Directly before the deposition, the substrates were cleaned by argon ion bombardment under the pressure of 2.00 Pa using a 13.56 MHz generated DC self-bias of -180 V for 15 minutes to remove any contamination and native oxidation. Subsequently, the targets separated by shutters from the substrates were cleaned by argon ions at 1.26 Pa for 15 minutes using the same power of cathodes as for the deposition. The rotation of the substrate was set to 5 rotations per minute. The distance between each target and the substrate was 110 mm. The argon flow was fixed at 80 standard cubic centimetres per minute (sccm), and the nitrogen flow was set to 20 sccm for all depositions. The samples were deposited at ambient temperature (abbreviated RT; without intentional heating, < 50 °C) and at high temperature (abbreviated HT; 580°C). For HT samples, the temperature of the substrates was maintained for 1 h before the deposition to stabilise the working conditions.

Results

Mg-Co-Ni-Cu-Zn-O

Sputtering from segmented targets led to a complex chemical evolution with increasing oxygen flow due to different sputtering yields of poisoned targets and different affinities of the elements to oxygen. The evolution was similar for bot RT and HT, as is shown in Fig. 1.

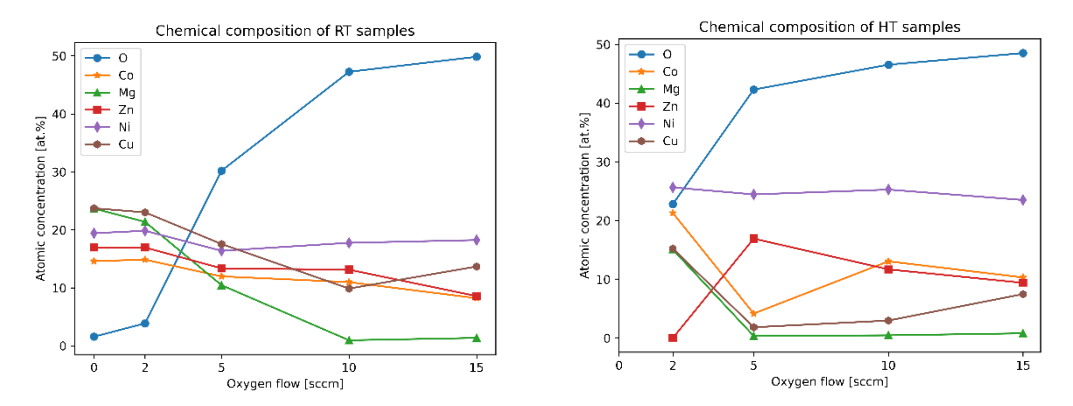


Figure 1. Chemical evolution of the Mg-Co-Ni-Cu-Zn-O system with different oxygen flows during the deposition.

Such complex evolution in chemistry also led to a complex evolution in the crystalline structure, as is illustrated in Fig. 2. While RT coatings required close to fully occupied oxygen sublattice to be crystalline, HT coatings showed a wider crystalline region and more than one phase.

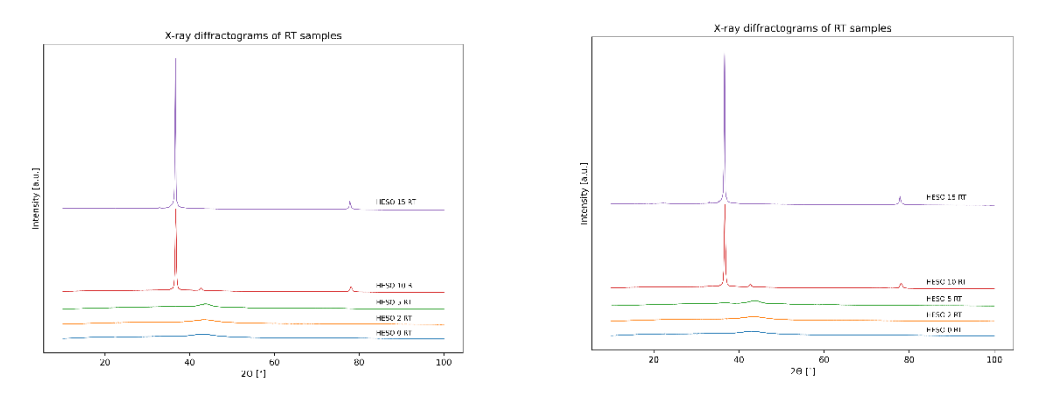


Figure 2. Chemical evolution of the Mg-Co-Ni-Cu-Zn-O system with different oxygen flows during the deposition.

The surface and cross-section morphology is showed in Fig. 3. The coatings are relatively dense, while the coatings with the highest oxygen contents exhibited a looser structure more relevant for electrochemical applications.

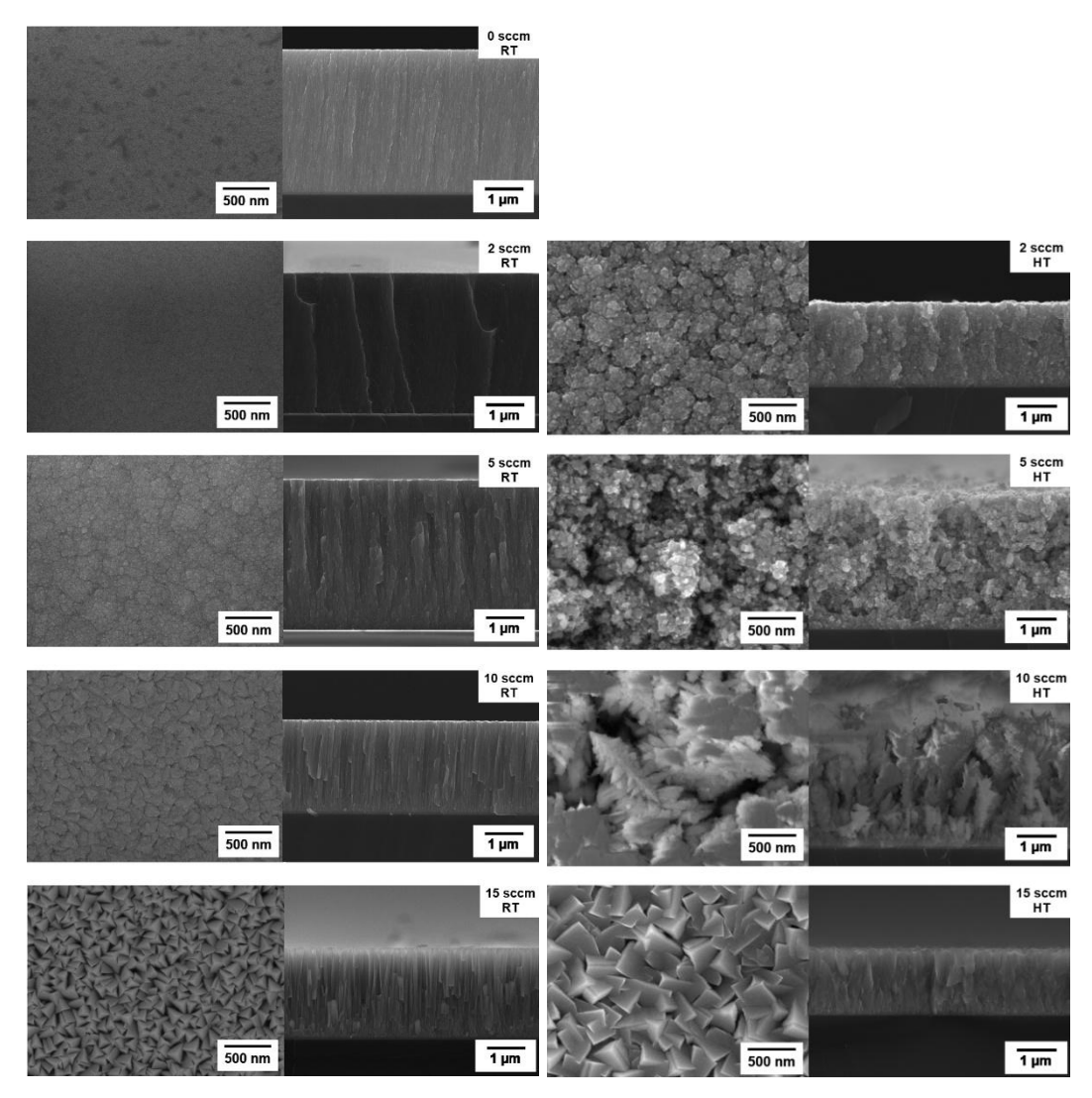


Figure 3. Surface and cross-section morphology evolution.

Cr-Mn-Fe-Ni-Cu-O

The evolutions of the chemical composition, microstructure and morphology of the coatings are in principle similar to the hitherto presented system. Moreover, comparison of depositions from a single compound target yielded predominantly amorphous coatings, while changes in the chemical composition given by the use of segmented targets yielded crystalline coatings. This showed the importance of the chemical composition tuning.

Conclusions

Magnetron sputtering has shown a great promise for the preparation of thin films for Li- and Na-ion battery anodes. It allows for easy change of chemical composition including tailored design of the vacancies on the metallic and oxygen lattice. Further optimization can also significantly increase the multi-level porosity of the coatings enhancing possible battery capacity and performance.

Acknowledgments

This research was supported by project LM2018097, funded by the Ministry of Education, Youth and Sports of the Czech Republic.

- 1. H. Zhang, et al., Ener. Stor. Mater. 36 (2021) 147-170.
- 2. B. Ouyang, Y. Zeng, *Nature Commun.* 15 (2024) 973.
- 3. X. Zou, et al., Chem. Commun. 59 (2023) 13535.
- 4. J. Asenbauer, et al., Sust. Ener. Fuels 4 (2020) 5387.
- 5. S.A. Firstov, et al., *Powder Metall. Met. Ceram.* 52 (2014) 560-566.
- 6. M.C. Gao, J.W. Yeh, P.K. Liaw (eds.), Springer, 2016.
- 7. X. Liu, et al., *EcoMat* 4 (2022) e1226.
- 8. T.X. Nguyen, Chem. Eng. J. 430 (2022) 132658

Multiscale Structural Evolution in Lithium-ion Batteries Investigated by Operando Scanning Electron Microscopy

D. Trochta^{a, b}, O. Klvač^{a, b}, L. Novák^b, T. Kazda^a

^a Department of Electrotechnology, Brno University of Technology, Brno 616 00, Czech Republic

This study investigates lithium-ion battery degradation by tracking structural changes at both electrode and particle levels using operando scanning electron microscopy. Real-time imaging during cycling is correlated with electrochemical data, capturing electrode expansion and grain-level cracking. These multiscale observations reveal degradation mechanisms not evident electrochemically, supporting the design of more durable battery materials.

Introduction

Structural degradation in lithium-ion (Li-ion) batteries, such as electrode expansion and particle cracking, plays a critical role in limiting cycle life and overall performance [1]. These changes occur across multiple length scales and evolve dynamically during operation, making them difficult to capture using conventional exsitu or post-mortem methods. Operando scanning electron microscopy (SEM) addresses this challenge by enabling high-resolution imaging of structural changes in real time, directly correlated with electrochemical behavior [2][3].

In this study, we use operando SEM to investigate structural evolution during battery cycling. The method enables simultaneous tracking of electrode thickness and grain-level cracking under electrochemical operation. We also demonstrate how this approach captures irreversible electrode expansion and particle-specific mechanical responses. These insights highlight the potential of operando SEM for studying degradation mechanisms across length scales and supporting better material and electrode design.

Experimental

A full cell was assembled in-house using commercially available NMC (lithium nickel manganese cobalt oxide, LiNi_{1/3}Mn_{1/3}Co_{1/3}O₂) and LTO (lithium titanate, Li₄Ti₅O₁₂) electrodes, an ionic liquid electrolyte (Pyr13-TFSI, N-methyl-N-propylpyrrolidinium bis(trifluoromethanesulfonyl)imide), and a Whatman GF/C glass fiber separator. Electrochemical cycling was performed at 0.1C in the 1.3–2.8 V range using a Biologic potentiostat. Operando SEM imaging was carried out in a Thermo Fisher Scientific Quattro ESEM. Details of sample preparation and workflow are provided in previous works [4][5].

^b Thermo Fisher Scientific Brno, Vlastimila Pecha 12, Brno 627 00, Czech Republic

Results

Operando SEM was used to monitor structural changes during electrochemical cycling, focusing on both particle- and electrode-level behavior. By combining image-based analysis with electrochemical data, we identified distinct deformation mechanisms at different length scales.

Particle-Level Structural Evolution

Operando SEM imaging revealed distinct mechanical responses among individual NMC particles during electrochemical cycling. Figure 1 shows the voltage profile over two formation cycles, along with the area evolution of two tracked particles (A and B). Particle areas were automatically evaluated using the Phenom Particle Analyzer (Thermo Fisher Scientific), enabling consistent quantification across time points. [6]

Both particles initially contracted during delithiation, but their behavior diverged in later stages. Particle A developed visible cracks midway through the first charge, followed by an overall area increase dominated by crack propagation. Although partial closure occurred during lithiation, the particle did not return to its original size. [6]

In contrast, Particle B remained mechanically intact, showing symmetric and reversible area changes that closely followed the state of charge. These results suggest that once cracks form, particle expansion becomes governed by crack dynamics rather than lithium content, highlighting localized degradation that may contribute to electrode-scale mechanical instability. [6]

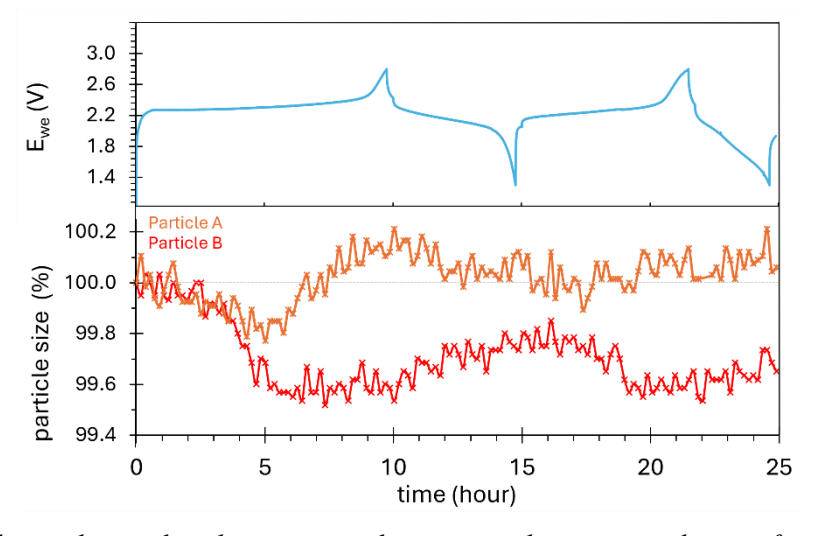


Figure 3: Electrochemical cycling curve with corresponding area evolution of selected NMC particles [6]

Electrode-Level Structural Changes

In addition to particle-scale observations, operando SEM enabled tracking of the full electrode cross-section during extended cycling. Figure 2 shows the evolution of NMC electrode thickness over 13 charge—discharge cycles. Thickness values were extracted from SEM images using a custom Python script developed for automated image analysis. [6]

To amplify mechanical effects, the cell was cycled beyond the standard voltage window, using an extended range of 0.8 to 3.3 V after initial formation. A clear

correlation was observed between electrode thickness and state of charge: expansion during delithiation and contraction during lithiation. However, this response was not fully reversible. With each cycle, both the minimum and maximum thickness values gradually increased. [6]

By the end of the test, the electrode had expanded by approximately 2.5 % relative to its initial state. This irreversible growth suggests cumulative mechanical deformation at the electrode scale, likely influenced by particle cracking, rearrangement, electrode binder and porosity evolution. [6]

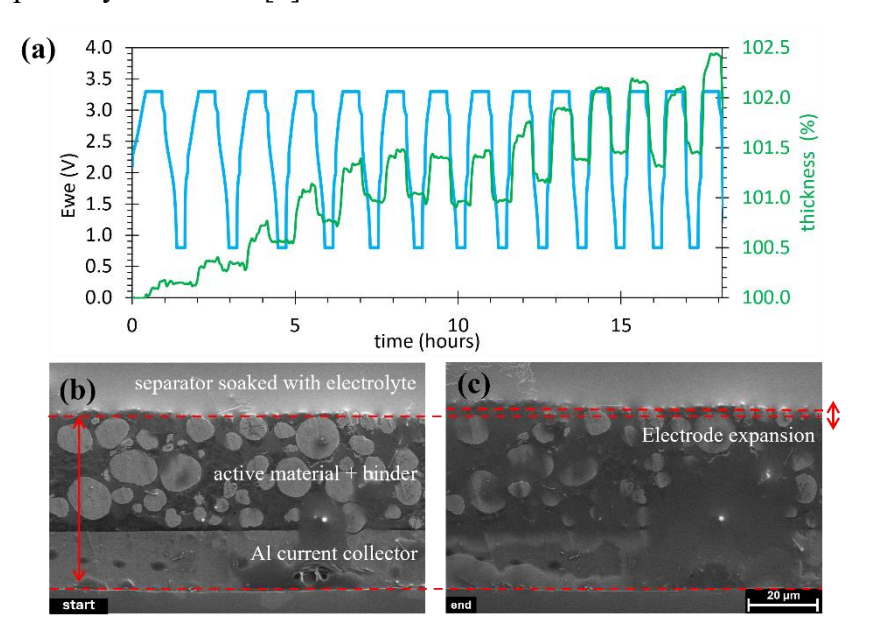


Figure 4: (a) Electrode thickness evolution during electrochemical cycling (b) SEM image of the electrode before cycling (c) SEM image of the electrode after cycling [6]

Conclusions

Operando SEM enabled real-time visualization of structural changes in a working lithium-ion cell across multiple length scales. At the particle level, crack formation altered the mechanical behavior of individual grains, decoupling their size evolution from the state of charge. At the electrode level, repeated cycling resulted in progressive and irreversible thickness growth, indicating accumulated mechanical deformation. These multiscale observations reveal degradation mechanisms that are not apparent from electrochemical data alone. Overall, the results demonstrate the value of operando SEM as a diagnostic tool for understanding battery failure pathways and guiding the design of more robust electrode architectures.

Acknowledgments

This work was supported by the specific graduate research of the Brno University of Technology No. FEKT-S-23-8286 and created in cooperation with Thermo Fisher Scientific Brno.

References

1. J. S. Edge et al., *Physical Chemistry Chemical Physics*, **23**, 8200-8221 (2021).

- 2. J. Wu, M. Fenech, R. F. Webster, R. D. Tilley, and N. Sharma, *Sustainable Energy & Fuels*, **3**, 1623-1646 (2019).
- 3. S. Zhou et al., Current Opinion in Electrochemistry, 41, 101374 (2023).
- 4. O. Klvač, D. Trochta, and T. Kazda, Advanced Batteries Accumulators and Fuel Cells 25th ABAF, p. 38, Brno (2024).
- 5. D. Trochta, O. Klvač, T. Kazda, and L. Novák, *Advanced Batteries Accumulators and Fuel Cells 25th ABAF*, p. 144, Brno (2024).
- 6. O. Klvač, D. Trochta, L. Novák, P. Priecel, M. Bornhöft, T. Kazda, and Z. Liu, *Energy Storage Materials*, accepted for publication (2025).

The Application of Synchrotron-based XRD and X-ray Tomography in Battery Research

D. Lia and J. Zhua

^aDepartment of Chemistry – Ångström Laboratory, Uppsala University, Sweden

In situ or operando characterization techniques using synchrotron facilities, which can monitor the internal changes of batteries in real-time under actual working conditions, are of great significance for revealing the working principles of batteries, analyzing failure mechanisms, and evaluating performance of battery components. Among them, synchrotron-based XRD and X-ray tomography have attracted wide attention from researchers due to their advantages of high temporal resolution, non-destructive testing, and ease of operation. This presentation will focus on some specific applications of using synchrotron-based XRD and X-ray tomography in the research of rechargeable batteries, based on the research work of our group in the fields of metal-air batteries, lithium-ion batteries, lithium-sulfur batteries, and aqueous zinc-ion batteries. The combination of these two techniques is possible at several beam lines. It is expected that this presentation will arouse broader interest in these techniques among our peers and promote the in-depth development of related research.

Enhanced Natural Clay Materials for Supercapacitor Energy Technologies

B. Mladenova^a, M. Dimitrova^a, G. Ivanova^a, A. Stoyanova^a

^aInstitute of Electrochemistry and Energy Systems, Bulgarian Academy of Sciences, Acad. G. Bonchev Str., 10, 1113 Sofia, Bulgaria

In recent years, supercapacitors have found widespread application as energy sources for fast-charging devices. A key factor for their efficiency is the choice of electrode material. Increasing research efforts are being directed towards the development of electrodes with optimized structure and improved interfacial diffusion. Priority is given to environmentally friendly and sustainable materials.

This study investigates the potential of clay-based materials as low-cost and ecofriendly components for electrodes in solid-state supercapacitors. These materials are characterized by a high specific surface area, ion-exchange ability, and good stability, which makes them suitable for energy applications. To enhance their electrical conductivity and capacitive properties, the clays were modified with various additives.

Composite electrode materials were synthesized and subsequently characterized in terms of structure and morphology using XRD, SEM, BET, and other *ex situ* analyses. Their electrochemical properties were evaluated through cyclic voltammetry, galvanostatic charge-discharge, and electrochemical impedance spectroscopy.

The results show that the addition of conductive modifiers significantly improves the electrochemical performance of the composite materials. Despite their limited conductivity, clay compounds provide a high specific surface area and a favorable porosity that facilitate ion diffusion. These properties make them suitable as carriers for active components, creating a cost-effective and environmentally sustainable basis for the development of electrodes for supercapacitors.

Acknowledgement

Part of the experimental work was carried out using the equipment of the research infrastructure "Energy Storage and Hydrogen Energy" (ESHER), provided by the Ministry of Education and Science of the Republic of Bulgaria under Grant Agreement No. D01-349/13.12.2023.

Electrochemically Deposited Nickel-Molybdenum Layers on Nickel Substrates for Hybrid Supercapacitors

L.Soserov^a, V. Bachvarov^b, R. Rashkov^b, M. Arnaudova^b, E. Lefterova^a, A. Stoyanova^a

^aInstitute of Electrochemistry and Energy Systems - Bulgarian Academy of Sciences, 1113 Sofia, Bulgaria

bInstitute of Physical Chemistry -Bulgarian Academy of Sciences, 1113 Sofia, Bulgaria 1 stefanov@iees.bas.bg

Hybrid supercapacitors have emerged as a promising energy storage solution, occupying the niche between conventional capacitors and lithium-ion batteries. The combination of high power density and increased energy capacity renders them optimal for applications such as energy recovery systems in vehicles and portable electronics. The integration of electrical double-layer and pseudocapacitive mechanisms, facilitated by Faraday redox reactions, has been demonstrated to enhance performance. The achievement of optimal performance in hybrid systems is contingent upon the structural and electrochemical characteristics of the electrode materials. Consequently, the design of advanced architectures with controlled morphology, porosity, and crystallinity is imperative.

Electrodeposition is a rapid and economical approach to fabricating electroactive materials directly onto conductive substrates. This method allows the fabrication of stable, binder-free electrodes with effective electrical contact. These features are highly desired for supercapacitor applications.

In the present study, nickel-molybdenum (Ni-Mo) coatings were electrochemically deposited onto nickel foam at varying current densities (3–8 Adm⁻²). The materials obtained were subjected to an extensive characterization process, which included the application of a number of physicochemical techniques.

These analyses were complemented by electrochemical evaluations performed in a 2 M KOH electrolyte, including cyclic voltammetry (CV) and galvanostatic charge-discharge (GCD) testing. The long-term cycling stability exhibited an exceptional capacity retention over 5,000 cycles, particularly for coatings with elevated molybdenum content (~20 wt. %), underscoring their considerable promise as electrode materials for hybrid supercapacitor systems.

Acknowledgement

The equipment used at the research are provided by the National Roadmap for Research Infrastructure 2020 -2027 "Energy storage and hydrogen energetics (ESHER)", approved by DCM No 354/29.08.2017 and updated by DO1-349/13.12.2023 under Grant Agreement DO1-160/28.08.2018.

Multilayered Nickel-Based Gas Diffusion Electrodes for Water Electrolysis in Zero-Gap Configuration

G.Borisov^a, E.Petkucheva^a, B.Mladenova^a, E.Slavcheva^a

^aInstitute of Electrochemistry and Energy Systems, Bulgarian Academy of Sciences, Acad. G. Bonchev Str., 10, 1113 Sofia, Bulgaria

Alkaline zero-gap water electrolyzers represent a relatively recent and promising technology for generating ultra-high-purity hydrogen (>99.9999%). These systems offer several advantages, including compact design, high current densities, operation across a broad temperature range (20°C to 95°C), and energy efficiency exceeding 75%.

This report examines the electrochemical performance of a pilot-scale alkaline water electrolyzer (DUAL Cell), which utilizes a ceramic diaphragm (Zifron Perl 500) and multilayered electrodes. Both the anode and cathode are built on a nickel foam framework, providing mechanical support for a microporous active layer with a highly developed surface area. This active layer is composed of nickel powder bound with polytetrafluoroethylene (PTFE, or Teflon).

The electrochemical activity and corrosion resistance of the electrodes were thoroughly evaluated using a standard three-electrode setup with cyclic and linear voltammetry, in a 25% KOH electrolyte at room temperature. The results showed that a current density of 200 mA·cm⁻² was achieved at an applied voltage of 2 V, without any signs of degradation.

Following initial characterization, the electrodes were assembled into a laboratory-scale prototype of the DUAL CELL electrolyzer [Utility Model No. 5061], which integrates design features from both traditional alkaline and modern polymer electrolyte membrane (PEM) electrolyzers.

Diaphragm conditioning was carried out in situ by circulating 25% KOH through the system for 24 hours at room temperature. Voltammetric measurements were then performed under conditions approximating real-world operation. At 80° C and 2 V cell voltage, the system reached a current density of $800 \text{ mA} \cdot \text{cm}^{-2}$.

The results demonstrate stable electrochemical performance and consistent behavior between the two individual cells, even during prolonged accelerated testing at room temperature.

Acknowledgement

This work was financed by the European Union – NextGenerationEU through the Bulgarian National Recovery and Resilience Plan (Project № BG-RRP-2.017-0027"Hydrogen Generator in a Zero-Gap Packaged Design"). Part of the experimental work was carried out using the equipment of the research infrastructure "Energy Storage and Hydrogen Energy" (ESHER), provided by the Ministry of Education and Science of the Republic of Bulgaria under Grant Agreement No. D01-349/13.12.2023.

The Effect of Electrolyte Structure on the ORR and OER Kinetics in Solid Oxide Cells

D. Budáč^a, V. Miloš^b, M. Carda^a, M. Paidar^a, K. Bouzek^a

^aDepartment of Inorganic Technology, University of Chemistry and Technology, Prague, Czech Republic

^bMathematical Institute, Charles University, Prague, Czech Republic

This work explores how microstructure and crystallographic orientation influence oxygen transport in solid electrolytes used in high-temperature solid oxide cells. Using impedance spectroscopy combined with advanced data analysis, distinct processes related to bulk transport and interfacial oxygen exchange were identified. Grain boundaries in polycrystalline materials were found to strongly impede oxygen transport, while having limited effect on the incorporation and release of oxygen at the electrolyte surface. Surprisingly, similar transport-limiting behavior was also observed at the surfaces of single crystals, attributed to the presence of space-charge layer. Furthermore, the crystallographic orientation of single-crystal electrolytes significantly affected both bulk transport and surface exchange, with some lattice orientations favoring oxygen incorporation while others promoted oxygen release. These results demonstrate that both microstructural features and atomic-scale lattice arrangement play a critical role in oxygen transport, and should be carefully considered when designing solid electrolytes for efficient electrochemical devices.

Introduction

Solid oxide cells (SOCs) are advanced energy conversion systems with considerable promise for integration into the hydrogen economy, functioning efficiently as both solid oxide electrolysers and fuel cells. Their high performance is attributed to enhanced electrochemical kinetics enabled by high operating temperatures, typically up to 900 °C. SOCs comprise three essential components: a dense solid electrolyte and two porous electrodes. The electrolyte plays a crucial role by enabling selective ionic transport while maintaining electronic insulation and providing a gastight barrier between the electrodes.

In practical applications, polycrystalline ceramic electrolytes are employed. Although often treated as structurally uniform, these materials are composed of crystalline grains separated by grain boundaries (GBs). It is well established that GBs can impede oxygen ion transport, largely due to the segregation of impurities and the formation of space-charge layers, i.e. a nanoscale dopant gradient at the grain surface, resulting in reduced ionic conductivity compared to single-crystal counterparts. Nevertheless, the impact of GBs at the three-phase boundary (active sites, simultaneous contact of pore, electrode and electrolyte) remains unresolved [1,2]. Some studies suggest GBs enhance oxygen incorporation and release, while others indicate the opposite effect, with evidence based primarily on oxygen isotope exchange experiments

rather than direct electrochemical characterization. Furthermore, the influence of electrolyte crystallographic orientation within the electrolyte lattice on ionic processes is still not well understood.

This work seeks to clarify these uncertainties by combining systematic experimental investigations with a novel approach to analyzing impedance data using distribution of relaxation times (DRT) methodology, aiming to resolve the long-standing discrepancies in the field.

Experiments

Commercially available monocrystalline 13YSZ (13 mol.% Y₂O₃ · ZrO₂) substrates with crystallographic orientations <100>, <110>, and <111> (1 mm thickness, 25 mm diameter) were employed as model systems. A polycrystalline reference sample (<poly>) of identical dimensions was fabricated in-house via uniaxial pressing of combustion-synthesized 13YSZ powder [3]. All electrodes were prepared by screen-printing a suspension of commercially available A-site deficient LSM ((La_{0.8}Sr_{0.2})_{0.95}MnO_{3-δ}). Initially, a circular counter electrode (CE, 12 mm diameter) and a concentric reference electrode (RE, 1 mm width with a 3 mm gap from the CE) were deposited via screen-printing on one side of the substrate and sintered at 1150 °C for 3 hours. Subsequently, a circular working electrode (WE, 12 mm diameter) was carefully aligned opposite the CE on the reverse side and sintered under identical conditions.

The assembled cells (<100>, <110>, <111>, and <poly>) were mounted in an alumina housing placed inside a tubular furnace for electrochemical characterization. A three-electrode assembly was used to investigate the oxygen evolution (OER) and oxygen reduction (ORR) reactions via electrochemical impedance spectroscopy (EIS). Spectra were recorded over a range of applied potentials (0 to ± 1 V vs. RE) at operating temperatures between 700 and 850 °C. The oxygen partial pressure in the working electrode gas stream was systematically varied, while a constant flow of pure O₂ was maintained in the CE+RE compartment to ensure RE potential stability.

The acquired EIS data were corrected for stray inductance and subsequently analyzed via an in-house implementation of the distribution of relaxation times (DRT) method [4], employing the Gold deconvolution algorithm [5] to resolve convolved electrochemical processes.

Results

DRT deconvolution of the EIS data revealed up to six distinct processes at 800 °C, with characteristic frequencies centered around 8×10^4 , 6×10^3 , 500, 200, 20, and 1 Hz, depending on the experimental conditions. The majority of these features were associated with charge transfer and oxygen sorption/desorption phenomena predominantly attributed to the LSM electrodes and were therefore considered irrelevant to the primary focus of this particular study. Notably, the high-frequency process at $\sim 8\times10^4$ Hz was consistently exhibited by < poly> at 700 °C and could be unambiguously assigned to a grain boundary response (**GB**) effects within the electrolyte.

Unexpectedly, a comparable signal also emerged in the monocrystalline specimens, which lack the traditional concept of GBs. This response was ascribed to the presence of a surface space-charge layer (SCL), effectively behaving as a "virtual grain boundary". The corresponding process reflects oxygen ion transport within the near-surface region of the electrolyte: from the surface into the bulk under ORR conditions, and from the bulk toward the surface during OER. This mechanism parallels the transport behavior across GBs in polycrystalline electrolytes, indicating that similar electrostatic barriers may form even in morphologically defect-free single-crystals.

A second electrolyte-related process was identified at approximately 6 kHz, consistent with findings from our previous work [6]. Under ORR conditions, this feature corresponds to the incorporation of oxygen anions (I) into the YSZ lattice, whereas during OER, it reflects the release (R) of oxygen anions from the lattice to the electrolyte surface. Consequently, the influence of electrolyte structure and GBs can be evaluated by analyzing the polarization resistance associated with two key processes: GB and I/R in polycrystalline electrolytes, and the analogous SCL and I/R steps in single-crystalline samples.

As expected, the **GB** resistance was substantially higher in < poly > compared to **SCL** resistance in the monocrystalline specimens, reflecting the presence of GBs throughout the bulk of the polycrystalline electrolyte. In contrast, **I/R** resistance exhibited no significant variation between the < poly >, < 100 >, and < 110 > samples. This finding indicates that while GBs strongly impede long-range oxygen ion transport within the electrolyte, they have only a limited effect on the interfacial kinetics of oxygen anion incorporation into, or release from, the crystalline YSZ lattice.

While the SCL and I/R processes exhibited consistent qualitative trends across <100> and <110>, their absolute polarization resistances varied with crystallographic orientation. <100> showed the highest SCL and I resistances during ORR and the lowest SCL and R during OER. In contrast, <111> displayed the lowest resistances for both SCL and I (under the detection limit), but the highest for SCL and R. These results suggest that the <100> orientation hinders oxygen ion incorporation into the lattice while facilitating its release, whereas <111> promotes incorporation but impedes release. This behavior is consistent with the atomic-scale lattice geometry of the respective orientations, as the <111> plane features a more open structure than <100>, potentially offering lower energy barriers for incorporation but higher for release.

Conclusions

The DRT analysis revealed that grain boundaries hinder bulk oxygen transport in polycrystalline electrolytes, while space-charge layers at monocrystalline surfaces produce similar effects. Grain boundaries have minimal impact on oxygen incorporation/release at the electrolyte interface. Importantly, the orientation of monocrystalline electrolytes significantly affects both interfacial and bulk oxygen transport, underscoring the critical role of lattice geometry in SOC performance.

Acknowledgement

This work was supported by the Technology Agency of the Czech Republic under project no. TK04030143.

- 1. J. Shim et al., Acta Mater., 60(1), 2012
- 2. R. De Souza et al., Phys. Chem. Chem. Phys., 10(15), 2008
- 3. M. Carda et al., *Energies*, **15**(7), 2022
- 4. Masicko, 10.5281/zenodo.8176605, 2023
- 5. T. Bergmann, ChemPhysChem, 23(13), 2022
- 6. V. Miloš, J. Electrochem. Soc., 2022

Synthesis the Non-Agglomerated Unzipped Multi-Walled Carbon Nanotubes as Electrode Materials for Fuel Cells

M. O. Danilov^a, G. I. Dovbeshko^{b,c}, S. S. Fomanyuk^a, O. P. Gnatyuk^b, V. Boilko^{b,c}, O. Bezkrovnyi^c, B. M. Romanyuk^d, T. Sabov^d, I. A Rusetskyi^a, G.Ya. Kolbasov^a

^aVernadskii Institute of General and Inorganic Chemistry, National Academy of Science of Ukraine, 32-34 Palladin Avenue, 03680 Kyiv, Ukraine

^bInstitute of Physics, National Academy of Science of Ukraine, 46 Nauky Avenue, 03680 Kyiv, Ukraine^c Institute of Low Temperature and Structure Research, Polish Academy of Sciences, Okólna 2, Wrocław, 50-422, Poland^d V.E. Lashkaryev Institute of Semiconductor Physics of NASU, 03028 Kyiv, Ukraine

The possibility of synthesis non-agglomerated unzipped carbon nanotubes was investigated by the method of electrochemical anodic oxidation of multi-walled carbon nanotubes in sulfuric acid solutions, 7% water in ethylene glycol and 2.5 M ammonium fluoride in 7% water in ethylene glycol. It was found that dispersed unzipped multi-walled carbon nanotubes are synthesis during the anodic oxidation of multi-walled carbon nanotubes in a solution containing 2.5 M ammonium fluoride in 7% water in ethylene glycol, which do not undergo agglomeration during subsequent washing and drying. The production of such materials was proven using transmission electron microscopy and other physicochemical methods. Electrochemical investigation partially unzipped carbon nanotubes showed that they are good catalysts in the oxygen reduction reaction. Their characteristics as a material for oxygen electrode are identical to platinum deposited on carbon nanotubes.

Introduction

Nanocomposite materials that can combine the properties of nanosized catalysts and their carriers should be used to increase the current in oxygen electrodes by forming a unique matrix with a synergistic effect. Recently, research centers have focused on catalyst carriers such as graphene oxide, partially unzipped multi-walled carbon nanotubes (PUMCNTs). However, in the process of synthesis of such materials, agglomerates of these nanotubes are obtained. Therefore, to increase the current, it is better to obtain non-agglomerated nanotubes. To synthesis partially unzipped multiwalled carbon nanotubes, two methods with a controlled degree of opening of carbon nanotubes are used: chemical [1] and electrochemical method [2]. As a result of synthesis, graphene-like unzipped carbon nanotubes are obtained. With a controlled degree of unzipping of multi-walled carbon nanotubes in a sulfuric acid solution using Raman spectroscopy and BET surface area measurements, it was found that the unzipping of CNTs begins with surface etching, then moves to partial and complete unzipping, and then fragmentation and aggregation [1]. But with these methods of production, even pre-dispersed nanotubes were obtained in an agglomerated state [3]. To obtain de-agglomerated dispersed MWCNTs for various composites, epoxy or polymer composites are used [3].

Experimental

The aim of our work was to study the possibility of electrochemical synthesis of non-agglomerated unzipped multi-walled carbon nanotubes. For this purpose, electrochemical anodic oxidation was carried out in sulfuric acid solutions [4], 7% water in ethylene glycol and 2.5 M ammonium fluoride in 7% water in ethylene glycol.

The synthesis materials were studied using TEM, XPS, X-ray phase analysis and IR spectroscopy. It was shown that in an electrolyte based on ethylene glycol with ammonium fluoride, dispersed unzipped multi-walled carbon nanotubes are obtained, which does not undergo agglomeration during subsequent washing and drying. Such nanotubes, which do not contain polymer filler, are not synthesis in other electrolytes and are not described in the literature. A micrograph of such nanotubes is shown in Figure 1 shows unzipped nanotubes synthesis in a different electrolyte.

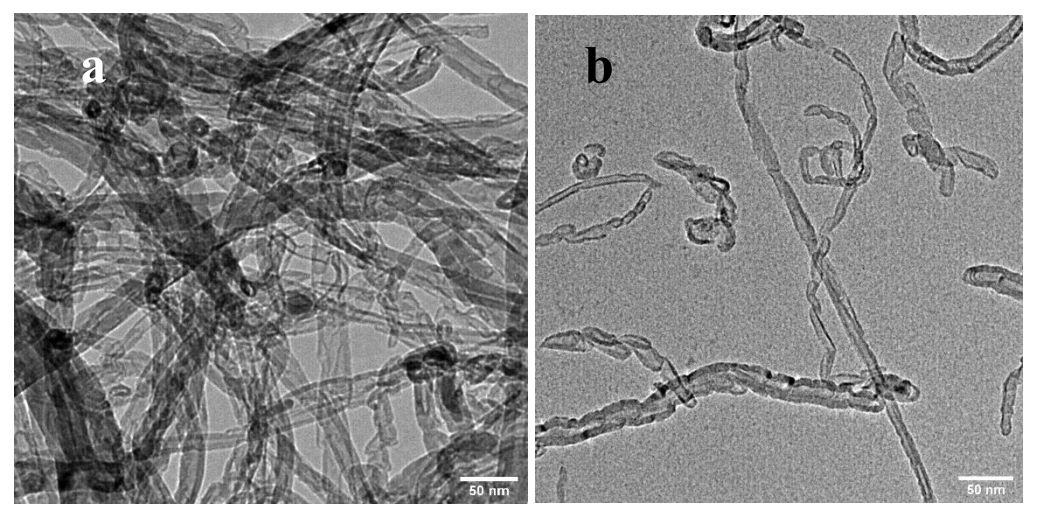


Figure 1. Micrographs of samples of partially unzipped multi-walled carbon nanotubes synthesis in 7% water solution in ethylene glycol (a) in 2.5 M NH₄F in 7% bidistilled water solution in ethylene glycol (b)

Results and discussion

Oxygen electrodes were made from these materials and investigated in a fuel half-cell in an alkaline electrolyte. The studies were carried out on a fuel half-cell, with a zinc electrode used as the anode. The fuel half-cell with gas diffusion electrodes are described in [5]. The discharge characteristics of oxygen electrodes made of materials based on unzipped nanotubes in various electrolytes are shown in Figure 2. The obtained results show that PUMWCNTs based materials without supported catalyst are catalytically active materials for the manufacture of oxygen electrodes, which is confirmed by a comparison of their characteristics with those of the MWCNTs - based electrodes with platinum coating. Therefore, with deposition of a catalyst, such materials can be promising candidates as a catalyst support for oxygen electrodes of fuel cells.

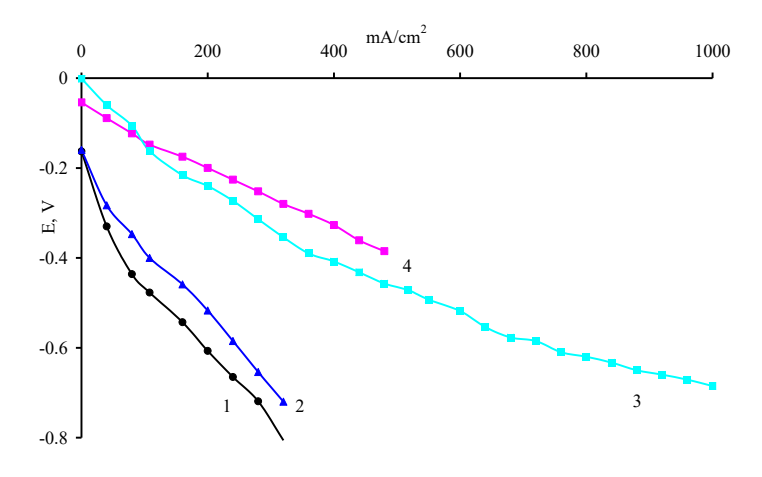


Figure 2. Current-voltage characteristics of oxygen electrodes with an active layer made of different electrode materials: 1 - partially unzipped multi-walled carbon nanotubes in sulfuric acid, 2 - partially unzipped nanotubes synthesis in a 7% water in ethylene glycol solution; 3 - partially unzipped nanotubes synthesis in a $2.5 \, \text{M NH}_4\text{F}$ ammonium fluoride solution in a 7% water in ethylene glycol solution during anodic oxidation; 4 - MWCNTs with deposited Pt.

It is worth to mention that the electrochemical synthesis non agglomerated PUMWCNTs were stable over six months subject to testing in the fuel half-cell by a galvanostatic mode (at the current density of 200 mA cm⁻² at the oxygen electrodes).

Conclusions

Non-agglomerated partially unzipped multi-walled carbon nanotubes were obtained by electrochemical synthesis in a solution of ammonium fluoride in ethylene glycol. Due to this structure of non-agglomerated partially unzipped carbon nanotubes, it was possible to obtain the same characteristics in oxygen electrodes as those of electrodes based on carbon nanotubes with deposited platinum. Oxygen electrodes based on non-agglomerated unzipped multi-walled carbon nanotubes showed stable characteristics during six months of long-term testing.

- 1. B. Xiao, X. Li, X. Li, B. Wang, C. Langford, R. Li, X. Sun. *J. Phys. Chem. C.*, **118**, 881 (2014).
- 2. M.O. Danilov, I.A. Rusetskyi, S.S. Fomanyuk, G.Ya. Kolbasov. *Theoretical and Experimental Chemistry*, **60**(2), 108 (2024).
- 3. P.-C. Ma, S.-Y. Mo, B.-Z. Tang, J.-K. Kim. *Carbon*, **48**(6), 1824 (2010).
- 4. M.O. Danilov, G.I. Dovbeshko, I.A. Rusetskyi, V.I. Pekhnyo, A.S. Nikolenko, G.Ya. Kolbasov. *Applied Physics A*, **126**(10), 764 (2020).

DDM Activated Stainless Steel Electrodes for Alkaline Electrolysis

E. Petkucheva^a, G. Borisov^a, N.Borisov^a, E. Slavcheva^a

^aAcad. Evgeni Budevski Institute of Electrochemistry and Energy Systems (IEES), Bulgarian Academy of Sciences (BAS), Acad. G. Bonchev Str., bl. 10, 1113 Sofia, Bulgaria

The development of durable, low-cost electrocatalysts for the oxygen evolution reaction (OER) in alkaline media is critical for advancing water electrolysis and sustainable hydrogen production. This study introduces a novel, facile activation technique—Dip and Drying Method (DDM)—applied to stainless steel substrates, including mesh (SSM) and net (SSN), to significantly enhance their OER performance without the need for external catalyst deposition. Unlike conventional approaches that rely on NiFe-based coatings prone to detachment and degradation, DDM leverages the intrinsic catalytic properties of stainless steel, inducing surface activation through KOH treatment and controlled iron leaching. This process exposes nickel sites that form Fedoped NiOOH, a highly active OER phase.

The DDM-treated electrodes demonstrate a substantial reduction in overpotential (>100 mV at $100 \text{ mA} \cdot \text{cm}^{-2}$) and exhibit excellent stability at industrial current densities (up to $650 \text{ mA} \cdot \text{cm}^{-2}$ at 2.0 V), rivaling the performance of state-of-the-art membrane-based electrolyzer systems.

To evaluate their practical applicability, the electrodes were integrated into a zero-gap alkaline water electrolyzer configuration. In this design, the anode, cathode, and diaphragm are assembled in direct contact, minimizing ionic resistance and maximizing current density output. The compact architecture enables high-efficiency operation with reduced voltage losses, making it particularly suitable for scalable and energy-efficient hydrogen production. The robust performance of the DDM-treated stainless steel electrodes in this zero-gap configuration highlights their potential for deployment in commercial alkaline electrolyzers and other electrochemical energy devices such as metal—air batteries.

Acknowledgement

This work was financed by the European Union – NextGenerationEU through the Bulgarian National Recovery and Resilience Plan (Project № BG-RRP-2.017-0027"Hydrogen Generator in a Zero-Gap Packaged Design"). Part of the experimental work was carried out using the equipment of the research infrastructure "Energy Storage and Hydrogen Energy" (NISEVE), provided by the Ministry of Education and Science of the Republic of Bulgaria under Grant Agreement No. D01-349/13.12.2023. Part of the experimental work was carried out using the equipment of the research infrastructure "Energy Storage and Hydrogen Energy" (ESHER), provided by the Ministry of Education and Science of the Republic of Bulgaria under Grant Agreement No. D01-349/13.12.2023.

Effect of Tetraglyme on Electrochemical Characteristics of LiMn₂O₄-AC System in Aqueous Electrolyte Li₂SO₄- H₂O-TG

N.I. Globa^a, Yu. V Shmatok^a

^aV.I. Vernadsky Institute of General and Inorganic Chemistry of the NAS of Ukraine, 32/34 Palladina Ave., Kyiv 03142, Ukraine

The paper discusses the effect of tetraglyme concentration on the specific electrical conductivity and phase homogeneity of lithium sulfate aqueous solutions. The effect of electrolyte composition on the specific, kinetic and cyclic characteristics of LiMn₂O₄-activated carbon electrode system is investigated.

Introduction

Safety issues and high cost of traditional lithium-ion batteries (LIBs) hinder their widespread use in large-scale energy storage devices. Alternative LIBs with aqueous electrolytes are considered to be more cost-effective and environmentally friendly. In addition, the high conductivity of aqueous electrolytes improves the kinetic capabilities of electrode systems based on intercalation and conversion electrode materials [1][2][3]. However, aqueous electrolytes have some limitations that hinder their widespread use in lithium-ion systems. First, it is a narrow electrochemical stability window (1.23 V), which limits the range of battery output voltage. Secondly, the formation of gaseous products complicates the formation of solid electrolyte interface (SEI) with low charge transfer resistance. This negatively affects the stability of the specific capacity of electrode materials and their kinetic properties during cycling [4]. An effective SEI at the electrode-electrolyte interface can be created by adding an organic solvent to the aqueous electrolyte. The organic solvent reduces the number of free water molecules and partially replaces them in the lithium solvation shell and affects the SEI composition. The paper discusses the capacitive, specific and kinetic characteristics of LiMn₂O₄ paired with an activated carbon electrode in 2M Li₂SO₄ H₂O-TG electrolytes.

Experimental

Spinel LiMn₂O₄ was synthesized by solid-state method from a mixture of electrolytic manganese dioxide and lithium carbonate [5]. Phase composition and structure parameters of spinel samples were investigated by X-ray diffraction (XRD) method on a DRON 4-07 diffractometer with Cu-Kα radiation. Morphology was studied by scanning electron microscopy (SEM) method on a JSM-6700F (JEOL, Japan). According to XRD data, the obtained cathode material is pure lithium manganese spinel LiMn₂O₄ with a cubic structure. According to SEM data, spinel particles had the appearance of agglomerates of arbitrary shape, with sizes up to 40 µm, which consisted of particles 100-200 nm in size. Electrolytes were prepared using double-distilled water and Li₂SO₄ salt (99.5%, Sigma Aldrigh) and tetraethylene glycol dimethyl ether (tetraglyme, TG, 99%, Sigma Aldrigh). Tetraglyme was introduced into the electrolyte composition instead of water in amounts of 0, 2.5, 5, 7.5 and 10 vol. % at a constant salt concentration of 2 mol/L. The specific electrical conductivity of electrolytes was determined by conductometry method on an Instek LCR-84 device in the temperature range from -25 °C to +70 °C at a frequency of 200 kHz. Electrochemical tests were carried out in 2- or 3-electrode teflon cells with an activated

carbon counter electrode (83 % of Kausorb 212 activated carbon, 10 % of carbon black P-267E and 7 % of F-4D binder) and Ag/AgCl as a reference electrode. Working LiMn₂O₄ electrode was prepared by mixing the as-synthesized active materials, conductive carbon black C-Nergy Super C65 (Imerys Graphite and Carbon, Belgium) and poly(vinylidene difluoride) Solef 6020 (Solvay, Belgium) as a binder at a weight ratio of 80:10:10 and using dimethylacetamide as a solvent. A grid made of stainless steel AISI 321 was used as a current collector. Electrochemical investigations were performed on a battery testing system (Neware, China) and SPG-200 or P-30 potentiostats in different testing modes. Operating currents for galvanostatic tests were expressed in C units (1C = 148 mA/g).

Resalts and Discussion

According to the results of conductometric studies, it is shown that the addition of TG affects the specific electrical conductivity of electrolytes and leads to a change in their freezing temperature and the temperature range of phase homogeneity. An increase in the content of tetraglyme in the electrolyte composition leads to a gradual decrease in the specific electrical conductivity of the solutions, which, for example, at a temperature of 25 °C is 78.8, 72.8, 65.3, 61.3 and 53.3 mS/cm for 2M Li₂SO₄ aqueous solutions with a tetraglyme content of 0, 2.5, 5, 7.5 and 10%, respectively. At the same time, there is a narrowing of the temperature range of homogeneity due to a decrease in the separation temperature of water and tetraglyme.

All presented in Fig. 1(a) cyclic voltammograms have two pairs of redox peaks characteristic of LiMn₂O₄. The peak potentials in composite electrolytes are 140-180 mV more negative and slightly less intense than in a simple aqueous electrolyte. The difference observed in the nature of the CVA peaks can be explained by the change in the Gibbs free energy caused by the formation of a competing water-ether bond in the electrolyte system, in addition to the main water-water hydrogen bond. This leads to a change in the structure of the primary solvation shell of Li⁺, a decrease in the number of free water molecules in the electrolyte volume, and a change in the number of solvated SO₄²⁻ anions. [6]. Based on the CVA data obtained at scan rates of 0.3–1 mV/s, the lithium diffusion coefficient was calculated using the Randles-Shevchyk equation [7]. The obtained values are in the range of $0.7 \times 10^{-10} - 1.4 \times 10^{-9}$ and have a slight tendency to decrease with increasing TG concentration. Further analysis of CVA data allows to determine the controlling mechanism of lithium intercalation/deintercalation. For this purpose, the logarithmic dependence log(i) = blog(v) + log(a) was used, where the value of the parameter b, which reflects the control mechanism, is determined by the slope of log(i) and log(v). The obtained values of the coefficient b are in the range of 0.75–0.9 and tend to increase with increasing TG concentration.

The dependences of specific capacity on cycle number and current density were determined by the galvanostatic cycling method in the current density range of 1.5–50C. The corresponding results are presented in Fig. 1(b). The constant charge/discharge current density was 3/1.5 C and after every 100 cycles the discharge current was sequentially increased (3 cycles per each current density) to 5, 10, 20, 30, 40 and 50 C. The specific capacity of LiMn₂O₄ on the first cycles does not significantly depend on the composition of the Li₂SO₄-H₂O-TG electrolyte. However, with repeated increases in current density after 100, 200, 300, and 400 cycles, the specific capacitances in cells with mixed electrolytes remain more stable. Analysis of the impedance spectroscopy results showed that during the cycling process, the increase in resistance in cells with aqueous-organic electrolytes is significantly smaller compared to the similar resistance of a cell with 2M Li₂SO₄ H₂O electrolyte. Thus, such aqueous-organic electrolytes with

low TG content demonstrate high efficiency in an aqueous lithium electrochemical system and are not much more expensive than a conventional aqueous electrolyte, which makes them an excellent alternative to expensive water-in-salt electrolytes.

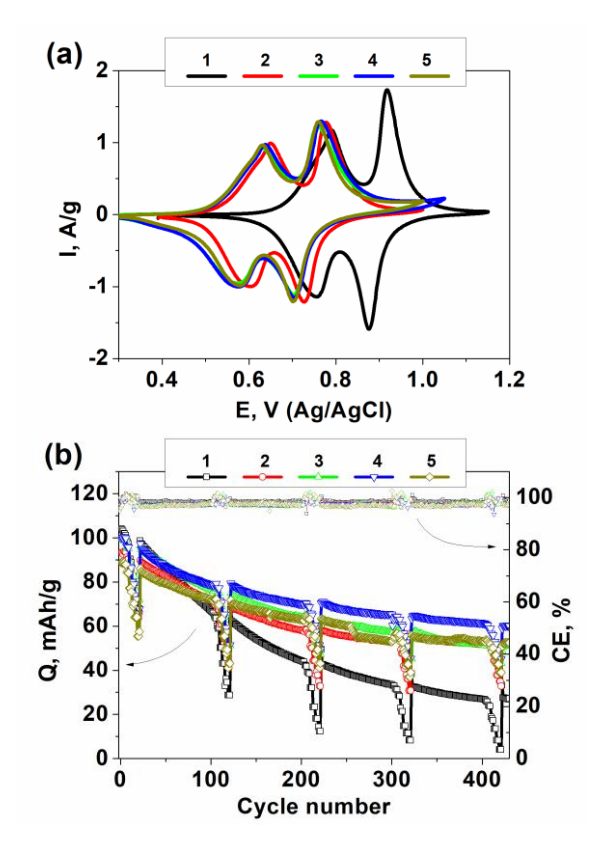


Figure 1. (a) CVA curves of LiMn₂O₄ in different electrolytes composition, (b) dependence discharge capacity on cycle number and current density. Electrolyte composition: I-2M Li₂SO₄ H₂O, 2-2M Li₂SO₄ H₂O:TG (97.5:2.5), 3-2M Li₂SO₄ H₂O:TG (95:5), 4-2M Li₂SO₄ H₂O:TG (92.5:7.5), 5-2M Li₂SO₄ H₂O:TG (90:10).

- 1. A.Eftekhari, Adv. Energy Mater., **8**(24), 1801156 (2018).
- 2. N. Alias and A. A. Mohamad, *J. Power Sources.* **274**, 237 (2015)
- 3. A.von Wald Cresce and K. Xu, *Carbon Energy*, **3**(5), 721 (2021).
- 4. D. Chao, W. Zhou, F. Xie, C. Ye, H. Li, M. Jaroniec, S.-Z. Qiao, *Sci. Adv.*, **6**, 4098 (2020).
- 5. Yu. V. Shmatok, N. I. Globa, V.A. Sirosh, S.A. Kirillov, *Surface*, **15**(30), 185 (2023).
- 6. L. Zhang, Y. Chen, *Energy Mater.*, **1**,100004 (2021).
- 7. H.-C. Shin, J.-Y. Choi, J. M. Kim, M.-S. Park, W.-S. Yoon, T. Kim, W. Choi, *Electrochem. Sci. Technol.*, **11**(1), 14 (2020).
- 8. X. Zhang, X. Lan, Y. Feng, X. Wang, S., S. Kong, Q. Li, *Adv. Mater. Interfaces*, **10**(4), 2202035 (2023).

Organic/Water Mixed Electrolyte for Aqueous Dual-Ion Batteries

Y. He^a, J. Červenka^a

^aDepartment of Thin Films and Nanostructures, FZU-Institute of Physics of the Czech Academy of Sciences, Cukrovarnická 10/112, 162 00 Prague 6, Czech Republic

The solvents used in aqueous dual-ion batteries (ADIBs) have not yet been systematically studied in depth. Therefore, this work focuses on organic/water mixed solvents and their application in ADIBs, aiming to understand why organic solvents traditionally employed in lithium-ion batteries can also be utilized in ADIB systems.

We first combine dimethyl carbonate (DMC) as the solvent with Zn(OTf)₂ as the primary salt, and fine-tune the solvation structure by introducing a trace amount of water. Water molecules insert between DMC and OTf anions, facilitating the dissociation of OTf and solvent molecules at the surface of the expanded graphite (GP) cathode during anion intercalation. Due to the low solubility of Zn(OTf)₂ in DMC, undissolved salt particles remain suspended in the electrolyte, while the overall solvation structure is significantly altered. The resulting salt particle suspension electrolyte (SPSE), with an optimized trace water content, exhibits excellent fluidity, high-voltage charge/discharge plateaus, and good compatibility with both Zn metal or natural graphite anodes and the GP cathode, achieving outstanding battery performance with a specific capacity of 178.66 mAh/g at a current density of 10 mA/g.^[1]

In parallel, water is also introduced into an ether-based solvent system using dipropylene glycol methyl ether (DGME). In this electrolyte, 5% vinylene carbonate (VC) is added as an additive, and 4 M Zn(OTf)₂ is dissolved. The effect of the water-to-DGME volume ratio on battery performance is systematically investigated. At an optimal ratio of 1:4 (water:DGME), the GP-Zn ADIB demonstrates a specific capacity of 118 mAh/g at 100 mA/g.^[2]

Acknowledgments

Y.H. gratefully thanks the financial support of the European Union and the Czech Ministry of Education, Youth and Sports (Project: MSCA Fellowships CZ FZU III-CZ.02.01.01/00/22 010/0008598).

- 1. Y. He, F. Yu and J. Červenka, J. Mater. Chem. A, 13, 15871 (2025).
- 2. Y. He, S. Xiao and J. Červenka, ACS Sus. Chem, Eng., 13, 8363 (2025).

Zn/Li Dual-Ion Batteries with Water-in-Salt Electrolytes

L. Kavana

J. Heyrovsky Institute of Physical Chemistry, Academy of Sciences of the Czech Republic, Dolejskova 3, CZ-18223 Prague 8, Czech Republic

The paper will present the first systematic investigation of electrochemical materials, i.e. substrates, active electrode materials, and electrolyte components, relevant to the emerging field of Zn/Li dualion batteries utilizing chloride-based waterin-salt electrolytes (WiSE). Among the tested substrates, titanium stands out by offering the widest electrochemical stability window. In contrast, carbon, a common additive and substrate material in these systems, exhibits instability at potentials above ca. 2.2 V vs. Zn2+/Zn, raising concerns about its suitability for high-voltage electrode materials, such as LiMnPO4. We demonstrate that LiFePO4 (olivine) serves as a highly stable positive electrode material in WiSE, delivering good charge capacity and cycling performance. Notably, we observe a positive shift in its formal potential with increasing Li+ concentration in WiSE. This study further highlights the often-overlooked impact of electrolyte impurities in WiSE. Trace amounts of Mn²+, commonly present in commercial-grade ZnCl2, can inadvertently mimic the electrochemical signature of LiMnPO4, potentially leading to misinterpretation of results [1].

Acknowledgment

This work was financially supported by the project "The Energy Conversion and Storage", funded as project No. CZ.02.01.01/00/22_008/0004617 by Programme Johannes Amos Comenius, call Excellent Research, and by the Czech Science Foundation (grant No. 23-05895S).

References

1. SUPIŇKOVÁ, T., ZUKALOVÁ, M., KAKAVAS, N., XU, J., NIU, W., EICKEMEYER, F.T., GRAETZEL, M., KAVAN, L., Electrolyte effects and stability of Zn/Li dual-ion batteries with waterin-salt electrolytes, J. Power Sourc., 655 (2025) 237983.

Microemulsion Redox Flow Batteries for Cheap Stationary Energy Storage

J. Kršek^a, M. Marek^a, A. Taccori^a, P. Mazúr^a

^aDepartment of Chemical Engineering, University of Chemistry and Technology Prague, 16628 Praha 6, Czechia

The growing share of renewables in global energy production necessitates scalable, efficient, and affordable stationary energy storage. Redox flow batteries (RFBs) are promising for grid applications due to their safety, independent scalability of power and capacity, and long cycle life [1]. However, conventional vanadium-based RFBs face challenges with vanadium cost and availability. Organic redox-active species, like vitamin or dye derivatives, offer improved sustainability and cost-efficiency, but their poor aqueous solubility limits practical application [2].

Microemulsions (mEs), made of water, non-polar solvent, surfactant and cosurfactant, offer a unique energy storage medium. They can dissolve non-polar organics while maintaining high ionic conductivity and non-flammability of the aqueous phase [3]. This enables using organic molecules in aqueous RFBs without their costly synthetic modifications. However, mEs present significant compatibility challenges, particularly for the membrane, which is a crucial component affecting battery's performance and durability. In the contact with organic solvent of mE, polymeric membranes can degrade, swell or lose integrity, leading to reduced selectivity, increased internal resistance, or even short-circuits [4][5].

This work focuses on the screening of commercially available membranes to evaluate their applicability in mE RFBs. The screening procedure using a model mE (water, toluene, sodium dodecyl sulphate (SDS), and butanol) consists of: i) Chemical stability testing of membranes immersed in the mE for a week with subsequent swelling ratios and visual inspection after to see the changes in membrane morphology and to identify chemically and mechanically stable materials; ii) Membrane's ohmic resistance measurements by electrochemical impedance spectroscopy (EIS) in a laboratory-scale single-cell with blank mE as electrolyte, area specific resistance (ASR) was evaluated and its time evolution over 24 hours of continuous operation; iii) Permeation tests, where selected low-resistance membranes are exposed to mE electrolyte containing a model redox-active species (e.g., ferrocene) on retentate side of the membrane, while the cross-over of active species to permeate is monitored via UV-VIS spectroscopy to determine the permeability.

Preliminary results show that while many membranes degrade or dissolve in the mE environment, several candidates (F-930-Reinforced, FS-830, F1850, Nafion 115) exhibit both chemical stability and acceptable ASR ($< 40 \,\Omega.\text{cm}^2$). For example, F-930-Reinforced, which had previously shown extremely high resistance in electrolytes containing supporting salts, displayed much improved and stable performance in blank mE, suggesting a favorable interaction with the uncharged medium [4]. However, permeation testing revealed measurable cross-over of ferrocene even through stable membranes, underlining the need to consider both resistance and selectivity in the membrane selection process [5].

In conclusion, the current study demonstrates that membrane behaviour in microemulsion environments differs substantially from conventional aqueous systems. While some commercially available membranes show promise for use in mE RFBs, further investigation is required to evaluate long-term durability, chemical compatibility with diverse redox-active species and the influence of electrolyte

composition (e.g., pH, ionic strength). In the next phase of our research, selected membrane—electrolyte systems will be tested under full-cell charge—discharge cycling to assess their mid-term durability, battery efficiencies and performance stability and practical usability. These tests will allow us to move beyond material characterization toward real battery operation and bring the development closer to functional application. The outcomes of this screening provide a foundation for the future development of affordable and sustainable RFB systems based on microemulsions and organic redox chemistries, supporting the broader transition to decentralized renewable energy infrastructures [6][7].

Acknowledgments

This work was supported by the project "The Energy Conversion and Storage", funded as project No. CZ.02.01.01/00/22_008/0004617 by Programme Johannes Amos Comenius, call Excellent Research.

- 1. Weber, A.Z., Mench, M.M., Meyers, J.P., Ross, P.N., Gostick, J.T., & Liu, Q. (2011). Redox flow batteries: a review. Journal of Applied Electrochemistry, 41(10), 1137–1164
- 2. Ouellette, R.J., & Rawn, J.D. (2015). Properties of Organic Compounds. In Principles of Organic Chemistry (pp. 33–64). Elsevier.
- 3. Paul, B.K., & Moulik, S.P. (2001). Uses and applications of microemulsions. Current Science, 80(8), 990–1001.
- 4. Zheng, Y., et al. (2023). Non-aqueous organic redox active materials for a bicontinuous microemulsion-based redox flow battery. Materials Today Energy, 34, 101286.
- 5. Barth, B.A., Elgammal, R.A., Liu, T.L., et al. (2022). Microemulsions: Breakthrough Electrolytes for Redox Flow Batteries. Frontiers in Chemistry, 10, 885705.
- 6. Darling, R.M., Gallagher, K.G., Kowalski, J.A., Ha, S., & Brushett, F.R. (2014). Pathways to low-cost electrochemical energy storage: a comparison of aqueous and nonaqueous flow batteries. Energy & Environmental Science, 7(11), 3459–3477.
- 7. Li, M., Wang, Z., Xu, Q., & Wang, W. (2021). Recent development of organic redox-active materials for redox flow batteries. Energy Storage Materials, 34, 529–550.

Temperature Changes During Repeated Cooling of a Lead-Acid Battery

P. Křivík^a

^aDepartment of Electrotechnology, Brno University of Technology, Faculty of Electrical Engineering and Communication, 616 00 Brno, Czech Republic

This paper deals with the study of the influence of ambient temperature on the dynamics of temperature changes in a lead-acid battery. For this reason, 3 temperature sensors were placed in the battery under investigation and temperature changes were measured, examining the increase and decrease of temperatures in the internal environment of the battery when the ambient temperature changes.

Introduction

A lead-acid battery is often exposed to repeated changes in ambient temperature during operation. Actual temperature of a lead-acid battery affects its capacity, performance, internal resistance or cycle life. The optimal temperature for the operation of lead-acid batteries is 20 °C. Lower temperatures cause an increase in internal resistance, a decrease in power and capacity. Higher temperatures cause a decrease in internal resistance and therefore an increase in power, but the speed of all parasitic reactions that cause a decrease in cycle life (self-discharge, corrosion, electrolysis of water during charging) also increases.

When the ambient temperature changes, the highest temperature changes are detected through the side walls of the battery container, which are in contact with the electrolyte and plates. The bottom of the container is thicker than the side walls, the top lid is not in contact with the electrolyte, and the air layer prevents major temperature changes due to its low thermal conductivity.

Experiment

To investigate the dynamics of temperature changes inside a lead-acid battery during repeated changes in ambient temperature, a maintenance-free 12 V ZAP Plus Calcium 74 Ah battery with dimensions of 275 x 175 x 190 mm was used. The battery is composed of 6 cells connected in series and placed in a container made of ABS plastic, which has a reinforced bottom. Individual cells are separated by plastic partitions.

Three Pt100 temperature sensors were placed in the vertical YZ plane passing through the center of the battery. To protect against aggressive electrolyte, the sensors were covered with a layer of epoxy resin before insertion. The first sensor was placed between the outer edge of the plate and the plastic container in the area of the 1st cell (no. 1), the second sensor was placed between the plate and the plastic partition in the area of the 2nd cell (no. 3) closer to the center of the battery, and the last third sensor was placed in the middle of the battery (in the direction of the Z axis) between the plate and the plastic partition in the area of the 3rd cell (no. 5). To install the temperature sensors, it was necessary to remove part of the battery cover, and after installing the sensors, this part was replaced with a layer of plastic to prevent electrolyte evaporation and to limit temperature changes in the upper part of the battery.

For this battery, experiment was performed in a charged state to measure the temperature changes of the lead-acid battery during repeated cooling from 20 $^{\circ}$ C to -40 $^{\circ}$ C

In this experiment, the battery was placed from a room temperature of 20 °C into a freezer box tempered at -40 °C for 1 h and then moved back to room temperature for 1 h. The battery was placed in the freezer box in this way 3 times, then moved to room temperature for 15 h. During the experiment, the temperature of all temperature sensors was recorded at 1-minute intervals.

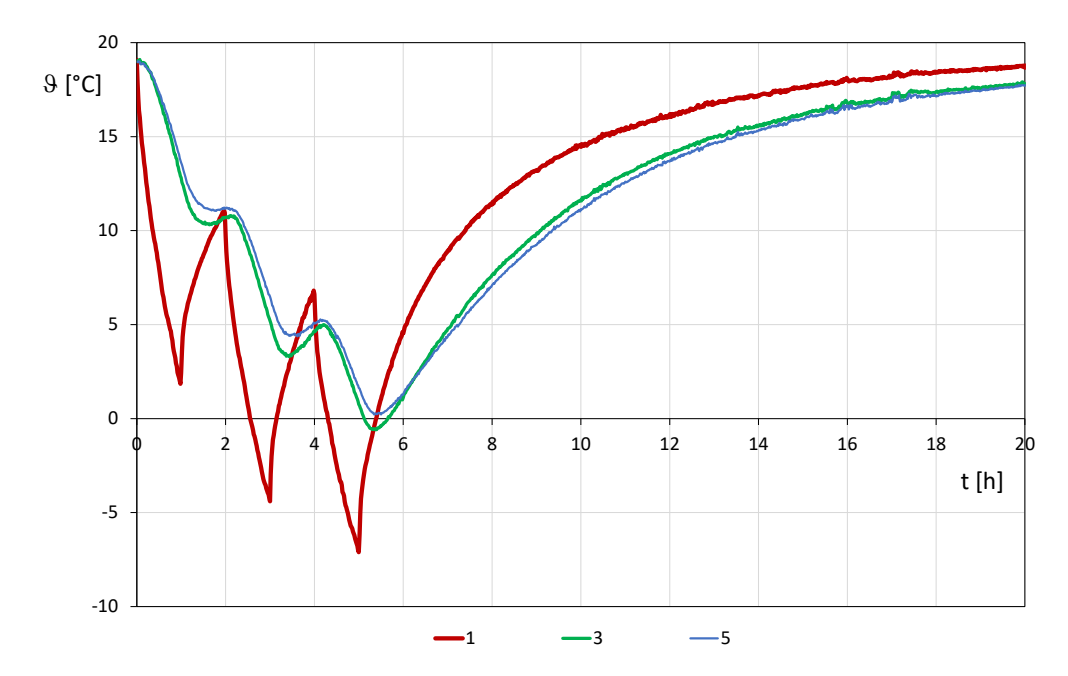


Figure 1. Temperature profile of 3 measured points in a lead-acid battery during repeated 1-hour cooling from $20 \,^{\circ}\text{C}$ to $-40 \,^{\circ}\text{C}$ and 1-hour heating back to room temperature of $20 \,^{\circ}\text{C}$.

Fig. 1 shows the temperature profile of 3 sensors after repeatedly placing the battery in the freezer and warming it back to room temperature. A significant difference can be seen between the temperature profiles of the sensor near the side wall of the battery container compared to the temperature profiles of the other sensors. This sensor has the highest temperature drop from the 1st minute to a temperature of 2 °C after an hour of cooling. For sensors further from the side wall, a more significant temperature drop was detected after 20 minutes. After moving the battery to room temperature, the sensor near the side wall of the battery container again has a sharp temperature increase from the 1st minute of heating, after 1 hour of heating the temperature of this sensor reaches about 11.5 °C. For the other sensors, the cooling process continues and after 20 minutes of battery heating does the cooling process stop. The temperature increase on these sensors during 1 h of heating practically does not occur due to slow heat transfer processes to the internal areas of the battery and the temperature stabilizes at 10.5 °C for sensor no. 3 and 11.5 °C for sensor no. 5, which is a temperature close to the temperature of sensor no. 1 near the side wall of the battery container. In the next round of cooling, the temperature of the sensor near the side wall of the battery container drops sharply again to -4 °C after an hour of cooling. For the other sensors, the cooling process is similar to the 1st round, the temperature at the end of the 2nd cooling is around 5 °C for sensor no. 5 and 4 °C for sensor no. 3. During the next heating, the temperature of the sensor near the side wall of the battery container rises sharply to 7 °C at the end of heating. For the other sensors, cooling down takes place again in the first 20 minutes, followed by a slight increase in temperature to 5 °C at the end of heating for both sensors. This is a difference compared to the 1st heating round, where the temperature increase almost was not observed due to the smaller difference between the ambient temperature

and the temperature of the sensors. The higher temperature gradient in the 2nd heating round led to higher temperature changes for all sensors. This trend was also confirmed by the 3rd cooling and heating round. After the end of the 3rd cooling round, the temperature of the sensor near the side wall of the accumulator container reached -7 °C. The temperature of the other sensors reached a minimum value of about 0 °C after 20 minutes of heating following the 3rd cooling round. In the remaining 15 hours, the accumulator was moved back to room temperature and the temperatures of all sensors gradually increased to 20 °C.

Conclusion

The experiments show a different temperature profile for the sensor near the side wall of the battery container compared to the temperature profiles of other sensors located inside the battery. The point of contact of the active materials with the side wall of the container has also the highest temperature gradient at the beginning of the experiment, which further increases the rate of temperature changes. On the contrary, the slowest temperature changes was observed, as expected, in the center of gravity of the battery (sensor 5). At the beginning, there is almost no temperature change for this sensor, only after 20 minutes can a gradual temperature change be observed as the ambient temperature gradually reaches the internal parts of the battery and the temperature gradient also increases in the internal areas of the battery.

Acknowledgments

This work was supported by the specific research of the BUT FEKT-S-23-8286.

- 1. H. A. Kiehne, Battery Technology Handbook, second edition, 2003
- 2. D. Valkovska, M. Dimitrov, T. Todorov, D. Pavlov, Journal of Power Sources 191 (2009), 119–126
- 3. H. Frank Gibbard, Journal of the Electrochemical Society, Volume 125, Issue 3, (1978) 353–358
- 4. D. A. J. Rand, R. Woods, R. M. Dell, Batteries for electric vehicles, 1998
- 5. D. Pavlov, Journal of Power Sources 64 (1997), 131–137
- 6. T. R. Crompton, MSc, BSc, Battery Reference Book, Third Edition, 2000
- 7. D.Berndt, Journal of Power Sources 100 (2001), 29–46

Hierarchically Porous Metal-Organic Gel Hosting Catholyte for Limiting Iodine Diffusion and Self-Discharge Control in Sustainable Aqueous Zinc-I₂ Batteries

H. K. Machhi^{a,b}, S. S. Soni^a, J. Červenka^b

^aDepartment of Chemistry, Sardar Patel University, Vallabh Vidyanagar 388 120, Gujarat, India

^bDepartment of Thin Films and Nanostructures, FZU-Institute of Physics of the Czech Academy of Sciences, 162 00 Prague 6, Czech Republic

Rechargeable aqueous zinc-iodine batteries (AZIBs) represent excellent zinciodine redox chemistry and emerged as a promising aspirant due to their high safety, low cost, ease of fabrication, and high energy density. Nevertheless, the high dissolution induced iodide diffusion toward the zinc anode brings self-discharge, which governs the capacity fading and poor cycling life of the battery. Herein, a multipurpose spongelike porous matrix of a metal organic gel to host a substantial amount of iodine-based catholyte and uniform distribution of iodine with controlled iodide diffusion is introduced. Limiting the iodine diffusion due to increased viscosity provides superior electrochemical performance of this promising cathode for solid-state AZIBs. As a result, AZIBs delivering high performance and long-term stability are fabricated with a capacity of 184.9 mAh g⁻¹ with a superior capacity retention of 95.8% even after 1500 cycles at 1 C rate [1]. The unique concept of self-discharge protection was successfully evaluated using open-circuit voltage (OCV) method. Moreover, prototype flexible band-aid-type AZIBs were fabricated, which delivered 166.4 mAh.g⁻¹ capacity with 96.4% coulombic efficiency even under the bend conditions after 100 cycles and successfully applied to real-scale wearable applications.

References

1. H. K. Machhi, K. K. Sonigara, S. N. Bariya, H. P. Soni, S. S. Soni, ACS Appl. Mater. Interfaces, 13, 21426 (2021).

Direct Contact Prelithiation of Silicon/Graphite Anodes for Lithium-Ion Batteries

D. Capkova^{a, b}, D. McNulty^a, T. Kazda^b, K. M. Ryan^a

^aDepartment of Chemical Sciences & Bernal Institute, University of Limerick, Limerick, V94 T9PX, Ireland

^bDepartment of Electrical and Electronic Technology, Faculty of Electrical Engineering and Communication, Brno University of Technology, Technická 10, 616 00 Brno, Czech Republic

Silicon is a promising candidate for anode material in lithiumion batteries due to its high theoretical capacity. High content silicon anodes suffer from low cycle life due to significant volumetric expansion during cycling. Continuous reformation of the solid electrolyte interface consumes lithium, leading to capacity fade and reduced lifespan. Direct contact prelithiation is a simple and effective method to mitigate lithium losses during the formation cycles and battery operation. Prelithiation of the anode during cell manufacturing compensates for initial lithium losses and contributes to improved cycle life of lithium-ion batteries. In this study, the process characteristics of direct contact prelithiation and its impact on battery performance are experimentally investigated. Silicon/graphite composite anodes were mechanically prelithiated using lithium foil and subsequently integrated into lithium-ion coin cells.

Introduction

Advanced energy storage technologies are essential for modern life, especially as global energy challenges continue to intensify. Lithium-ion (Li-ion) batteries are widely recognised for their high energy and power densities, enhanced safety, excellent cycling stability, low weight, low self-discharge rates, and fast-charging capabilities [1]. These attributes have enabled their widespread adoption in portable electronics, electric and hybrid vehicles, e-bikes and scooters, stationary storage systems, and aerospace applications [2]. Despite their success, commercial Li-ion batteries are constrained by limited gravimetric and volumetric energy densities, posing a challenge to meet the increasing demands of grid-scale storage and electric transportation. Current cathode materials typically include metal oxides such as lithium nickel manganese cobalt oxide (NMC) and lithium nickel cobalt aluminum oxide (NCA), as well as lithium iron phosphate (LFP), while graphite remains the dominant anode material [3]. However, with a theoretical capacity of only 372mAh g⁻¹, graphite anodes are approaching their theoretical limits in practical applications [4]. To address this limitation, high-capacity anode materials are under investigation, including germanium (Ge), tin (Sn), antimony (Sb), magnesium (Mg), aluminum (Al), gallium (Ga), phosphorus (P), and zinc (Zn), with silicon (Si) emerging as the most extensively studied candidate [5].

Silicon-based anode materials encounter several critical challenges that limit their practical application. The lithiation/delithiation processes induce substantial volumetric expansion of silicon (~300%), resulting in structural pulverization and subsequent loss of electrical connectivity within the electrode [6]. This mechanical degradation exposes

fresh silicon surfaces directly to the electrolyte, promoting electrolyte consumption through continuous formation of the solid electrolyte interphase (SEI) layer, which contributes to low initial Coulombic efficiency (ICE). Furthermore, the intrinsically slow lithium-ion diffusion kinetics in silicon electrodes generate significant lithium concentration gradients, which hinder complete lithium extraction during cycling [7]. Compounding these issues, silicon's poor intrinsic electrical conductivity (2.52 × 10-6 S cm-1) causes electrically isolated fragments upon pulverization [8]. These factors limit the cycling stability, rate capability, and Coulombic efficiency of silicon-based anodes.

To improve the initial Coulombic efficiency (ICE) and mitigate lithium loss due to SEI reformation, prelithiation of the anode can be employed. Various prelithiation methods (chemical, electrochemical, and direct contact) have been developed [9]. Direct contact prelithiation using a lithium foil is a simple, cost-effective, and scalable method [10]. Therefore, the present study focuses on the examination of direct contact prelithiation of silicon/graphite anodes using lithium metal foil for Li-ion batteries.

Experimental

The anodes with 20 % silicon (Si), 60 % graphite (Gr), 30 % conductive additive, and 10 % carboxymethyl cellulose (CMC) were prelithiated for different times (15, 30, 60, 120, and 240 min) and analysed electrochemically in half cells. The prelithiation was done by the application of electrolyte on the electrode, and a lithium metal foil was placed on the top. The electrode was washed, dried and used in a coin cell with a GF/A separator and electrolyte in a composition of 1 M lithium bis(trifluoromethanesulfonyl)imide (LiTFSI) in 1,2-dimethoxyethane (DME) and 1,3-dioxolane (DOL) in a ratio of 2:1 + 10 % LiNO₃ and 10 % fluoroethylene carbonate (FEC).

Results and Discussion

The prelithiated Si/Gr anodes for various times (15, 30, 60, 120, and 240 min) are shown in Figure 1. The prelithiation of \sim 50 % was achieved after 15 min, \sim 80 % after 30 min,

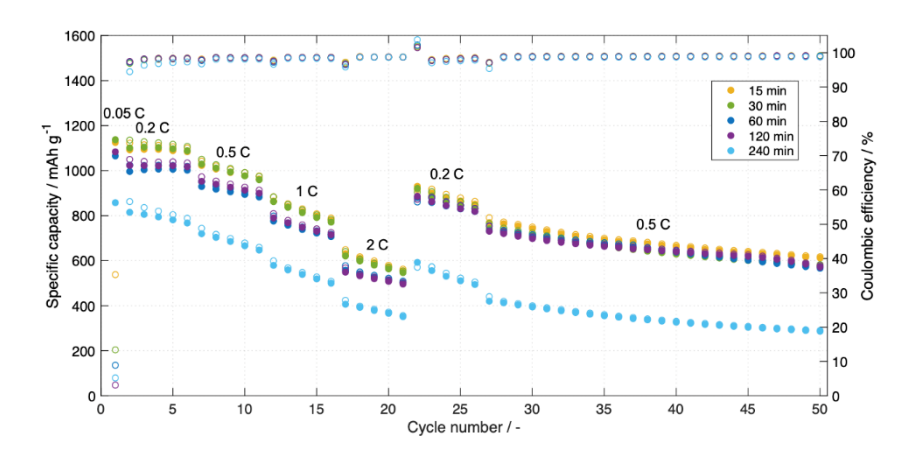


Figure 1. Specific capacities of Si/Gr anodes prelithiated for various times.~90 % after 60 min, ~95 % after 120 min, and ~90 % after 240 min. However, the electrolyte evaporated after 240 min and a significant capacity decrease was observed compared to the rest of the cells, where capacities were comparable.

Performance and Stability of a CdSe Photoanode in a Photoelectrochemical Cell

S. V. Chivikov^a, I. A.Rusetskyi^a, A.M.Davydov^a

^aV.I.Vernadskii Institute of General and Inorganic Chemistry of the NAS of Ukraine, 32/34 Academic Palladin Avenue, Kyiv, 03142, Ukraine.

The characteristics of a CdSe photoanode in a high-voltage photoelectrochemical system were evaluated. The open-circuit voltage reached approximately 0.9 V, and the current density was around 5 mA/cm². However, improvements in solar energy conversion efficiency were accompanied by a significant loss of system stability. After one month, a notable decrease in the open-circuit voltage was observed, while the current density of the photoanode degraded even faster. The influence of electrolyte selection on the photoanode's performance is discussed.

Introduction

A reversible photoelectrochemical system with an open-circuit voltage of about 0.8V is described [1]. This is the result of attempts to improve the characteristics of the original version of the photoelectrochemical cell presented earlier [2]. Preliminary tests of the cell with the increased voltage showed that the system is reversible. It is capable of accumulating energy when illuminated and releasing it in the absence of light. The first sample demonstrated a current density of 0.2mA/cm² (3mA, anode area ~15cm²) at a voltage of 0.65..0.7V [1]. Unfortunately, after a pause in testing (a couple of months), it was found that the cell had lost its functionality. This was unexpected, as the original version with the electrolyte in the anode compartment based on polysulfide showed remarkable stability. Further work was primarily aimed at understanding the reasons for the loss of functionality of the reversible photoelectrochemical system with increased voltage. The goal was also to clarify the characteristics of the CdSe photoanode in the alkaline electrolyte K₃[Fe(CN)₆]/K₄[Fe(CN)₆]. In order to determine the causes of the loss of functionality, the photo cell was disassembled, and the performance of its components was assessed separately. It was found that there had been a significant decrease in the characteristics of the photoanode. With such characteristics of the photoanode, the cell could not be functional since a low photo potential (around 400mV) is insufficient to charge the cathode. A deposit was also found on the surfaces of the photoanode window and the walls of the cell that came into contact with the electrolyte. Therefore, it was necessary to improve the sealing of the cell leads to exclude the influence of the atmosphere (CO₂, O₂) on the composition of the cell's electrolyte. Stability tests of the CdSe photoanode in an electrolyte consisting of: KOH 0.9M; K₄[Fe(CN)₆]*3H₂O 0.12M; K₃[Fe(CN)₆] 0.15M were conducted. The same electrolyte composition was used in the anode compartment of the photo cell. A cell with improved sealing of the leads was also assembled. The cell was assembled to estimate the characteristics of the CdSe photoanode and to check how they change over time. Since testing the accumulation of solar energy was not the goal of the experiment, the cell was assembled in a two-electrode configuration without a cation-exchange membrane. Photoanodes sized approximately 2x1cm were used. These photoanodes were previously manufactured for other research according to the technology described earlier [2]. The second electrode consisted of a foam of nickel sized approximately 2x1x0.2cm. As in the previous versions, the cell housing parts were printed from polypropylene on a 3D printer.

Results and Discussion

Tests were conducted immediately after assembly. A colleague had doubts about the magnitude of the photopotential obtained in [1]. Therefore, it was suggested to conduct tests of the newly assembled photo cell together. A 300W incandescent lamp was used as the light source, and the cell was placed at a distance of about 40 cm from the lamp. The open-circuit voltage was approximately 0.875V. The short-circuit current was 8mA. The surface area of the photoanode directed towards the light, immersed in the electrolyte, was 0.9x1.9 cm. Accordingly, the current density was 4.7mA/cm². The dependence of the voltage on the photo cell on the load current is shown in Fig. 1.

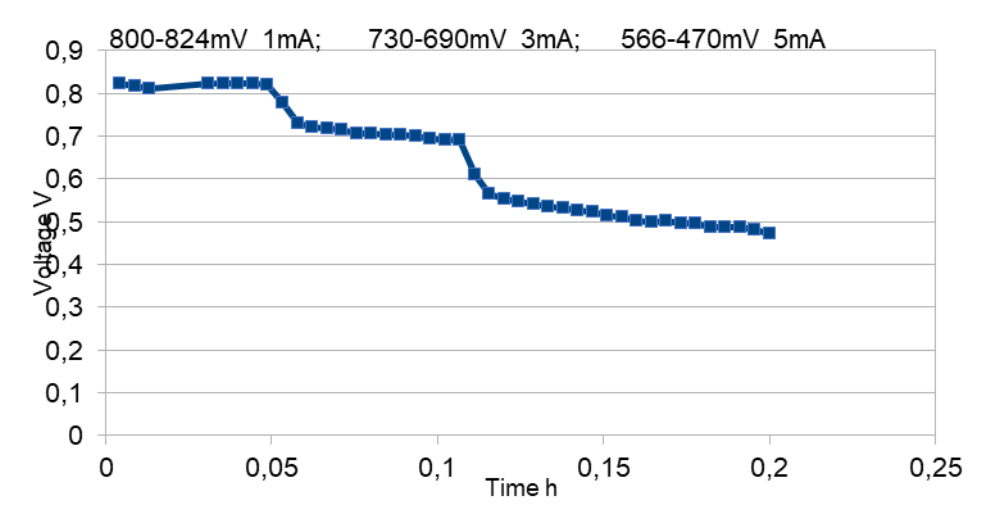


Fig. 1. The dependence of the voltage on the photo cell on the load current

Under sunlight, the indicators were higher, but they were not recorded properly. Changes in cell characteristics over time. The characteristics of the cell in terms of current density at the photoanode degraded very quickly. Already the next day, the values were significantly lower, and further results for current density were not recorded. The cell was periodically illuminated under reproducible conditions (60W incandescent lamp), and an open-circuit voltage measurement was taken. The open-circuit voltage was ~0.85V and was retained for a couple of weeks. The rapid decline in current density characteristics over time explains why low current density values were obtained for the cell described in [1]. During the preparation time of the cathode for the reversible cell, the characteristics of the anode decreased. Samples of photoanodes stored in the electrolyte for a month also showed a noticeable decrease in photopotential.

Let us provide a table of characteristics of photoanodes based on CdSe in different electrolytes Table I. The data for the last column is taken from [3]. This result indicates that the efficiency of the photoelectrochemical system largely depends on the choice of electrolyte. The used electrolyte improve productivity of the CdSe photoanodes in several times.

Table I. characteristics of photanodes based on CdSe in different electrolytes

Photoanode/ electrolyte	CdSe/ polysulfide/alkali	CdSe/ K3[Fe(CN)6]/alkali	CdSe/CdS/ V3+VO2+/acid
Open circuit voltage	0.4V	0.9V	0.67V
Short circuit current	1.5mA/cm2	4.7mA/cm2	1.4mA/cm2
stability	stable	day/month	Up to 5min
load	-	~0.7 at 1.8mA/cm2	-

Conclusions

The CdSe photoanode demonstrated high initial performance in the alkaline electrolyte $K_3[Fe(CN)_6]/K_4[Fe(CN)_6]$. The open-circuit voltage reached 0.9 V. The short-circuit current density was 5 mA/cm².

The use of the alkaline $K_3[Fe(CN)_6]/K_4[Fe(CN)_6]$ electrolyte leads to degradation of CdSe photoanode characteristics over time. The electrolyte itself is unstable and forms precipitates on the surfaces of containers during storage.

Further improvement of the system is related to the selection of a stable electrolyte and the study of the reasons for the decrease in the characteristics of the photoanode.

- 1. S.V.Chivikov, in Advanced Batteries Accumulators and Fuel Cells-25rd,108-109,(2024)
- 2. S.V.Chivikov, I.A.Rusetskyi, S.S.Fomanyuk et al., Journal of Physics: Conference Series, 2382(1), (2022)
- 3. J. Azevedo, T. Seipp, J.Burfeind, Célia Sousa et al., Nano Energy, 396–405, 22 (2016)

FT-IR and GC-MS Analysis of the Chemical Recycling Products of the PV Module

J. Vaněk^{a,b}, J. Jandová^a, P. Vanýsek^a, P. Maule^a, and M. Čepil^a

^a Department of Electrotechnology, Brno University of Technology, Brno, Czech Republic

^b Department of Electrical Engineering, Faculty of Military Technology Brno, Czech Republic

Photovoltaic modules are a key part of the shift to clean energy, but their increasing use brings challenges related to their recycling. This work focuses on the recycling of photovoltaic modules using a chemical method to decompose the binder of each functional layer. It also includes an analysis of the current recycling situation in the Czech Republic.

Introduction

In connection with the growing interest in solar energy, the number of installed photovoltaic modules is also increasing. The global photovoltaic boom has been record-breaking in recent years, as recently confirmed by the International Roadmap for Photovoltaics (ITRPV) study published by the VDMA Industry Manufacturers Association. In total, for example, more than 295 GW of photovoltaic modules had been sold in the global market in 2022. Although they can have a lifespan of up to 30 years, the issue of recycling them will be an issue in the future but needs to be addressed now. We have focused on investigating the current state of PV module recycling in the Czech Republic, mapping current recycling practices and PV module recycling [1].

By 2030, there will be up to 30 million photovoltaic modules in operation in the Czech Republic, which means nearly three modules per person. This is based on data from the Rema System, a company that deals with the collective collection of electrical waste. One of the companies that recycle photovoltaic modules in the Czech Republic is Dekonta IC. It has built a special recycling line in Kralupy nad Vltavou that focuses on solar modules. The line developed by Dekonta IC works on the mechanical principle of recycling. Dekonta IC has processed several tonnes of photovoltaic modules as part of the preparatory tests. At full operation, they expect to process 1,500 to 2,000 tonnes of modules per year [2].

Another company, which will be interesting to watch on this topic, is Technoworld, which has reportedly acquired recycling technology from Aquatest. Technoworld is part of the better-known company Asekol, which is also an authorized electrical waste collection company. An interesting innovation here is a technology called 'hot knife'. The technology has come to the Czech Republic from Japan and according to information should be quite unique on the world market. This hot knife works by cutting the cover glass very precisely and cleanly, leaving the cell sandwich intact. It performs a very clean separation which in turn allows for easier recycling. For the separation to be successful, it is necessary to use the same modules, or at least modules with similar parameters, so that the materials on the modules are not simply destroyed due to the wrong thickness of the extender. Therefore, it follows that it will be much more interesting for this recycling line to source material from large solar

power plants where there will be sufficient quantities of the same input material with the same parameters, rather than different modules from individuals in salvage yards.

Chemical delamination

Some of these limits of mechanical recycling can be solved by the chemical delamination of photovoltaic modules. The primary encapsulation material currently used in commercial photovoltaic modules is polyethylene vinyl acetate (EVA), a copolymer of ethylene and vinyl acetate [3][4][5]. EVA is a relatively inexpensive material with good optical transparency that has been used for many years in the construction of photovoltaic modules [4,5]. However, it is known to be susceptible to aging due to prolonged exposure to outdoor environmental conditions, leading to discoloration and the release of small amounts of acetic acid. Since EVA is used as an encapsulation material, its removal is crucial for module delamination. Therefore, the typical process that is most commonly reported is the heat treatment of the module, which leads to thermal degradation and, in some cases, burning of the EVA and back sheet materials [3]. While this process allows for rapid deconstruction and separation of the remaining parts, it generates gaseous emissions and precludes the possibility of recycling the encapsulation material. This problem can be avoided by using chemical means, as EVA has been shown to dissolve or react with a variety of solvents and solutions. These include substances such as toluene, xylene, sulfonic acid and lactic acid [5]. It is therefore likely that at least some EVA could theoretically be recycled by chemical means. Complete recycling of all EVA is unlikely due to the partial crosslinking of the bonds in the material.

Chemical recycling of photovoltaic modules is a promising approach to recover valuable materials from photovoltaic modules and minimize waste. While this technology has been explored and shows potential, it's important to note that the feasibility and success of chemical recycling depend on various factors, including the composition of the PV modules, the state of technology, and economic considerations.

In our previous research, it was found that the most advantageous method is to use heat to remove the Tedlar and EVA film layers, a relatively high temperature of 540-550 °C is required. This temperature can be reduced to 340 °C by pressure control. However, reaching these temperatures is still energy intensive and the cell surface may oxidize. The chemical process is simpler in this respect as it only requires a solvent. The disadvantage is the greater time requirement and the correct choice of chemicals for dissolution.

Experiment

The aim of this work was to investigate methods for chemical release of functional layers and recycling of single and polycrystalline solar cells using different solvents. The main focus is on the removal of the protective layers - mainly the EVA layer and the Tedlar back protective layer - from the silicon cell. In addition, chemical analysis in the infrared (IR) spectrum has been performed to determine how much material dissolves in the most effective solvents. Finally, the results are evaluated and the efficiency of the different methods used is assessed.

In addition to the solar cell, the solvents were also tested on a separate EVA film to determine its ability to disrupt its polymer structure. During the experiment, changes in the EVA layer, whether it showed signs of swelling or decomposition, were observed and recorded.

Table 1: Example of result for the EVA layer solved by toluene

Material	Toluene	Room temperature	Sample size	Sample weight before immersion	Sample weight after extraction	Sample weight after 24 hours drying
	ml	${}^{\circ}\!C$	mm	\boldsymbol{g}	\boldsymbol{g}	\boldsymbol{g}
EVA layer	40	22	25x18	0.58	9.6	0.4
Solar cell	40	22	25x15	8.95	19.1	8.55

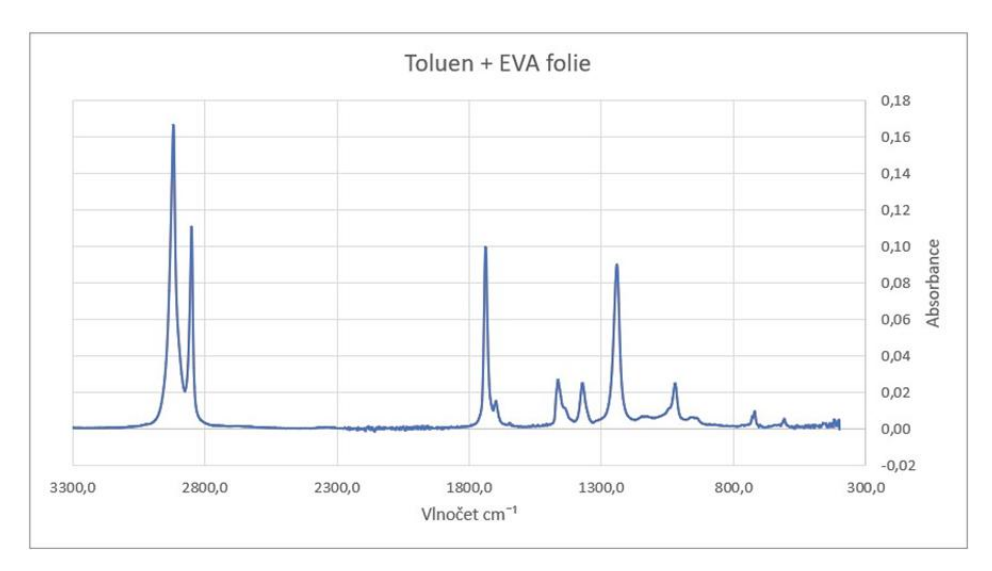


Figure 1 Sample FTIR spectra of toluene solvent and EVA film

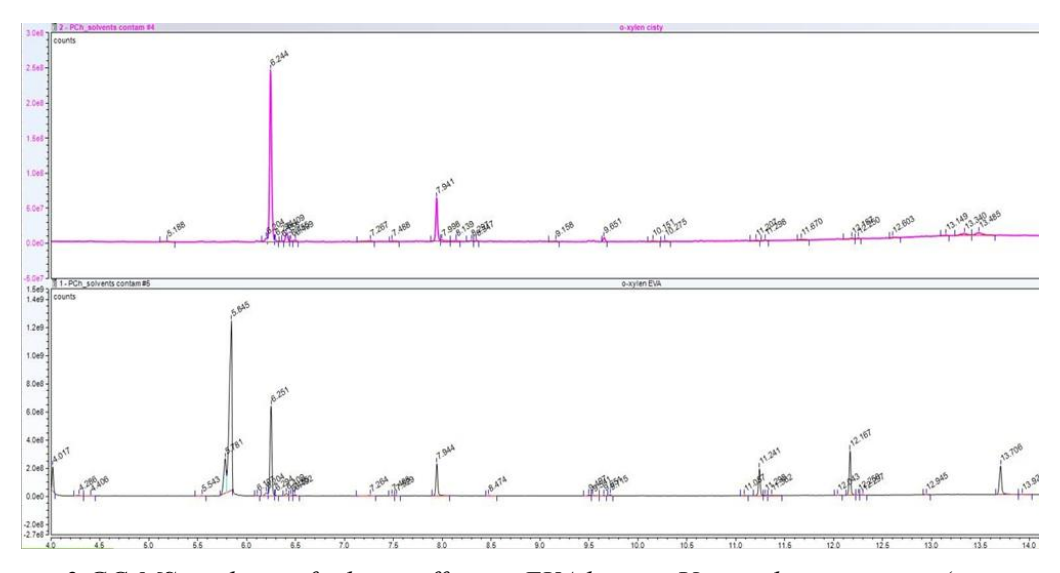


Figure 2 GC-MS analyses of toluene effect on EVA layer, - Upper chromatogram (pure toluene): One dominant peak at 4.705 min (corresponding to toluene alone-Lower chromatogram (toluene with EVA)

All used and compared solvents in experiments:

- 1. Toluene (chemically methylbenzene with formula $C_6H_5CH_3$)
- 2. Dimethylformamide, (abbreviated DMF is an organic compound with the formula $(CH_3)_2NC(O)H)$)

- 3. Acetone (propane-2-one or dimethyl ketone, CH_3COCH_3)
- 4. Methyl pyrrolidone (NPM) (1-methyl-2-pyrrolidone, C_5H_9NO)
- 5. Ethyl acetate (acetic acid ethyl ester, $CH_3COOOCH_2CH_3$)
- 6. O-xylene (ortho-xylene is an aromatic hydrocarbon with formula C_8H_{10})

Conclusion

Overall, six different solvents were compared, and it can be concluded that toluene and o-xylene are the most effective for the chemical recycling of solar cells, while safety precautions for their use must be carefully considered, especially in terms of toxicity and flammability. For practical use in industrial conditions, it will be important to choose a solvent that offers the optimum combination of efficiency, safety and environmental friendliness.

Acknowledgments

This work was supported by Brno University of Technology grant No. FEKT-S-23-8286 and was supported by the Faculty of Military Technology, University of Defense.

- 1. Philipps, S. Photovoltaics report—Fraunhofer ISE; 2025. Available from: https://www.ise.fraunhofer.de/en/publications/studies/photovoltaics-report.html.
- Z. Kamenzova, Češi se učí recyklovat soláry. První z nich doslouží už za pár let.
 Online. Hospodářské noviny. 2023. [web] z: https://archiv.hn.cz/c167267330-cesi-se-uci-recyklovat-solary. [cit. 2024-11-01].
- 3. D.W. Zeng, M. Born, and K. Wambach. J. Environ. Sci. 2004, 16, 889–893.
- 4. Chitra; Sah, D.; Lodhi, K.; Kant, C.; Saini, P.; Kumar, S., Sol. Energy 2020, 211, 74–81.
- 5. Czanderna, A.W.; Pern, F.J.. Sol. Energy Mater. Sol. Cells 1996, 43, 101–181.
- 6. Final_Report_End-of-Life_Pathways_For_Photovoltaic_Backsheets.pdf [online]. https://www.coveme.com/files/immagini/green-solutions/Final_Report_End-of-Life Pathways For Photovoltaic Backsheets.pdf
- 7. J. Vanek, P. Maule K. Jandová and F. Langer, The Electrochemical Society, 2021. s. 281-289. ISSN: 1938-6737.

Conclusions

Prelithiation is an important step in full cell harmonisation to eliminate lithium losses during the formation cycles and improve cycle life of Li-ion batteries. The prelithiation of Si/Gr anodes was performed using various times. Different states of prelithiation were achieved and identified. Only after 15 min, the prelithiation was ~ 50 % and after 30 min it was ~ 80 %. The presented results regarding Si/Gr anode prelithiation will be used in a future full cell harmonisation.

Acknowledgments

D.C. acknowledges the EU Horizon 2023 research and innovation program under the Marie Sklodowska-Curie Postdoctoral Fellowship Grant no. 101152715 (SALSA project). This publication was supported by the project "The Energy Conversion and Storage", funded as project No. CZ.02.01.01/00/22_008/0004617 by Programme Johannes Amos Comenius, call Excellent Research, specific graduate research of the Brno University of Technology No. FEKT S 23-8286 and the European Union's Horizon 2022 Research and Innovation Program; grant agreement no. 101069738 (SiGNE Project).

- 1. J. Xu, X. Cai, S. Cai, Y. Shao, C. Hu, S. Lu and S. Ding, *Energy Environ. Mater.*, **6**, e12450 (2023).
- 2. G.-A. Nazri and G. Pistoia, *Lithium-Ion Batteries: Advances and Applications*, Elsevier, Amsterdam (2014).
- 3. S. B. Chikkannanavar, D. M. Bernardi, and L. Liu, *J. Power Sources*, **248**, 91 (2014).
- 4. **S.** Chen, C. Liu, R. Feng, Z. Chen, Y. Lu, L. Chen, Q. Huang, Y. Guan, W. Yan, Y. Su *et al.*, *Chem. Eng. J.*, 503, **158116 (2024).**
- 5. N. Nitta and G. Yushin, *Part. Part. Syst. Charact.*, **31**, 317 (2014).
- 6. Y. Deng, C. Li, R. Guo, Z. Xie, L. Huang, J. He, L. Xing, and W. Li, *Adv. Funct. Mater.*, **35**, 2415820 (2024).
- 7. F. K. Tareg and S. Rudra, *Mater. Today Commun.*, **39**, 108653 (2024).
- 8. W. J. Zhang, *J. Power Sources*, **196**, 13 (2011).
- 9. F. Holtstiege, P. Baermann, R. Noelle, M. Winter, and T. Placke, *Batteries*, **4**, 4 (2018).
- 10. B. Stumper, A. Mayr, K. Mosler, J. Kriegler, and R. Daub, *J. Electrochem. Soc.*, **170**, 060520 (2023).

Entropy Profile for Sodium-ion Batteries

M. Ceylana,

^a Department of Electronics, Gebze Technical University, Kocaeli, 41400, Turkey

Effective thermal management is a vital aspect in the design and operation of battery packs, particularly under high-rate charge/discharge conditions and in safety-sensitive applications. Heat generation of batteries arises from two primary sources. The irreversible heating depends on the internal resistance and current, whereas the reversible heat component, known as the entropic heating, is associated with entropy changes. These entropic heat variations have significant implications for thermal modeling and aging properties. The characteristic entropy coefficient can be defined as the temperature derivative of the open-circuit voltage (OCV), such as $\partial OCV/\partial T$.

While lithium based chemistries have been extensively studied in this regard, the thermal behavior of sodium-ion systems remains comparatively underexplored. This work aims to provide accurate parameterization of the entropy coefficient for a commercial sodium-ion cell across the whole SoC range by means of potentiometric measurements.

- 1. D. Bernardi, E. Pawlikowski and J. Newman, J. Electrochem. Soc., 132, 5 (1985).
- 2. J. Dahn, W. McKinnon, J. Murray, R. Haering, R. McMillan, and A. RiversBowerman, Phys. Rev. B: Condens. Matter Mater. Phys., **32**, 3316 (1985).
- 3. Y. Reynier, J. Graetz, T. Swan-Wood, P. Rez, R. Yazami, and B. Fultz, Phys. Rev. B: Condens. Matter Mater. Phys., 70, 174304 (2004).
- 4. J.Huang, C. Delacourt, P. Desai, and J. M. Tarascon. *J. Electrochem. Soc.*, **171**, 3 (2024).

Suitability of Sodium-Ion Based Battery Pack as a Cold-Start Alternative to a Conventional 12V/15Ah Lead Acid Starter Battery

T. Finsterle^a, J. Kasper^a, V. Knap^a, P. Hrzina^a

^aDepartment of Electrotechnology, Faculty of Electrical Engineering, Czech Technical University, Prague, Czech Republic

This study presents an experimental evaluation of a sodium-ion battery pack constructed from 18650-format cells, compared to a conventional lead-acid starting, lighting, and ignition (SLI) battery. With sodium-ion technology emerging as a promising alternative to lithium-ion and lead-acid chemistries, offering advantages in resource availability, cost-effectiveness, and cold-temperature performance, its potential for various applications warrants detailed investigation. A 4s11p sodium-ion SLI battery pack was assembled for this purpose and subjected to performance testing in a climate chamber across a temperature range from +10 °C to -20 °C. The results aim to assess the coldweather reliability and operational viability of sodium-ion cells relative to traditional battery solutions.

Introduction

The performance of conventional lead-acid starting, lighting, and ignition (SLI) batteries significantly deteriorates at low temperatures, leading to reliability issues in automotive and backup power applications. While lithium-ion batteries offer higher specific energy and better cold resistance, their cost, limited raw material availability, and safety risks make them less suitable for some large-scale or cost-sensitive applications.

Sodium-ion batteries (SIBs) are emerging as a promising alternative. Unlike lithium, sodium is abundant, inexpensive, and can be processed on the same production lines as lithium-based cells. Recent studies have shown that commercially available cylindrical SIBs, especially in the 18650 format, can achieve specific energies above 120 Wh/kg, lifespans exceeding 2000 cycles, and stable performance even at sub-zero temperatures [1] [2]. The chemical composition of these cells varies by manufacturer but typically includes a hard carbon anode and various types of layered metal oxide, polyanionic (phosphates), or Prussian blue analogues as cathodes [3].

Within this study, a battery pack using 44 SIB 18650 cells was assembled and compared to a standard 12 V lead-acid battery in terms of performance. The study builds upon scientific literature analyzing impedance behavior, cell construction, and performance under high discharge currents [4]. The aim of the study is to assess the suitability of these cells for use in starting and backup systems under harsh climatic conditions.

Methodology

A total of 44 SIB 18650 cells (approximately 3.0~V/1.3~Ah) were used. Each cell was measured using a voltmeter with 1 mV resolution. Cells exhibiting a voltage deviation greater than $\pm 50~mV$ were individually balanced through controlled charging

to ensure uniformity across the entire pack. The resulting 4s11p configuration provides a nominal voltage of approximately 12 V and a capacity of 14.3 Ah.

Pack Assembly

The cells were arranged so that four 18650 cells were first connected in series, forming eleven such quartets. These quartets were then connected in parallel, resulting in the final 4s11p configuration (Figure 1). Nickel strips ($8 \text{ mm} \times 0.12 \text{ mm}$) were used for the interconnections, and plastic holders ensured mechanical stability. The series connections were made using the same material, joined with a manual spot welder equipped with a dual electrode.

For safe operation at currents up to 200 A, power leads with a cross-section of at least 4 mm² and connectors rated above the maximum test current are recommended. For mechanical protection, mounting with plastic reinforcements or housing the pack in an insulating enclosure is advised. The pack does not include a battery management system (BMS) or temperature sensors; voltage and current will be measured externally.





Figure 1. The resulting configuration is 4s11p.

Test Plan

Testing is carried out in a climate chamber at four temperature points: $+10 \,^{\circ}\text{C}$, $0 \,^{\circ}\text{C}$, $-10 \,^{\circ}\text{C}$, and $-20 \,^{\circ}\text{C}$. At each temperature, the battery pack is subjected to pulse discharges at 40, 80, 160, and 200 A for durations ranging from 1 to 3 seconds.

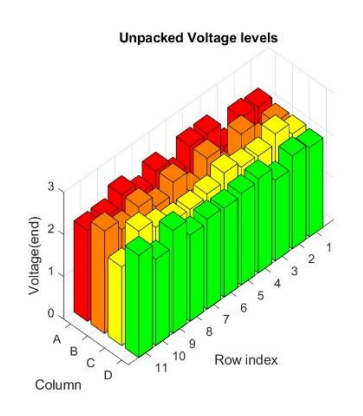
During and after each pulse, the following parameters are evaluated:

- Voltage drop (ΔV) within the first 500 ms
- Voltage recovery within 30 s
- Internal resistance evolution
- Surface temperature development during passive discharge (monitored by an external temperature sensor).

All measurements are conducted using the battery testing system Neware CE-6000, specifically on a channel rated at $60\,\mathrm{V}$ / $200\,\mathrm{A}$, designed for testing battery packs under high current loads.

Results

Initial Cell Voltage Before Assembly



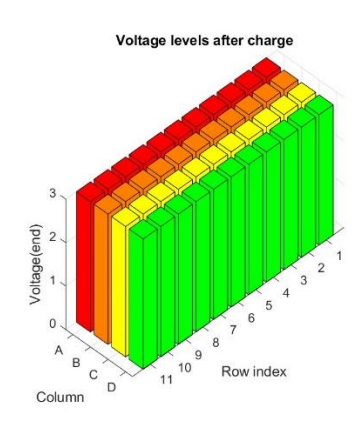


Figure 2. Voltage Distribution Across Pack Before and After Balancing Charge

TABLE I. Statistics.

	vmax	v average	vmin
Before Balancing	2.4340	2.1995	1.845
After Balancing	2.9998	2.9984	2.9979

Initial voltage measurements of the individual SIB 18650 cells revealed a noticeable spread ranging from 1.845 V to 2.434 V, with a standard deviation of 0.182 V (Figure 2). This variation indicates differences in state of charge (SoC), which may be attributed to storage conditions, manufacturing tolerances, or varying levels of self-discharge during logistics [1]. The lowest voltages were mainly observed in the lower rows of the array (rows 9–11), while higher voltages were more evenly distributed. Although the cells did not exhibit extreme deviations, each was individually charged to a uniform voltage to ensure balance in the 4s11p configuration. SoC equalization is critical to ensure uniform current distribution and to prevent overstressing of individual cells during cycling.

Acknowledgments

This work was supported by the Grant Agency of the Czech Technical University in Prague, grant No. SGS24/136/OHK3/3T/13, and the project "The Energy Conversion and Storage", funded as project No. CZ.02.01.01/00/22_008/0004617 by Programme Johannes Amos Comenius, call Excellent Research.

- 1. Y. Zhao et al., *Nanomaterials*, **14**, 1604 (2024).
- 2. K. Deshmukh et al., J. Mater. Sci., **60**, 3609–3633 (2025).
- 3. S. Manna, P. Verma, and S. Puravankara, *J. Power Sources*, **631**, 236234 (2025).
- 4. B. Wang et al., *iScience*, **3**, 110–133 (2018).

Low-Temperature Discharging Performance Comparison of Sodium-Ion and Lithium-Ion Cylindrical Batteries

J. Kasper^a, J. Kočí^a, K. Nováková^a, T. Finsterle^a, P. Hrzina^a, and V. Knap^a

^a Department of Electrotechnology, Faculty of Electrical Engineering, Czech Technical University, Prague, Czech Republic

study compares the low-temperature discharging performance of cylindrical sodium-ion (SIB) and lithium-ion (LIB) batteries using continuous current tests. Two 18650format SIB cells (high-energy and high-power variants) are evaluated alongside three LIB cells with different chemistries: NMC, LFP, and LTO. While NMC-based LIBs offer the highest energy at room temperature, their performance degrades rapidly below -30 °C. LFP and LTO cells show moderate to poor performance under cold conditions. In contrast, both SIB variants maintain stable operation down to -30 °C, with the highpower cell delivering usable energy even at -40 °C. These findings suggest that SIB technology, despite lower energy density, may offer superior performance in extreme cold environments, making it a promising candidate for lowtemperature applications utilizing secondary batteries.

Introduction

Reliable battery performance in low-temperature environments is critical for various applications, such as space missions, outdoor systems, and operations in cold climates.[1] Nevertheless, at low temperatures, lithium-ion batteries (LIBs) exhibit significant performance limitations, typically manifested as large overpotentials and severely reduced capacity due to hindered Li⁺ transport within the cell. Furthermore, electrolyte freezing is expected below $-30\,^{\circ}\text{C}$ for commonly used LiPF6 in ethylene carbonate/ethyl methyl carbonate solvents.[2] Efforts to improve the low-temperature performance of LIBs focus primarily on electrolyte and electrode engineering, targeting issues like ion desolvation and charge-transfer resistance at the electrode–electrolyte interface. Strategies include using low-freezing-point solvent mixtures, EC-free electrolytes, and engineered solid-electrolyte interphases (SEI) to enhance Li⁺ mobility

Another approach to achieving efficient low-temperature performance in energy storage systems is to adopt an alternative technology that exhibits more favorable behavior under such conditions. One promising candidate is the recently commercialized sodium-ion battery (SIB). SIBs offer the potential for lower cost and reduced dependence on critical materials, as they use the more abundant sodium and can employ aluminum instead of copper as the anode current collector.[3] Additionally, some manufacturers report lower operational temperature limits compared to those typical for LIBs. This improved behavior may be explained by the fact that, although SIBs suffer from sluggish Na⁺ diffusion at low temperatures, Na⁺ ions can desolvate more easily than Li⁺ ions, potentially enabling faster interfacial reactions, such as charging and discharging, under cold conditions[4].

In this work, two 18650 cylindrical SIB cells, a high-energy and a high-power variant with layered metal oxide-based cathodes, are systematically evaluated and compared with three LIB cells of the same format utilizing different chemistries. Continuous current discharge tests are conducted to investigate their performance in terms of available capacity, energy, and temperature rise in order to assess their application potential at low temperatures.

Results Summary

Among the cells investigated, those with nickel manganese cobalt (NMC)-based cathodes exhibit an energy density, and consequently discharge energy, that is approximately three times higher than that of cells using other chemistries, as illustrated in Fig. 1 a). However, -30 °C appears to be the functional discharge limit for NMC cells, as their energy output drops nearly to zero even at a low discharge rate of 0.3 °C.

Cells with lithium iron phosphate (LFP) cathodes provide slightly higher energy than sodium-ion batteries (SIBs) down to -20 °C. At lower temperatures, however, their performance deteriorates rapidly, making them unreliable. Cells with lithium titanate oxide (LTO) anodes maintain good discharge capability down to -20 °C, after which their performance also declines significantly. Nevertheless, LTO cells demonstrate the lowest energy capacity among all tested chemistries.

The results clearly show that SIBs, in both high-energy (HE) and high-power (HP) configurations, perform better at reduced temperatures. At -30 °C, they provided the highest energy output and maintained stable operation at 0.3 °C. As expected, HP cells, owing to their generally lower internal resistance, can deliver higher currents under extreme conditions. Their performance remained unaffected even at a higher C-rate of 1.0, as shown in Fig. 1 b).

Furthermore, this technology demonstrated reliable operation even at -40 °C, highlighting its potential for more effective rechargeable battery solutions in extremely cold environments.

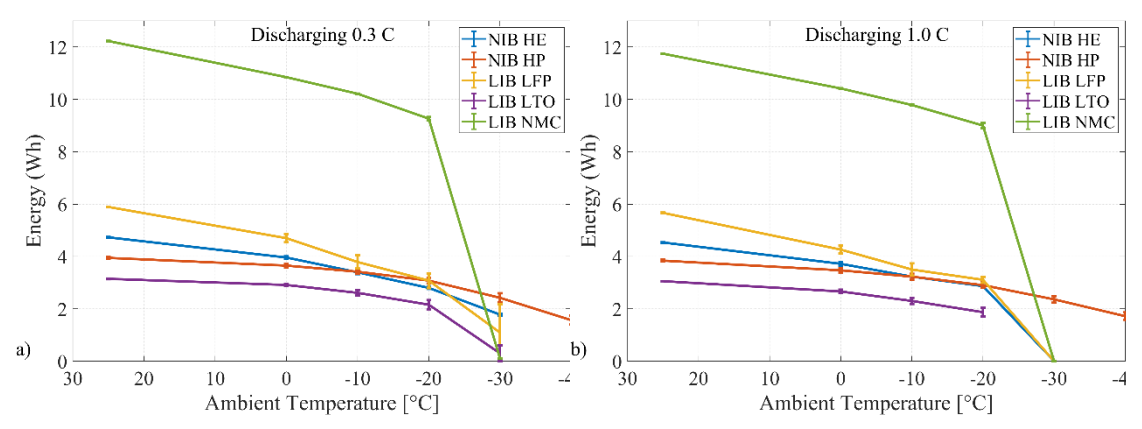


Figure 1. Available discharging energy at various temperatures for a) 0.3 C discharge, and b) 1.0 C discharge.

Acknowledgments

This work was supported by the Grant Agency of the Czech Technical University in Prague, grant No. SGS24/136/OHK3/3T/13, and the project "The Energy Conversion and Storage", funded as project No. CZ.02.01.01/00/22_008/0004617 by Programme Johannes Amos Comenius, call Excellent Research.

- 1. A. Gupta and A. Manthiram, Adv Energy Mater, 10 (2020).
- 2. G. Zhu et al., *J Power Sources*, **300**, 29–40 (2015).
- 3. C. Vaalma, D. Buchholz, M. Weil, and S. Passerini, *Nat Rev Mater*, **3**, 18013 (2018).
- 4. M. Li et al., Carbon Energy, 6 (2024).

Evaluation of Cycling Performance and Degradation Mechanisms in Commercial Sodium-ion Batteries

S. Narayanan^{a,b}, B. Rajagopalan^a, D. Ezhumalai^a, J. Reiter^a, M. Valtiner^b

^aInobat R&D and production centre, 919 42, Voderady, Slovakia

^bInstitute of Applied Physics, Technische Universität Wien, 1040 Vienna, Austria

Sodium-ion batteries (SIBs) have garnered significant attention in recent years as a promising alternative to lithium-ion batteries due to the abundant availability and low cost of sodium resources. The growing demand for efficient and sustainable energy storage solutions has intensified research efforts towards optimizing the performance of SIBs, yet their viability is constrained by limited cycle life. This study investigates the cycling performance and degradation behaviour of commercial 18650 cells manufactured by HAKADI, which employs NFM cathode and hard carbon anode. The cells were subjected to cycling at 1C rate in a constant current constant voltage (CCCV) mode. The cell retained 56% its initial capacity after 200 cycles, depicting a progressive loss in the capacity, further confirmed from differential capacity (dQ/dV) analysis. DCIR and post-mortem studies are planned to further elucidate degradation pathways. This work presents early insights into failure mechanisms in commercial SIBs and supports ongoing efforts toward improving cycle stability.

Since their commercialisation by Sony in 1991, Li-ion batteries (LIBs) have gained much attention as primary candidates for energy storage. LIBs have seen commercial success from portable electronic devices such as cell phones and laptops to electric vehicles (EVs) and grid-energy storage applications due to their unmatched energy density and excellent cycling performance. However, the current technology for LIBs faces a few challenges due to the increasing demand for lithium associated with large-scale applications, which has significantly increased the price of lithium since it is not naturally abundant. As a result, the widespread implementation of lithium has been hindered due to its limited reserves. Concerns about lithium depletion from rechargeable lithium-ion batteries have sparked interest in sodium-ion batteries (SIBs). As the fourth most abundant element on Earth, sodium presents a viable alternative for large-scale energy storage. With the growing demand for sustainable battery technologies, SIBs are gaining attention due to sodium's abundance and low cost.

Despite progress in cathode and anode materials, the long-term stability of commercial SIB cells remains a challenge. This study explores the long-term cycling performance of HAKADI 18650-format sodium-ion cells, utilizing NFM layered oxide cathodes and hard carbon anodes, which are among the few cylindrical SIB formats available for practical applications.

This study investigates the electrochemical degradation behaviour of commercial Hakadi 18650 format sodium-ion cells with a real capacity of 1500 mAh. The cells were subjected to extended cycling at a rate of 1C (Figure 1). They were cycled using a constant-current constant-voltage (CCCV) charging mode and a constant-current discharge between 1.5 V and 4.0 V. All tests were conducted under ambient laboratory conditions using a Neware battery cycler. The cycling protocol was chosen to mimic realistic scenarios in energy systems related to both stationary and mobile applications.

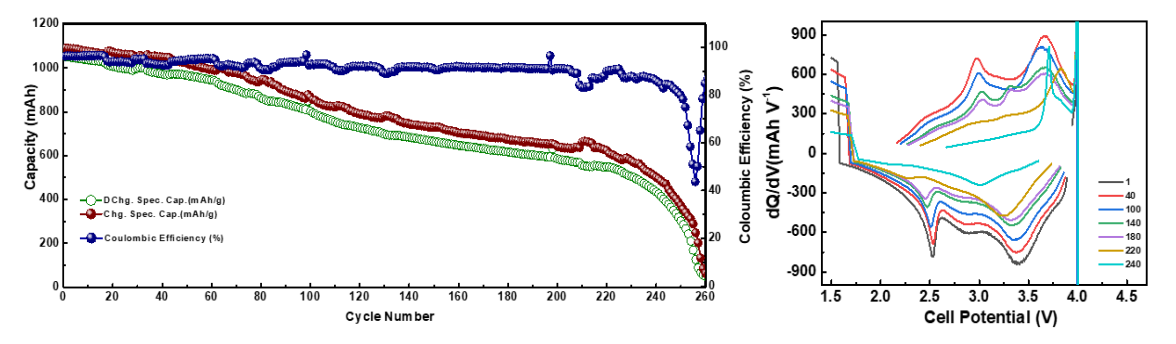


Figure 1. (Left) Capacity retention and coulombic efficiency of commercial Hakadi 18650 sodium-ion cells cycled at 1C within a 1.5–4.0 V window. A gradual decline in charge and discharge capacity is observed over 260 cycles, with a notable drop after 180 cycles. Coulombic efficiency remains stable initially but decreases significantly toward end-of-life. (Right) Differential capacity (dQ/dV) plots at selected cycles show progressive broadening and fading of redox peaks, indicating increased polarization and kinetic limitations during prolonged cycling.

Figure 1 shows the relationship between specific capacity and cycle number, along with the corresponding trends in coulombic efficiency (CE). A consistent decline in both charge and discharge capacities was observed over 260 cycles. The cells maintained over 80% of their initial discharge capacity for approximately 180 cycles. After this point, the decline became more pronounced, with capacity dropping to nearly zero, indicating accelerated degradation. This long-term trend clearly demonstrates the limitations of current commercial sodium-ion battery (SIB) chemistries under continuous 1C cycling.

Throughout the initial half of the test, the coulombic efficiency exhibited relative stability, maintaining a range of approximately 98% to 99%. This stability indicates that the charge and discharge processes were predominantly reversible. However, after 200 cycles, we observed increasing fluctuations and a noticeable decline in coulombic efficiency, particularly evident after 240 cycles. This behaviour points to the emergence of parasitic reactions, which may involve electrolyte decomposition, interfacial layer thickening, or irreversible side reactions at the electrode surfaces. These processes contribute to active sodium loss and result in a deterioration of charge storage efficiency.

While post-mortem or impedance-based analysis (e.g., DCIR) were not performed in this preliminary study, the electrochemical trends offer early indications of possible degradation pathways. The observed capacity fade and coulombic efficiency decline may be linked to structural changes in the NFM cathode, sodium loss or trapping in the hard carbon anode, and interfacial layer growth that could hinder Na⁺ transport. However, the exact mechanisms remain uncertain, and further studies, including impedance measurements and post-mortem analysis, are currently ongoing to better understand the underlying failure modes.

In summary, this work demonstrates the significant capacity fade and efficiency loss in commercial 18650 sodium-ion cells under high-rate cycling. The observed degradation highlights critical challenges for the long-term deployment of SIBs in real-world applications. Ongoing and future work will focus on microstructural analysis and

post-cycling diagnostics to reveal the specific degradation pathways and guide the design of more durable electrode materials and interfaces.

Acknowledgements

The project was carried out with support from EU StorAGE project (No. 101119913).

- 1. J. Wang and W. Azam, Geosci. Front., 15, 101757 (2024).
- 2. J. B. Goodenough, Energy Storage Mater., 1, 158–161 (2015).
- 3. V. Marangon et al., J. Power Sources, 634 (2025).
- 4. K. Bischof et al., J. Power Sources Adv., 27 (2024).
- 5. M. Jeong, H. Lee, J. Yoon, and W. S. Yoon, J. Power Sources, 439 (2019).
- 6. C. Deng et al., ACS Appl. Mater. Interfaces, 12, 51397–51408 (2020).

Solid Polymer Electrolytes for Li-ion and Post-Li-ion Batteries Based on Novel Salts and Plasticizers

L. Niedzicki^a, K. Rogala^a, M. Kasprzyk^a, M. Broszkiewicz^a

^aFaculty of Chemistry, Warsaw University of Technology, Noakowskiego 3, Warsaw 00-664, Poland

Lithium-conducting plasticized solid polymer electrolytes for Li-ion batteries and post-Li-ion batteries are developed based on common polymers, in-house developed lithium salts (e.g. LiTDI, LiPDI, LiPCP) and plasticizers (ionic liquids with our proprietary anions). In the presented work, results on new electrolytes will be shown — conductivity, lithium cation transference number, their compatibility and thermal properties.

Lithium-ion (Li-ion) batteries are powering our micromobility, passenger cars, buses, trucks, ferries, unmanned vehicles, and, soon, planes. They also serve as a base for the milliseconds-reaction energy storage systems that are supporting the growth of renewable energy production. However, the race for the best performance – quick charging, high power, high energy density – comes at the cost of safety. This is where the all-solid-state batteries (ASSBs) come in. Particularly, Lithium-Sulfur ASSBs combine safety and high energy density, but all ASSBs struggle with high power of charge and discharge due to poor ionic transport of solid electrolytes. All-solid-state Liion and post-Li-ion batteries require new solutions for electrolytes to be competitive parameters-wise with liquid-based Li-ion batteries. Thus, our approach is to employ new generations of lithium salts and plasticizers proprietary to our group.

During the presentation, we will present our newest results on solid polymer electrolytes development. Our plasticized polymer electrolytes show higher conductivity and potential for lower manufacturing cost compared to commercial and state-of-the-art solutions. They also exhibit high thermal stability (over 250°C), are not based on sophisticated nano- or microstructure, and are stable against moisture, making their application easier, scalable and less costly by enabling thermal techniques of coating and cell assembly (e.g. extrusion).

Hard Carbon-Tin Composite as High-Capacity Anodes for Sodiumion Batteries

A. Šimek^a, T. Kazda^a and O. Čech^a

^a Department of Electrical and Electronic Technology, Brno University of Technology, Brno 616 00, Czech Republic

Hard carbon and tin composites are being investigated as promising anode materials for sodium-ion batteries due to the high theoretical capacity of tin and the structural stability of hard carbon. Cyclic voltammetry reveals distinct alloying/dealloying peaks associated with sodium and tin phases, while initial galvanostatic cycles at 0.1 C show a clear voltage plateau associated with the formation of Na–Sn alloys. However, extended cycling at 0.2 C shows a significant decrease in capacity and suppression of tin-related activity, resulting in performance lower than that of the original hard carbon. These results highlight the potential and limitations of Sn additives and suggest directions for improving electrode design.

Introduction

The growing demand for sustainable and cost-effective energy storage has driven significant interest in sodium-ion (Na-ion) batteries as an alternative to lithium-ion (Li-ion) systems. While Li-ion batteries currently dominate the market due to their high energy density and proven technology, concerns about the availability of lithium sources, costs, and the geopolitical distribution of key raw materials and their processing capacities have highlighted the need for alternative technologies [1]. Na-ion batteries offer several advantages, including the availability and low cost of sodium, higher safety, and better performance at low temperatures. Although Na-ion systems generally have lower gravimetric energy density (100-160 Wh.kg⁻¹) compared to Li-ion (150-280 Wh.kg⁻¹) and lower operating voltage, they are increasingly considered suitable for applications such as stationary energy storage and low-cost electromobility, where cost and resource sustainability are critical [2].

Anode materials for Na-ion

Carbon materials are among the most promising anodes for Na-ion batteries because conventional graphite used in Li-ion systems cannot effectively accommodate larger sodium ions due to the mismatch in ion radius sizes (~1.02 Å for sodium and ~0.76 Å for lithium) [3]. This limitation has led to research into alternative carbons, such as hard carbon (HC) and soft carbon (SC), which offer disordered structures that enable sodium storage through intercalation, adsorption, and pore filling. Although their capacity is lower than that of graphite in Li-ion batteries, they provide a practical and scalable solution for Na-based energy storage, with HC being particularly notable for its stability and structural resilience [4].

Hard carbon is a widely studied anode material for Na-ion batteries, offering a reversible capacity of around 300 mAh.g⁻¹. Despite its stability, hard carbon suffers from low initial Coulombic efficiency and electrolyte decomposition. To address this

issue, alternative materials have been explored, including alloy-type anodes such as Sn, which offers high theoretical capacity (847 mAh.g⁻¹), excellent conductivity, and the ability to alloy with sodium. Sn forms Na₁₅Sn₄ through a multi-step alloying process, making it attractive for SIBs. However, during cycling, large volume expansion (~420 %) occurs, leading to mechanical degradation, unstable SEI formation, and poor long-term performance. Strategies to mitigate these issues include nano structuring, integration with conductive matrices (e.g., carbon), and electrolyte optimization. Sn-based composites show improved durability, but further development is needed to achieve scalable and stable anodes for practical Na-ion battery applications. [5]

Results and Discussion

To verify the electrochemical properties of Sn, a hard carbon-tin (HC-Sn) composite was prepared. For the initial research, 20% tin powder (FICHEMA) was added to hard carbon (Curranode type 2, 9 µm). The resulting electrode paste composition was 85 wt. % active material (HC-Sn 80-20), 5 wt. % conductive additive (Super P), and 10 wt. % carboxymethyl cellulose (CMC) binder. Demineralized water was used as the solvent. The electrode paste was prepared in a Fritsch Pulverisette 7 planetary mill using a ZrO bowl and 10 mm diameter ZrO balls. After mixing, a 200 μm layer was applied to carbon-coated aluminium foil using a K-hand coater. The applied layer was then dried at 50 °C, followed by cutting out electrodes with a diameter of 18 mm, which were pressed at a pressure of 30 kN and finally dried in a vacuum dryer at 130 °C. The dried electrodes were transferred to a Jacomex glove box (H₂O and O₂ < 1 ppm), where test electrochemical half-cells (EL-CELL) were assembled, containing the prepared electrodes as working electrodes, metallic sodium as the counter electrode, a Whatman GF/C separator, and 1M NaClO₄ in EC-PC 1-1 (v-v) electrolyte. Electrochemical characterization was performed on a 24-channel BioLogic BCS-805 battery cycler. The measurement procedure consisted of cyclic voltammetry at different scan rates (5; 1; 0.5; and 0.1 mV.s⁻¹) and galvanostatic cycling at 0.1 and 0.2 C. Both procedures were performed in the potential range of 0.01-2.5 V.

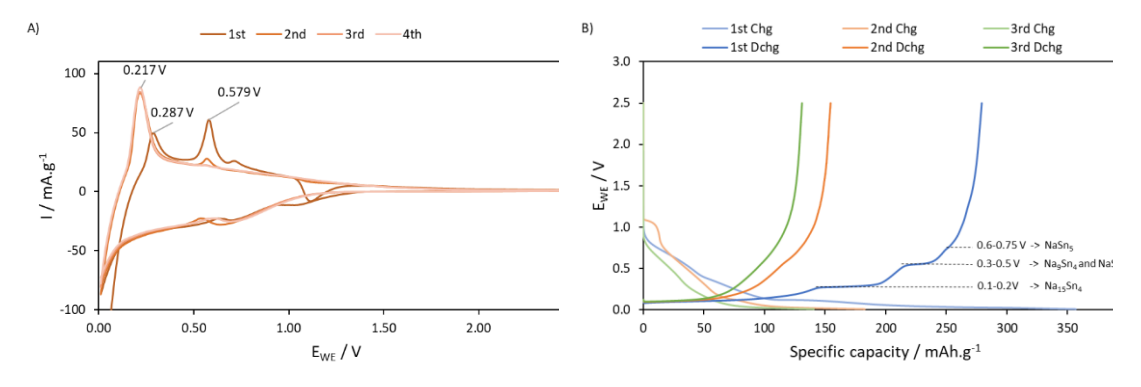


Figure 1. A) cyclic voltammetry at 0.1 mV.s⁻¹; B) formation cycles at 0.1C.

Figure 1.A) shows cyclic voltammetry of the HC–Sn composite recorded at 0.1 mV.s⁻¹ over four cycles. During the first cycle, a desodiation peak of HC appears at 0.29 V, which shifts to 0.22 V in subsequent cycles. This shift is caused by minor irreversible sodium intercalation, which changes the surface properties and reduces overpotentials after the first cycle. In addition, a pronounced anodic peak appears at 0.58 V, corresponding to the dealloying of sodium from the Na_xSn phases, indicating the electrochemical activity of the Sn additive. However, this peak gradually decreases with repeated cycles, probably due to volume expansion and pulverization of Sn

particles, leading to loss of electrical contact, increased resistance, and reduced reversibility of the alloy.

Figure 1.B) shows the galvanostatic discharge curves of the HC-Sn composite during the initial cycles at 0.1 C. During the first discharge, well-defined voltage plateaus are observed, corresponding to different phases of Na-Sn alloying, as highlighted in the figure. However, the HC-Sn composite exhibits a relatively low initial coulombic efficiency (ICE) of 78.2%, followed by a significant decrease in capacity in subsequent cycles. As the cycles progress, the voltage plateaus gradually disappear and the discharge profiles begin to resemble those of pure HC with reduced capacity. This degradation is likely caused by significant volume changes associated with the alloy and the distribution of the Sn alloy, which lead to particle cracking, structural instability, and loss of electrical connectivity, ultimately reducing the contribution of the active material to the capacity.

Conclusion

The addition of Sn to HC significantly increases the initial capacity of the anode through alloying reactions with Na. However, electrochemical performance suffers from poor cycling stability due to mechanical degradation of the active material. Future work should focus on improving structural integrity, e.g., by optimizing particle size and distribution or using buffering matrices, in order to fully exploit the potential of Sn-HC composites for practical Na-ion battery applications.

Acknowledgments

This work was supported by the specific graduate research of the Brno University of Technology No. FEKT-S-23-8286. Authors gratefully acknowledge the financial support of the Technology Agency of the Czech Republic (project No. TK04030083).

- 1. N. Tapia-Ruiz, S. R. P. Silva, T. B. M. Adair, S. Adamson, C. A. Bridges, G. Cibin, et al., J. Phys. Energy, 3(3), 031503 (2021).
- 2. J.-Y. Hwang, S.-T. Myung, and Y.-K. Sun, Chem. Soc. Rev., 46(12), 3529 (2017).
- 3. N. Yabuuchi, K. Kubota, M. Dahbi, and S. Komaba, Chem. Rev., 114(23), 11636 (2014).
- 4. Z. Jian, C. Bommier, L. Luo, Z. Li, W. Wang, C. Wang, P. A. Greaney, and X. Ji, Chem. Mater., 29(5), 2314 (2017).
- 5. J. K. Amai, The Effect of Micro-Sized Tin/Hard Carbon Composition on Sodium-Ion Battery Performance, Ph.D. Dissertation, 2025

Macroporous Carbon Additive Enhancing the Cycling Stability of Li-sulfur Batteries

M. Zukalová^a, T. Supiňková^a, and L. Kavan^a

^aJ. Heyrovský Institute of Physical Chemistry, Czech Acad Sci, Dolejškova 3, Prague 8, Czech Republic

Li-S batteries are particularly attractive due to their high theoretical capacity of 1675 mAh/g, the abundance of raw materials, low cost, and environmental friendliness of the system. Despite the undeniable progress made in the development of this technology in recent years, the main issue with Li-S batteries remains the decline in charge capacity during long-term cycling. This decline is primarily caused by the high reactivity of lithium polysulfides, which manifests as the so-called "shuttle effect"—a phenomenon where less reduced polysulfides oxidize more reduced ones, resulting in energy loss.

Various approaches have been proposed to address this issue, such as electrolyte modification using organic solvents that better dissolve polysulfides, or engineering the cathode surface—e.g., through the use of porous conductive carbon—to ensure rapid reduction of sulfur at the surface while trapping the formed polysulfides in the pores, preventing their diffusion to the anode.

In our research, we used monodisperse macroporous carbon (Figure 1) as the cathode material, prepared via glucose pyrolysis using silica spheres as a template. The Li-S battery with a cathode made from this macroporous carbon exhibited an initial capacity of over 700 mAh/g of sulfur. The capacity loss over 120 cycles at a rate of 0.1 C was less than 10%.

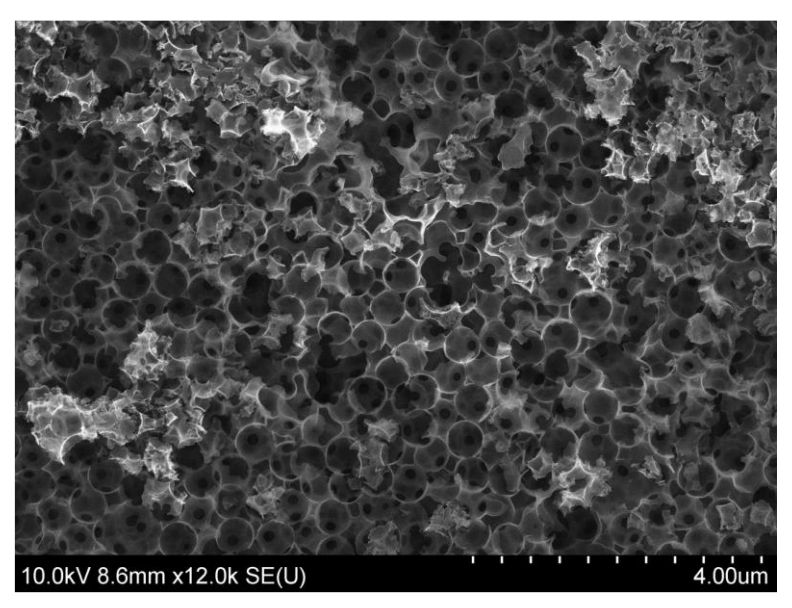


Figure 1: SEM image of macroporous carbon prepared by templating with monodisperse silica spheres

Acknowledgment

This work was supported by the EU Horizon Europe project No. 101202842/ANGeLiC.

Environmental Impacts of Alternative Fuels in Public Transportation

M. Fridrich^{a, b}, E. Sedláčková^a, J. Weinzettel^{a, b}

^aDepartment of Electrotechnology, Czech Technical University in Prague, Prague, Czech Republic

^bCharles University, Environment Centre Prague, Czech Republic

This study provides a detailed Life Cycle Assessment (LCA) study of public transport vehicles, delivering a comprehensive evaluation of both fossil fuel-powered and alternative fuel options. The research underscores the significance of renewable energy sources, focusing on fuels such as biomethane and electricity derived from advanced future energy grids, wind power, and photovoltaic systems. By exploring these alternatives, the study aims to highlight their potential to reduce the environmental impacts associated with public transportation. The study also indicates that biomethane could serve as a transitional energy source towards electric vehicles powered entirely by renewable energy. It evaluates each stage of a vehicle's life cycle (excluding the end-of-life phase) from production to use, while considering the vehicle's lifespan, ensuring a complete understanding of its environmental footprint.

Introduction

Urban transportation poses challenges like congestion, accidents, noise, air pollution, and greenhouse gas emissions. To mitigate these impacts, it is vital to optimize transport networks and promote sustainable mobility, prioritizing cleaner and more efficient modes of travel. Public transportation options include trams, trains, metros, and buses, with this study focusing on bus transport, particularly in smaller cities lacking rail systems. Buses play a key role in reducing traffic congestion and emissions, contributing significantly to urban mobility. Larger buses enhance comfort by offering more seating and luggage space but require careful infrastructure planning to ensure smooth traffic flow [1].

Choosing public transport, such as buses, over private cars can notably lower greenhouse gas emissions. In the U.S., public transportation reduces annual CO₂ emissions by 37 million tonnes, cutting individual emissions by 45% and improving air quality [2]. Over the past decade, the adoption of alternative fuel buses has risen. In 2012, diesel-powered buses accounted for 89% of new purchases globally but dropped to 72% by 2020, while hybrid, electric, and fuel cell buses increased from 6% to 15%, and CNG/LNG (Compressed Natural Gas/Liquefied Natural Gas) buses rose from 5% to 13%. Europe leads in the adoption of alternative powertrains, with 30% of new buses featuring electric variants, though it holds just 5.3% of the global bus market. Conversely, China dominates the global bus market with a 26.3% share, where 28% of new buses use alternative powertrains [3]. A critical environmental issue of bus transport is greenhouse gas emissions, alongside nitrous oxides (NOx) and particulate matter (PM2.5/10), which significantly affect air quality [4].

Results

A comprehensive cradle-to-wheel Life Cycle Assessment was carried out to assess the environmental impacts (EIs) associated with public transportation systems, with buses serving as a representative vehicle type. The study compared diesel-powered buses with those featuring electric powertrains and buses operating on bioCNG (compressed methane derived from biomass). The LCA study was conducted for the Czech Republic environment due to its geographical proximity and the characteristics of its energy sector. The Czech energy mix shows potential for reducing its dependence on fossil fuels and has a defined trajectory toward increasing the share of renewable energy sources in the long term. The scope of the LCA study included the whole life cycle of vehicle production and its usage (including fuel production and the effects of vehicle use over time). The end of life of the vehicle was excluded.

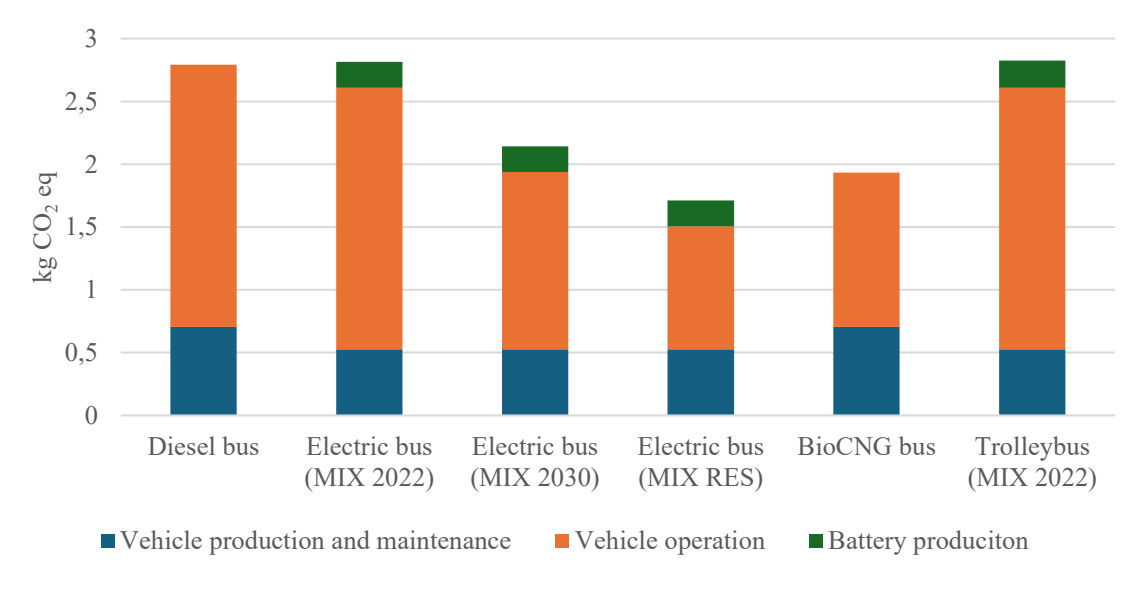


Figure 1: Comparison of selected vehicles in climate change impact category.

In addition, the EIs of vehicles' life cycle were divided into three categories: vehicle production and maintenance, battery production and vehicle operation (including fuel-related emissions and emissions from wear and tear). A brief examination, presented in Figure 1, indicates considerable potential for using alternative fuels derived from renewable energy sources. In the climate change impact category, the environmental impacts of electric vehicles powered by an energy mix with a higher share of renewable sources, as well as those of bioCNG-powered vehicles, are substantially lower compared to diesel buses. In general, buses powered by alternative fuels demonstrate lower environmental impacts compared to fossil-fuel-powered buses. Notable exceptions include the Electric Bus (MIX 2022) and the Trolleybus (MIX 2022), whose environmental performance closely aligns with that of the Diesel Bus. Across all bus variants and impact categories considered, the vehicle operation phase represents the largest contribution to total environmental impacts in categories particularly relevant to the transportation sector, such as particulate matter formation and photochemical ozone formation. Consequently, reducing emissions associated with vehicle operation remains a central priority. A more detailed evaluation with a focus on additional LCA Impact categories is going to be included in the full paper.

Acknowledgments

This work was supported by the Grant Agency of the Czech Technical University in Prague, grant No. SGS23/058/OHK3/1T/13 and by the Czech Science Foundation, grant No. 23-07984X.

- 1. De Dominicis, L., Berlingieri, F., d'Hombres, B., Gentile, C. et al., Report on the Quality of life in European cities, 2023, European Commission: Directorate-General for Regional and Urban Policy, Publications Office of the European Union (2023)
- 2. Andy Pei, 5 Environmental Benefits of Sustainable Transportation, https://transportation.ucla.edu/blog/5-environmental-benefits-sustainable-transportation, UCLA, (cited 12.12. 2024)
- 3. Mahmoud, M., Garnett, R., Ferguson, M., and Kanaroglou, P., Electric buses: A review of alternative powertrains, 62, p. 673–684, Renewable and Sustainable Energy Reviews (2016)
- 4. Simon, B., Tamaska, L., & Kováts, N., ANALYSIS OF GLOBAL AND LOCAL ENVIRONMENTAL IMPACTS OF BUS TRANSPORT BY LCA METHODOLOGIES, 38 (2), p. 155-158, HUNGARIAN JOURNAL OF INDUSTRIAL CHEMISTRY VESZPRÉM (2010)

Impact of Particle Size Distribution on the Behavior of Lithium-ion Batteries Under Dynamic Operation

N. Klusoňová^a, F. Kekula^b, J. Kasper^a, J. Zemen^a, J. Sadil^b, V. Knap^a

^aDepartment of Electrotechnology, Faculty of Electrical Engineering, Czech Technical University, Prague, Czech Republic

^bDepartment of Transport Telematics, Faculty of Transportation Sciences, Czech Technical University, Prague, Czech Republic

Understanding the impact of particle size distribution on the performance of lithium-ion batteries (LIBs) is critical for improving electrochemical models used in automotive applications. This work compares three physics-based models of varying complexity, each representing electrode microstructure and particle size effects to a different degree. The models were implemented using the Python Battery Mathematical Modelling (PyBaMM) framework and parametrized based on a modified dataset from Chen et al., with adjustments reflecting the characteristics of a commercial 21700 LG M50LT cell. Experimental validation was performed using voltage data measured under multiple repetitions of the Worldwide Harmonized Light Vehicles Test Cycle (WLTC), representing realistic automotive load conditions.

Introduction

Battery energy storage systems are essential in the transition to low-emission transport and renewable energy integration. Lithium-ion batteries (LIBs) dominate this field due to their high energy density, power capability, and decreasing costs. Despite significant advances in modeling battery behavior, most physics-based models still assume uniform particle size within electrodes, which oversimplifies the real microstructure composed of particles with varying sizes and morphologies [1][2][3]

To investigate how particle size distribution affects battery behavior, three physics-based models were implemented and compared: the Doyle-Fuller-Newman (DFN), Many-Particle Model (MPM), and Many-Particle Doyle-Fuller-Newman (MP-DFN). While the DFN provides a spatially resolved electrochemical description of the full cell assuming monodisperse particles, the MPM extends the single-particle approach by incorporating a continuous particle size distribution. The MP-DFN combines both features, allowing spatial resolution across the electrode and variation in particle radii.

The models were parametrized for a commercial cylindrical lithium-ion cell and validated using experimental voltage data recorded under the Worldwide Harmonized Light Vehicles Test Cycle (WLTC), a standard dynamic driving profile used to represent real automotive usage.

Models and Methods

All simulations in this work were performed using the open-source Python Battery Mathematical Modelling (PyBaMM) framework. Three electrochemical models of increasing complexity were implemented. Each model captures different aspects of lithium-ion cell behavior, particularly with respect to particle size assumptions and spatial resolution. The goal was to evaluate how these structural differences affect the predicted voltage response of a lithium-ion cell under dynamic conditions. All models were parametrized using a modified dataset by Chen et al. [4], with partial adjustments for the LG M50LT cylindrical cell [5].

Many-Particle Model

The Many-Particle Model builds on the Single-Particle Model (SPM) by introducing a continuous distribution of particle sizes. Instead of assuming a single representative radius, the model represents the electrode as a spectrum of spherical particles, typically weighted by surface area. While it neglects spatial variations in the electrolyte or across the cell thickness, it provides a more realistic approximation of intra-particle diffusion and reaction kinetics affected by particle size variability [6][7].

Doyle-Fuller-Newman model

The Doyle-Fuller-Newman model is a pseudo-two-dimensional (P2D) electrochemical model that includes spatial resolution along the through-thickness direction of the cell and within electrode particles. It assumes all particles have the same radius, simplifying the microstructure while maintaining key features of lithium transport in both solid and electrolyte phases. Due to its balance between physical realism and computational efficiency, the DFN model is widely used in battery modeling [8].

Many-Particle Doyle-Fuller-Newman model

The Many-Particle DFN model extends the DFN formulation by incorporating a particle size distribution at each point in the electrode. This additional dimension allows the model to reflect heterogeneous diffusion dynamics and interfacial kinetics more realistically. Despite assuming spherical particles, the MP-DFN captures effects such as reaction heterogeneity and voltage relaxation that are not well reproduced by simpler models. This model provides the most detailed representation of lithium-ion cell behavior among the tested models [8][9].

Experiment

Experimental data used for model validation were obtained from a degradation campaign using commercial 21700 cylindrical lithium-ion cells (LG M50LT, 5 Ah). Each cell was initially charged using a constant-current constant-voltage (CCCV) protocol up to 4.15 V, corresponding approximately to 95 % state of charge (SOC). Following a short rest period, a driving profile based on the WLTC was applied in the form of a simulated dynamic current load.

This protocol was designed to replicate realistic automotive usage conditions. The WLTC profile was applied repeatedly to approximate the cumulative current demand

of a full-scale automotive battery. Model predictions were then compared with voltage data measured under dynamic load conditions.

Preliminary results indicate an observable effect of particle size distribution on model predictions, which will be further discussed in the poster presentation.

Acknowledgments

This work was supported by the Grant Agency of the Czech Technical University in Prague, grant No. SGS24/136/OHK3/3T/13, TACR, project no. TN02000054, and the project "The Energy Conversion and Storage", funded as project No. CZ.02.01.01/00/22_008/0004617 by Programme Johannes Amos Comenius, call Excellent Research.

- 1. M. Doyle, T. F. Fuller, and J. Newman, *J Electrochem Soc*, **140**, 1526–1533 (1993) https://iopscience.iop.org/article/10.1149/1.2221597.
- 2. M. T. Castro and J. D. Ocon, *J Electrochem Soc*, **171**, 123506 (2024).
- 3. N. Klusoňová et al., J Power Sources, 627 (2025).
- 4. C.-H. Chen et al., *J Electrochem Soc*, **167**, 080534 (2020).
- 5. N. Stapf et al., *J Electrochem Soc*, **172**, 060513 (2025).
- 6. https://docs.pybamm.org/en/stable/source/examples/notebooks/models/MPM.ht ml.
- 7. T. L. Kirk, J. Evans, C. P. Please, and S. J. Chapman, (2020) http://arxiv.org/abs/2006.12208.
- 8. F. Brosa Planella et al., *Progress in Energy*, **4**, 042003 (2022) https://iopscience.iop.org/article/10.1088/2516-1083/ac7d31.
- 9. https://docs.pybamm.org/en/stable/source/examples/notebooks/models/DFN-with-particle-size-distributions.html.

Assessing Battery Separator Integrity: Microstructure, Phase, and Safety Analysis

G. Kratošová^a, G. S. Martynková^a, S. Holešová^a, and L. Plesník^{a, b}

^a Nanotechnology Centre, CEET, VSB-Technical University of Ostrava, 17. listopadu 2172/15, 708 33 Ostrava, Czech Republic

^b Faculty of Materials Science and Technology, VSB-Technical University of Ostrava, 17. listopadu 2172/15, 708 33 Ostrava, Czech Republic

The structural integrity of battery separators is essential for ensuring the safety and performance of lithium-ion batteries. Study highlights the need for continuous development, optimization, and modification of separator materials, with a focus on controlling their physicochemical properties and behaviour under operational stress. A combination of advanced techniques—including scanning electron microscopy (SEM), energy-dispersive X-ray spectroscopy (EDS), X-ray diffraction (XRD), and Fourier-transform infrared spectroscopy (FTIR)—is applied to characterize separator structure, composition, and thermal stability. Correlative analysis enables a more comprehensive understanding of degradation mechanisms and structural changes over time. Particular attention is given to postmortem analysis of damaged separators, which helps identify failure modes and root causes of safety-related issues in cells. These findings will contribute to improved material design, quality control, and long-term battery reliability.

Overview

The separator in lithium-ion batteries is a critical component that physically separates the cathode from the anode while allowing the transport of electrolyte ions. Its mechanical, thermal, and chemical properties significantly influence the battery's performance, lifespan, and, most importantly, safety. Since the separator may be exposed to extreme temperatures, mechanical stress, or chemical degradation during operation, it is essential to closely monitor its behavior under various operating conditions and states of the battery. Understanding these changes is crucial not only for predicting potential failures but also for designing optimal separator compositions and modifications that can enhance the overall stability and safety of the battery system.

To analyze the chemical composition, structural properties, morphology and degradation state of the battery separator material, a set of complementary analytical techniques is utilized. X-ray diffraction (XRD, Ultima IV, Rigaku, Japan) was employed to identify crystalline phases and assess the degree of crystallinity of the polymer separator, providing insight into its structural arrangement and changes in end-of life state. Scanning electron microscopy (SEM, JEOL JSM 7610F+, Japan) combined with energy-dispersive X-ray spectroscopy (EDS, Oxford Instruments, UK) was used to examine the surface morphology and to perform elemental mapping on both sides of the separator. Fourier-transform infrared spectroscopy (FTIR, Nicolet iS50, ThermoScientific, USA) was used to detect characteristic functional groups and

molecular bonds, aiding in the identification of the polymeric composition. Moreover, CPEM correlation method (AFM+SEM) was employed to combine advantages of both imaging methods in revealing the microstructure separator changes and visualizing the depth profile of polymer material. The polymer separator membrane, along with other cell components, was obtained through manual disassembly of a discharged Li-ion battery.

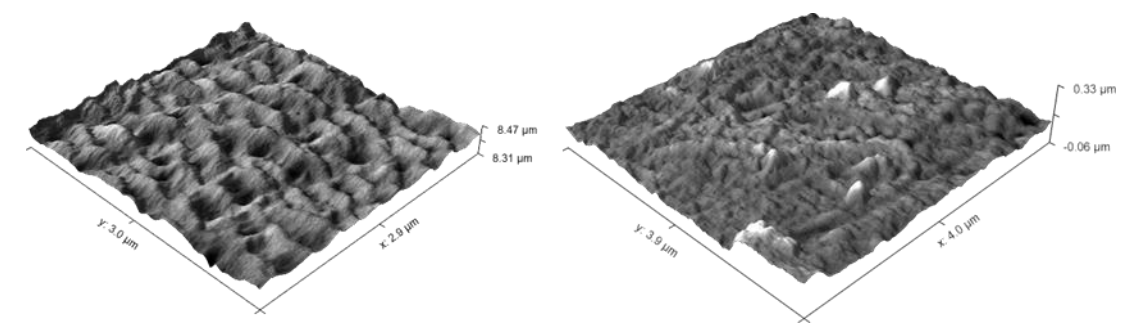


Figure 1. A) CPEM of original Celgard separator; B) CPEM of failure Celgard separator

Conclusion

The importance of integrating microscopy, crystalline lattice diffraction, and thermal methods into modern battery research and safety assessments are discussed. Separators play a crucial role in ensuring the safety of lithium-ion batteries, as they prevent direct contact between the electrodes while allowing ion transport. One of the most serious risks in battery operation is thermal runaway—a dangerous chain reaction that can lead to overheating, fire, or even explosion. Well-designed separators can significantly reduce this risk by maintaining structural integrity under high temperatures and shutting down ion flow when overheating occurs. As the demand for safer and more reliable energy storage systems grows, the future of battery safety will increasingly rely on the development of advanced separator materials with enhanced thermal, mechanical, and chemical properties as well on advanced analytical investigation of separators in various states of use.

Acknowledgments

The work was supported by the project MATUR - Materials and technologies for sustainable development within the Jan Amos Komensky Operational Program (project reg. No.CZ.02.01.01/00/22_008/0004631) and the REFRESH - REFRESH - Research Excellence For REgion Sustainability and High-tech Industries (project reg. No.CZ.10.03.01/00/22_003/0000048) via the Operational Program "Just Transition" and and CZ.10.03.01/00/22_003/0000045 "Circular enonomy R&D Centre – CirkArena, The Operational Programme Just Transition".

- 1. G. S. Martynková, G. Kratošová, S. Brožová, S. K. Sathish, in *Recyclability, circular economy, and environmental aspects of lithium–sulfur batteries*. Lithium-Sulfur Batteries: Materials, Challenges and Applications, p. 653–72 (2022).
- 2. J. Choi, P. J. Kim, in *A roadmap of battery separator development: Past and future*. Curr Opin Electrochem, **31**(2022).

Development of an Effective Second-Life Protocol for Rechargeable Batteries for Medical Electronic Devices

M. Rae^a, M. Ottaviani^b, M. Singh^a

^aDepartment of Mathematics and Statistics, the University of Limerick, Limerick V94T9PX, Ireland

^bDepartment of Physics, Technological University of the Shannon, Moylish Campus, Limerick V94EC5T, Ireland

> Many medical electronic systems (MESs) in hospitals rely on rechargeable batteries to ensure an uninterrupted power supply (UPS) – a necessity for many MESs such as ventilators, infusion pumps, and multiparameter physiological monitors. Thus, battery monitoring systems (BMSs) are paramount in ensuring this reliability. Hospitals often lack sufficient BMSs, therefore, premature battery replacement is common; owing to a more rigid and systematic battery replacement process as opposed state of health (SoH)-based replacements. The integration of a more scientifically rigorous BMS and maintenance scheme for MES batteries will significantly improve the lifespan and efficiency of rechargeable battery use and the recycling/repurposing of batteries. This study proposes a BMS suitable for hospitals to address this shortcoming while also attaining the appropriate data for performing end-of-life (EoL) diagnostics and forensic analysis of battery degradation. The model will optimise battery use and suggest the second life use-case based on the batteries' expected degradation trends.

Overview of the Problem and Solution Approach

Hospitals are increasingly significant consumers of rechargeable batteries due to the development of more MEDs that include a rechargeable battery for ensuring UPS or portable operation. The approximated annual battery consumption rate in a single large hospital was 97,000 in the USA, 2007 [1]. Furthermore, the global medical battery market size is estimated to grow from 1.74 billion USD in 2025 to 2.77 billion USD by 2034 with Europe holding approximately 28% of this global medical battery market in 2024 [2]. Improving the lifespan and recycling of these batteries is essential for fostering a greener and more sustainable future of using battery operated devices. One promising approach for improving this factor is by assigning a second-life for the batteries which have reached their EoL (SoH < 70-80%). This requires monitoring the state of charge (SoC) and SoH during battery use in addition to some degradation diagnosis once the SoH reaches the EoL range. Machine learning models demonstrate significant potential in reverse aging and degradation modelling using non-invasive measurements taken at a single point in time [3][4][5]. Furthermore, the accuracy of such models is greatly enhanced by the availability of previous cycling data. Such models provide valuable insights into the cell's internal structural and chemical degradation mechanics which is crucial to forecast future degradation based on different use cases. Forecasting the degradation of second life batteries in various use-case scenarios will significantly enhance the efficiency, safety, and confidence in allocating

batteries with SoH < 70-80% to a second use [4]. This will ultimately drive the confidence in policy changes necessary to support and enforce this essential improvement in battery recycling in hospitals. This presentation will focus on the key modelling developments and machine learning approaches to bridge the gap in battery aging forensics and determination of the optimal second life use-case for rechargeable batteries based on their current SoH and degradation characteristics. It will also relate to the significance of policy research and the need for engineering, modelling, and policy developments to work in parallel.

Machine Learning BMS

SoH and SoC are significant parameters to monitor and predict during battery use as they directly impact the efficiency and reliability of the battery. Numerous BMSs have been developed and presented in the available literature, however many of these prioritise extreme accuracy over practicality and computational efficiency. While a highly accurate BMS is desired, it may not be practical to measure the required features or to attain the required number of observations necessary for the model to work. Therefore, we propose a BMS that favours coarse datasets with practical and non-invasive measurements and high computational efficiency. Simple artificial neural network architectures, such as multilayer perceptron (MLP) and long short-term memory (LSTM), have been successfully implemented for efficient SoC estimation and prediction using extremely coarse datasets with non-destructive measurements [6].

Second-Life Protocol.

The information from the BMS coupled with single-point-in-time measurements are leveraged to perform forensic analysis at the EoL of the battery cell. This will determine the mode of degradation during the cells previous use-case and subsequently determine the optimal second-life use-case scenario for the specific cell. However, the integration of such a system into the health sector will need to be accomplished with a rigorous analysis of policies. While a perfect BMS and second-life forecasting model can be developed considering all practicality of the hospital settings, it is essential that the proposed solution considers the legislative policies surrounding its integration and adoption in the health sector.

Acknowledgments

This ongoing work is possible due to the collaboration between MACSI centre and Bernal Institute at the University of Limerick, Ireland; the Physics and Medical Science Departments of the Technilogical University of the Shannon, Ireland; and the Brno University of Technology, Czech.

- 1. J. D. Plisko, D. Choinière, American Nurse Journal, (2007).
- 2. R. Patil and A. Shivarkar, *Precedence Research*, Report 4455, (2025).
- 3. M. Ansari, S. B. Torrisi, A. Trewartha, S. Sun, *Journal of Energy Storage*, **81**, (2024).
- 4. K. Inwoo, K. Hyunjae, A. Seongha, O. Jihoon, K. Minsoo, W. C. Jang, p. 3784-3794, *Energy & Environmental Science*, **18**(8), (2025).

- 5. C. R. Birkl, M. R. Roberts, E. McTurk, P. G. Bruce, D. A. Howey, *Journal of Power Sources*, **341**, (2017).
- 6. M. Rae, M. Ottaviani, D. Capkova, T. Kazda, L. J. S. Maria, K. M. Ryan, S. Passerini, M. Singh, *Journal of Power Sources*, **646**, p. 236929, (2025).

Advancing High-Energy Battery Technologies: Scaling High-Si and High-Ni NMC9055 Cells to Mass Production

B. Rajagopalan^a, D. Ezhumalai^a, S. Narayanan^{a,b}, J. Reiter^a

^aInobat R&D and production centre, 919 42, Voderady, Slovakia

^bInstitute of Applied Physics, Technische Universität Wien, 1040 Vienna, Austria

InoBat, a subsidiary of Slovakia-based InoBat i.s.a., is pioneering lithium-ion battery technology through vertically integrated, in-house R&D and manufacturing. The company focuses on full-cycle innovation—from coin cell research to pilot-scale production of large-format cells (10Ah-60Ah). In collaboration with Wildcat Discovery Technologies (WDT), InoBat employs high-throughput (HTP) screening to accelerate the discovery of optimized cathode, anode, and electrolyte chemistries by up to tenfold. A key achievement is the development of GEN4 B-chemistry containing high-nickel NMC9055 cathodes paired with high-silicon (Si-Gr) anodes, validated through hierarchical testing from coin cells to 1Ah multilayer pouch (MLP) cells. Optimized formulations reduced nickel dissolution and anode volume expansion, delivering up to 1,000 cycles at 80% state of health. Chemistry was successfully scaled to a 33Ah format, achieving energy densities exceeding 330 Wh/kg and obtaining UN38.3 certification.

InoBat: Pioneering Advanced Lithium-Ion Batteries Through In-House Innovation

InoBat, a subsidiary of Slovakia-based InoBat j.s.a., specializes in the in-house research, development, and manufacturing of advanced lithium-ion batteries for both domestic and international clients. Operating under one roof, the company conducts end-to-end development—from coin cell R&D and small-format cells to the production of large-format cells (ranging from 10Ah to 60Ah) on a pilot production line.

InoBat oversees every stage of the battery manufacturing process, from slurry preparation to cell formation, all carried out under strict cleanroom and dry room conditions to ensure high-quality prototyping.

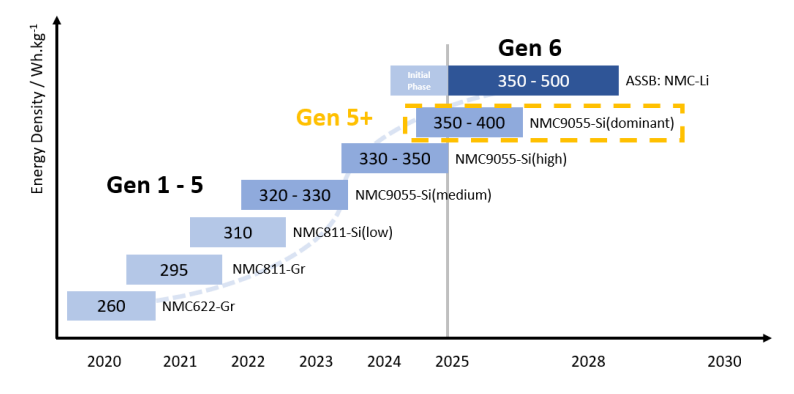


Figure 1 Inobat roadmaps on chemistry development.

The company's research activities are designed to deliver highly accurate and reliable results. InoBat successfully developed and optimized various cell chemistries to meet evolving energy density targets. InoBat, in collaboration with WDT, is using high-throughput (HTP) screening to identify and develop novel cathode, anode, and electrolyte compositions. This approach significantly accelerated the discovery processed by approximately tenfold compared to traditional research methods. Figure 1 presents the InoBat cell chemistry development roadmap, outlining the progression of cell generations from GEN1 through GEN6.

<u>Lab-scale development and validation of GEN4 high-Ni NMC9055/Si-Gr based B-cell chemistry</u>

The research and development program implemented a comprehensive screening process across all key battery cell components—including the electrolyte, anode, cathode, and separator to achieve targeted specific key performance indicators (KPIs). For example, electrode materials were evaluated across a range of formulations comprising different binders, conductive additives, and active materials obtained from various suppliers, each exhibiting unique physicochemical properties. The candidate selection and subsequent validation were performed across multiple hierarchical stages, beginning with coin-type cells and progressing through single-layer pouch configurations to multilayer pouch cells with capacities up to 1Ah. The failure and degradation mechanisms of cell chemistry were investigated using Incremental Capacity Analysis (ICA, dq/dv).

A key achievement of the collaborative research and development program is the development of GEN4 B-Chemistry: a high-silicon anode paired with a high-nickel NMC9055 cathode which is engineered to deliver enhanced longevity and efficiency. The GEN4 A-chemistry serves as the baseline formulation, delivering an energy density of 320–330 Wh/kg. Building on this foundation, B-chemistry was developed through targeted modifications of passive components, enabling energy densities exceeding 330 Wh/kg. A HTP screening process is being conducted to identify the optimal cathode composition with consistent properties that deliver reliable performance. Similarly, high-silicon (High-Si) hybrid anodes combined with graphite are being systematically evaluated through various configurations to achieve enhanced electrochemical performance. Electrolyte formulations are being strategically optimized to suppress nickel dissolution from high-nickel NMC9055 cathodes and to alleviate anode volumetric expansion and contraction during repeated electrochemical cycling, thereby enhancing overall cell stability and longevity. Figure 2 presents the cycling stability of large-format 1Ah multilayer pouch (MLP) cells incorporating the fully optimized high-nickel NMC9055 cathode and high-silicon (High-Si) anode. The performance was evaluated by comparing electrodes scaled up on a manufacturing line with those using electrodes from labs scale and baseline A-chemistry. The optimized B-chemistry electrodes demonstrated excellent stability, achieving up to 1,000 cycles with 80% state of health—an impressive result, particularly for cells utilizing highnickel NMC cathodes and high-silicon (High-Si) anodes. The enhanced performance observed in the scaled-up electrodes is attributed to optimized slurry preparation and film casting processes, which contribute to improved electrode homogeneity, microstructure, and overall electrochemical stability.

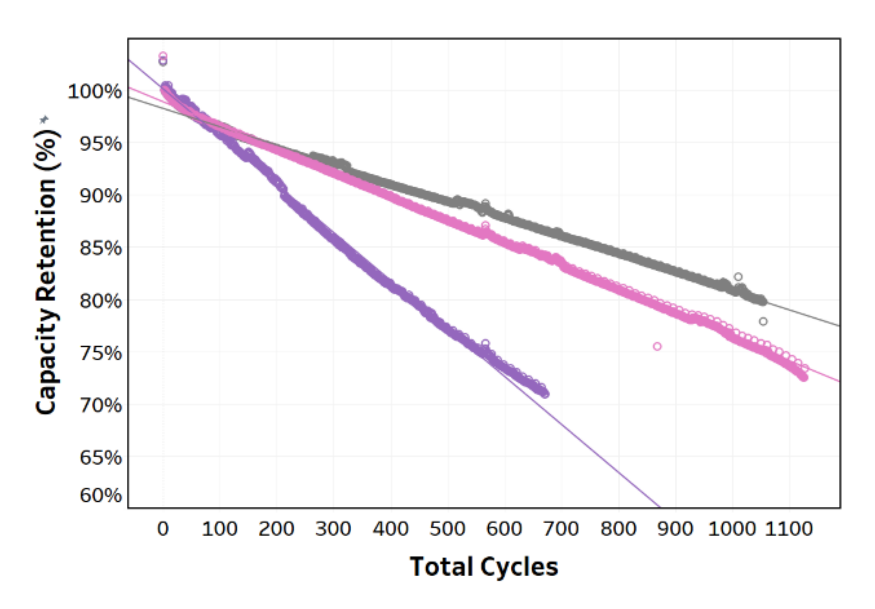


Figure 2 Cycling stability analysis of 1Ah GEN4 B-chemistry cells incorporating lab scale anode and cathodes (black) scaled up on a manufacturing line, and (pink) fabricated at laboratory scale. (blue) Battery cell containing B- chemistry cathode and A-chemistry anode produced in a manufacturing line. All cells were cycled between 2.5 V and 4.2 V at a C/3 rate under ambient temperature conditions.

Scaled up in a 33Ah cells.

Following successful validation in 1Ah cells, the NMC 9055/Si-Gr based Inobat B-cell chemistry was scaled up to a 33Ah format and meet the targeted energy density of >330Wh/kg. The scaled-up cells were subjected to extensive validation, including thorough safety and electrochemical performance assessments, ultimately achieving UN 38.3 certification.

Acknowledgments

The project was carried out with support from the EU-funded Important Project of Common European Interest (IPCEI) initiative, EU StorAGE project (No. 101119913), and SILION (co-financed by the *Technology Agency of the Czech Republic (TS01030029 TACR)*.

- 1 K.V. Graae, *J. Power Sources.*, **570**, 232993 (2023).
- 2. X. Zhang, *Energy storage Materials.*, **56**, 562 (2023).
- 3. Z. Cui, Adv. Mater., 36, 2409272 (2024).

Comprehensive Digital Twin for Stationary Battery Energy Storage

M. Sedlařík^a, P. Vyroubal^a, P. Tomíček^b, M. Mačák^c, M. Šedina^a, T. Kazda^a

 Department of Electrical and Electronic Technology, Faculty of Electrical Engineering and Communication, Brno University of Technology, Brno, Technická 10, 616 00, Czech Republic

^b Department of Microelectronics, Faculty of Electrical Engineering and Communication, Brno University of Technology, Brno, Technická 10, 616 00, Czech Republic

^c Electric Vehicle Technologies Transport Technologies, AIT Austrian Institute of Technology GmbH, Vienna, Austria

This work focuses on digital twin designed for stationary energy storage systems employing second-life lithium-ion batteries. The concept combines real-time monitoring of the physical system with a virtual counterpart built upon semi-empirical models, data-driven algorithms and reduced-order physical models. This hybrid modeling approach enables continuous estimation of critical battery parameters, including State-of-Charge, State-of-Health and internal temperature. By considering the higher variability of second-life cells, the proposed architecture supports advanced diagnostics, predictive maintenance strategies, and improved system performance.

Introduction

Digital twin technology is an important tool in the energy sector [1][2], offering new possibilities for monitoring, diagnostics and control of battery energy storage systems. A digital twin acts as a virtual counterpart of a physical system, using real-time operational data to estimate internal states, detect early signs of degradation, and predict system behavior over time. This approach allows for more efficient operation, improved safety and better maintenance planning.

Its application is particularly relevant in the field of stationary lithium-ion (Liion) battery systems, which play a significant role in supporting the integration of renewable energy into the power grid. These systems benefit from the high energy density, long cycle life and low self-discharge of Li-ion cells [3]. However, as these batteries age, their performance gradually declines due to calendar and cyclic degradation, leading to capacity loss and increased internal resistance. These effects become even more pronounced when batteries are reused in second-life applications, such as stationary storage systems following their retirement from electric vehicles.

Second-life batteries present additional challenges due to the higher variability in their electrical and thermal behavior. [4] This makes accurate tracking of their condition more difficult, yet even more necessary. In this context, a digital twin can provide valuable insights by continuously estimating key parameters such as State-of-Charge (SOC), State-of-Health (SOH), and Remaining Useful Life (RUL), enabling early detection of potential failures, supporting predictive maintenance strategies, and improving safety.

This work introduces a digital twin concept tailored specifically to stationary storage systems using second-life Li-ion batteries. The system uses physics-based models, data-driven methods, and ECMs to describe the battery storage system from different perspectives. The objective is to ensure the safe, efficient, and sustainable operation of battery storage systems across their prolonged service life.

Experimental

The experiment was conducted on a battery pack composed of NMC-based pouch cells arranged in an 8s3p configuration. The entire system (see Figure 1) is structured into two principal layers. The physical layer includes the battery storage system itself, the Battery Management System (BMS), which ensures proper battery operation, and the Monitoring System, which acts as an interface between the digital layer of the twin and the physical battery.

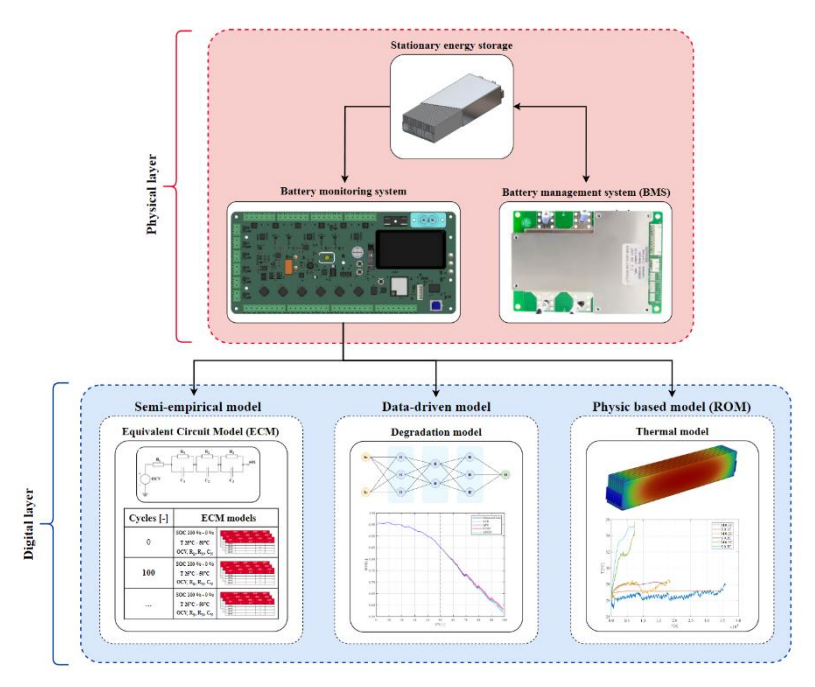


Figure 1. Pearson Correlation Analysis between input features and SOH.

The digital layer is represented by a combination of multiple modeling approaches that together describe the key characteristics of the battery storage system. These models differ in both methodology and complexity. Since the primary goal of the digital twin is to estimate the system states in real time, computationally intensive models need to be reduced to enable real-time analysis.

The semi-empirical model, based on an Equivalent Circuit Model (ECM), was characterized using the Galvanostatic Intermittent Titration Technique (GITT) method, which involves discharge pulses at 0.3 C followed by hourly rest periods, continued until the cut-off voltage of 2.65 V. This procedure enables the extraction of dynamic responses to current changes and allows identification of the RC elements across the full SOC range. These elements provide a simplified representation of the underlying electrochemical processes occurring within the battery. The thermal model is formulated using the finite element method (FEM), while the battery behavior in Ansys Fluent is also described using the ECM-based approach. The resulting coupled model is subsequently reduced to enable real-time analysis.

The data-driven degradation model, implemented as a feed-forward neural network, was developed using cycling data obtained under controlled conditions across

a range of temperatures (5 °C, 25 °C, and 45 °C) and depths of discharge (70 %, 90 %, and 100 %). This comprehensive dataset enables the model to account for a wide spectrum of aging mechanisms occurring under various thermal and operational stressors. In total, 500 full cycles were carried out on eight Li-ion cells to ensure sufficient statistical relevance and model generalizability. Discharge currents of 0.33 C/0.33 C were employed during the training phase, while test data included discharge rates of 0.2 C/0.3 C to evaluate the model's predictive performance under slightly shifted operational regimes.

Degradation indicators used for model development include variations in voltage slope during both charge and discharge phases, current decay duration during the constant voltage step, and features extracted from Incremental Capacity Analysis (ICA). Particular emphasis is placed on the analysis of charging cycles, as this phase offers higher practical relevance for integration into real-world battery management systems.

Conclusion

This work presents a comprehensive digital twin framework specifically designed for second-life Li-ion batteries in stationary energy storage applications. The proposed architecture integrates semi-empirical ECMs, data-driven neural networks, and physics-based thermal models to create a robust virtual representation of the physical battery system. The validation results demonstrate exceptional accuracy with the ECM model achieving 0.33% Root Mean Square Error (RMSE). The neural network implementation, utilizing a simple architecture with 3 hidden layers and 10 neurons, employed the Levenberg-Marquardt algorithm with linear transfer functions, achieving 1.4% RMSE when using charging cycles only and 1.9% RMSE with reduced input features.

Acknowledgments

This work was supported by the BUT specific research program (project No. FEKT-S-23-8286).

- 1. M. Liu et al., Energy, vol. 331, 2025
- 2. S. Ren, S. Chai, Z. Yang et al., Procedia Computer Science, vol. 261, 2025
- 3. C. R. Birkl, M. R. Roberts et al., ", Journal of Power Sources, vol. 341, 2017
- 4. M. F. Roslan, P. R. Satpathy, T. Prasankumar et al., Journal of Energy Storage, vol. 123, 2025

Advanced Application of Elimination Voltammetry with Linear Scan in Electroanalysis and Electrotechnology

L. Trnková^a

^aDepartment of Electrical and Electronic Technology, Faculty of Electrical Engineering and Communication, Brno University of Technology, Technická 10, 616 00 Brno, Czech Republic

Voltammetric methods are among the most widely used electrochemical techniques in both electroanalysis and electrotechnology, but their informative value in research is often insufficient. Therefore, the linear variable polarization potential (CV, LSV) techniques were extended in elimination voltammetry with linear scan (EVLS), which eliminates some chosen particular currents and preserves others. The method is used to investigate in detail the electrode/electrolyte interface and the reaction mechanisms of electrode processes. The article shows how valuable EVLS is for the characterization of materials and for obtaining new information about the catalytic effects of substances in electrochemical processes. The possibilities of EVLS application and the perspectives of its development are demonstrated in examples of the latest research.

Voltammetric methods have undergone various developments, which were initiated not only by the desire to increase sensitivity, selectivity and stability in electroanalysis but also by understanding the processes occurring at the electrode/electrolyte interface in electrotechnology [1]. To achieve these goals, there are hardware solutions using new technologies and materials, and software solutions using existing instrumentation.

We present an easily implementable software solution to the main shortcomings of linear sweep voltammetry, such as low sensitivity, high capacitive current content and the problem of overlapping signals in the form of elimination linear scan voltammetry - EVLS [2][3][4][5][6][7][8]. The method is based on the validity of the different behavior of individual partial currents (capacitive I_c , diffusion I_d , kinetic I_k) on the scan rate v and on the validity of the linear combination of these currents creating the total voltammetric current. The most pronounced dependence of the current component on the scan rate can be expected for the capacitive current component, where the exponent for v is one, i.e., $I_c = f(v)$. A smaller influence of the scan rate is noticeable for the diffusion current component, where the exponent is one half, $I_c = f$ $(v^{1/2})$. The kinetic component of the current is independent of the scan rate, which corresponds to an exponent equal to zero, $I_c = f(v^0)$. EVLS is able to eliminate or preserve certain selected current components $(I_c, I_d \text{ and } I_k)$ by sensing the total currents at different scan rates. One scan rate is the reference and the corresponding total current is the reference total current (I_{ref}). The current is measured at double and half the scan rate $(I_{2ref}, I_{1/2ref})$, then the integer is equal to 2. The integer (integer multiple) can be different, but from the point of view of possible errors in the EVLS procedure, it has been proven that integer 2 is more suitable [9][10].

We found that increased sensitivity and selectivity in electroanalysis can be expected especially in the case of a fully adsorbed electroactive particle subjected to an

irreversible electrode process, where the elimination of kinetic and capacitive currents while preserving the diffusion current provides a theoretically confirmed peak counter signal. This special peak-counterpeak signal was experimentally proved and subsequently used many times. [3][4][8][11][12][13][14][15].

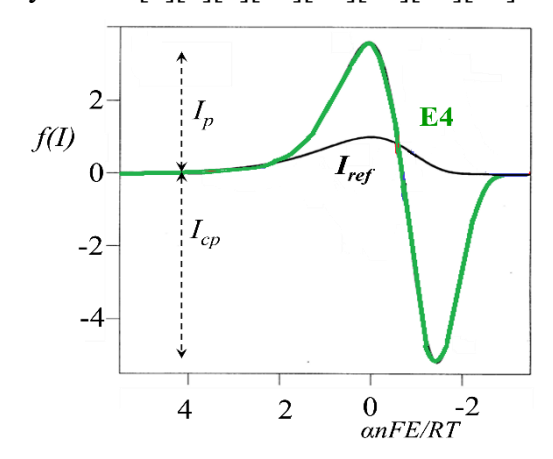


Figure 1. The theoretical EVLS curve of the function E4 (the elimination of I_c and I_k and conservation of I_d) for an adsorbed electroactive species, the x-axis corresponds to the dimensionless value $\alpha nFE/RT$.

Like any method, EVLS has its advantages and disadvantages, which we highlight through a SWOT analysis (Strength, Weakness, Opportunity, Treats). Nevertheless, EVLS offers a new tool that contributes to a better understanding of electrochemical processes and their mechanisms. Our latest research has shown that:

EVLS can be successfully used to test the electrode set-up and its proper function by cyclic voltammetric recordings of electrochemical probes such as $[Fe(CN)_6]^{3-/4-}$, $[Rb(NH_3)]^{3+/2+}$, $[IrCl_6]^{2-/3-}$. For reversible diffusion-controlled electron transfer without further complications (Nernst-type process), the EVLS function eliminating the diffusion component of the current (labeled E5 and E6) should provide a zero current line [16][17].

EVLS is a promising tool for determining the values of capacitive current components. Functions with elimination of diffusion and kinetic currents are included in this application. The remaining capacitive current can be an indicator of changes in the capacitance of the electric double layer [6][17].

EVLS is capable of using the elimination function E4 (elimination of I_c and I_k and conservation of I_d) to very quickly and easily detect the adsorption state of the electrochemically investigated substance by providing a characteristic peak-counterpeak signal (Figure 1) [2][3][4][5][6][10][11][13][14][15][18][19].

EVLS has found wide application in electrode materials, where the electrode surface can be pre-treated in such a way that scanning of the electrode at different scan rates takes place on the same surface (one of the most important prerequisites for successful evaluation of voltammetric data). This requirement is successfully met by a boron-doped diamond electrode (BDDE), which can be electrochemically pre-treated using a long-term polarization of the electrode at very negative or positive potentials with concentrated sulfuric acid. Pretreatment at negative potentials results in a hydrogen-terminated surface, and at positive potentials in an oxygen-terminated surface. Each type of chemical surface termination has different electrochemical features, and EVLS is able to contribute to revealing these features (J. Electroanal. Chem. 2025, accepted).

The outputs of the elimination functions should be understandable for correct and plausible interpretation. The content of EVLS is open for discussion, change, enrichment and closer sharing by the electrochemical community. EVLS results obtained under different experimental conditions can be a source for improving current or newly designed applications. In this way, EVLS can significantly contribute to R&D&I (Research & Development & Innovation) processes not only in electroanalysis but also in electrotechnology [6][10].

Acknowledgments

The author thanks all collaborators and students (Masaryk University, Mendel University, Charles University, J. Heyrovský Institute of Physics, University of Pardubice, Palacký University in Olomouc, Pavol Jozef Šafárik University in Košice) who participated in the research, development and innovation of EVLS. The author thanks the Grant Agency of the Czech Republic (GACR), the Ministry of Education, Youth and Sports (MEYS), and the company Metrohm of the Czech Republic for financial and work support. This work was supported by the specific graduate research of the Brno University of Technology No. FEKT-S-23-8286.

- 1. V. Adam, J. Hubalek, R. Kizek, *Int. J. Electrochem. Sci.*, **8**, 4363 (2013).
- 2. L. Trnkova, Chem. Listy, 95, 518 (2001).
- 3. L. Trnkova, J. Electroanal. Chem., **582**, 258 (2005).
- 4. L. Trnkova, J. Electroanal. Chem., 905, 9 (2022).
- 5. L. Trnková, *Chem. Listy*, **112**, 802 (2018).
- 6. L. Trnková, Chem. Listy, 118, 520 (2024).
- 7. L. Trnkova, O. Dracka, J. Electroanal. Chem., 413, 123 (1996).
- 8. L. Trnkova, R. Kizek, O. Dracka, *Electroanalysis*, **12**, 905 (2000).
- 9. O. Dracka, J. Electroanal. Chem., 402, 19 (1996).
- 10. X. C. Li, L. Trnkova, V. Hrdlicka, T. Navratil, *Talanta*, **284**, 14 (2025).
- 11. L. Trnkova, *Talanta*, **56**, 887 (2002).
- 12. L.Trnkova, F.Jelen, J. Petrlova, V.Adam, D. Potesil, R.Kizek, *Sensors*, 5, 448 (2005).
- 13. L. Trnkova, F. Jelen, I. Postbieglova, *Electroanalysis*, **15**, 1529 (2003).
- 14. L. Trnkova, F. Jelen, I. Postbieglova, *Electroanalysis*, 18, 662 (2006).
- 15. L. Trnkova, I. Postbieglova, M. Holik, *Bioelectrochemistry*, **63**, 25-30 (2004).
- 16. X. C. Li, J. Cechal, L. Spanhel, S. Tiscani, J. Martinik, R. Oborilova, L.Trnkova *Electrochim. Acta*, **475**, 12 (2024).
- 17. X. C. Li, I. Triskova, L. Trnkova, *Electrochim. Acta*, **442**, 11 (2023).
- 18. N. Aladag, L. Trnkova, A. Kourilova, M. Ozsoz, F. Jelen, *Electroanalysis*, **22**, 1675 (2010).
- 19. F. Jelen, A. Kourilova, S. Hason, R. Kizek, L. Trnkova, *Electroanalysis* **21**, 439-444 (2009).

Reduced Modeling of Lilon Battery Thermal Abuse

P. Vyroubal^a, M. Sedlařík^a, M. Mačák^b, M. Šedina^a, T. Kazda^a

^a Department of Electrical and Electronic Technology, Faculty of Electrical Engineering and Communication, Brno University of Technology, Brno, Technická 10, 616 00, Czech Republic

^b Electric Vehicle Technologies Transport Technologies, AIT Austrian Institute of Technology GmbH, Vienna, Austria

Thermal abuse in lithium-ion (Li-ion) batteries represents a major safety concern across a wide range of applications, from portable devices to electric mobility systems. This study reviews the fundamental thermal mechanisms that can lead to hazardous conditions and examines advanced physical modeling techniques used to capture these phenomena. Special attention is given to reduced-order modeling (ROM), which offers a balance between computational efficiency and predictive accuracy. A practical case study is used to compare modeling approaches, and the relevance of these methods for battery pack design and thermal safety diagnostics is discussed.

Introduction

Lithium-ion (Li-ion) batteries are currently the dominant energy storage technology due to their high energy density and long cycle life. However, as their usage becomes more widespread, the risk of failures also increases—especially under extreme conditions such as mechanical damage, overcharging, or exposure to high temperatures. One of the most critical safety concerns is thermal runaway: an uncontrollable rise in temperature that can lead to cell failure, fire, or even explosion [1].

Understanding and predicting this phenomenon requires sophisticated models capable of capturing the complex physico-chemical processes involved. In the literature, a distinction is commonly made between physics-based models derived from first principles and simplified, reduced-order models that lower computational demands while still providing useful predictive capabilities [2].

Accurate modeling of thermal runaway is essential for the development of safer battery systems.

Experimental

Experimental validation is a crucial component in the development of models aimed at predicting thermal runaway in lithium-ion batteries. No model—whether physics-based or reduced-order—can be considered reliable without verification against real-world measurements. Experiments are not only essential for validating simulation outcomes but also for determining key input parameters necessary for model calibration, such as specific heat capacity, thermal conductivity of individual cell layers, reaction rates at various temperatures, and the onset conditions for thermal runaway.

The most commonly used experimental methods include:

Thermal Oven Test

In this method, a cell is placed inside a laboratory oven and gradually heated until thermal runaway is triggered. Parameters such as temperature, time to failure, pressure, and gas evolution are monitored. This test is considered a standard procedure due to its reproducibility and controlled conditions. Finegan et al. [3] utilized this method in combination with X-ray tomography to observe structural changes within the cell during runaway.

Nail Penetration Test

This test simulates mechanical abuse by driving a metal nail through the battery cell, causing an internal short circuit that may lead to thermal runaway. Temperature response, propagation rate, gas formation, and potential explosion are monitored. Diekmann, J. et al. [4] used data from this test to validate a physics-based model, achieving a simulation error below 5%, indicating high model accuracy.

Overcharge Test

This method investigates cell behavior when charging beyond the specified voltage limit. Overcharging induces excessive heat due to parasitic electrochemical reactions. Experiments monitor the voltage threshold at which temperature rises, impedance shifts, and eventual thermal runaway occurs. These tests are widely used in the automotive industry, where overcharging is a common fault scenario.

Accelerating Rate Calorimetry (ARC)

In this specialized test, the cell is placed inside a calorimeter to measure the rate of heat generation. This technique is especially valuable for calibrating kinetic parameters in thermal models. It allows estimation of heat release as a function of temperature and determination of the energy profile of individual reactions, such as SEI decomposition or oxygen release from the cathode.

X-ray and Neutron Tomography

These imaging techniques provide insight into structural changes within the battery cell during thermal runaway. Such data are extremely valuable for developing multi-layered models that differentiate between the thermal properties of the anode, cathode, and separator.

When combined with numerical modeling, experimental data play a key role in the iterative calibration of thermal runaway models. Parameters such as specific heat capacity or activation energies of chemical reactions can be fine-tuned to achieve the highest possible agreement between simulation outputs and experimental measurements.

Validation is carried out not only at the level of individual cells, but also for entire battery modules or packs. In such cases, simulations focus on the propagation of thermal runaway between cells, the effectiveness of thermal barriers, and the performance of cooling systems. Experimental investigations often involve multichannel thermal imaging, flame propagation speed measurements, or acoustic emission analysis.

In practice, these data are used not only to develop accurate models but also to inform the design of safety features such as pressure relief devices, thermal insulation layers, or early fault detection algorithms implemented within battery management systems (BMS). By combining simulation and experimental approaches, it is now possible to predict thermal runaway with high accuracy, significantly enhancing the safety of lithium-ion batteries in real-world applications.

Conclusion

Although thermal runaway modeling has advanced significantly over the past decade, several challenges remain. One major issue is the complex behavior of cells within larger assemblies, where intercell interactions, variations in thermal conductivity, and component aging can strongly influence overall system dynamics.

Another limitation is the lack of open-access experimental data, which makes independent model validation difficult. Battery manufacturers often do not disclose detailed information about the internal structure of their cells, restricting accurate parameterization in simulations.

Future developments are expected to focus on hybrid models that combine physics-based approaches with machine learning techniques. Such models will enable better adaptation to specific battery types, respond to changing operating conditions, and offer faster computational performance. Another emerging trend is the use of digital twins—virtual replicas of battery systems that allow real-time predictive maintenance and operational optimization.

Thermal abuse modeling of Li-ion batteries is essential for ensuring safe deployment. Physics-based models provide high accuracy but are computationally intensive. In contrast, simplified models offer faster simulations at the cost of certain assumptions. In practice, both modeling approaches are complementary, particularly in the design of battery management systems (BMS) and in multi-scale or hierarchical simulation frameworks.

Acknowledgments

This work was supported by specific graduate research of the Brno University of Technology No. FEKT-S-23-8286.

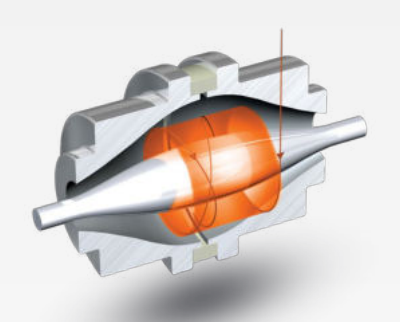
- 1. A. Mallarapu, V. Boovaragavan, Electrochemical Society Meeting Abstracts, 2024.
- 2. Z. Wei, Singapore: Springer, 2024. ISBN 978-981-97-4639-2.
- 3. D. P. Finegan, M. Scheel, J. B. Robinson et al., Nature Communications, vol. 6, 6924, 2015.
- 4. Diekmann, J. et al. (2020), Journal of The Electrochemical Society, 167(90504).





Pragolab

Špičkové služby a přístroje z oboru analytické chemie, mikroskopie, materiálografie a fyzikálního měření pro český a slovenský trh. Již více než 30 let.



ORGANICKÁ ANALÝZA A SEPARAČNÍ TECHNIKY



MIKROSKOPIE A PŘÍPRAVA VZORKŮ PRO METALOGRAFII



FYZIKÁLNÍ A MATERIÁLOVÉ ANALÝZY

plynová chromatografie ICP-OES příprava vzorku elementární analýza elektrochemie testery akumulátorů EIS SEA analýza povrchů separační techniky DVS reologie atomová spektroskopie GC temperace kapalinová chromatografie UV-VIS spektrometrie GC-MS lyofilizátory konfokál B.E.T. lims mikroskopie materiálografie metalografie technická čistota optická mikroskopie elektronová mikroskopie koncentrátory CHNSO analýza AAS analýza částic HPLC hmotnostní spektrometrie centrifugy extruze ICP-MS servis AIR monitoring XPS widefield textura spotřební materiál NMR DLS automatické dávkování iGC TOC analýza RVC stopped-flow cirkulární dichroismus XRF XRD



From High-end **Potentiostats** to **Battery Cyclers**.



ENERGY: FROM ACADEMIA TO INDUSTRY



- Powerful/intuitive software: Suits experts & beginners alike
- From 1 pA to 800 A: Extensive product range
- Integrated EIS for internal resistance characterization
- Extensive online support library/Multiple yearly upgrades

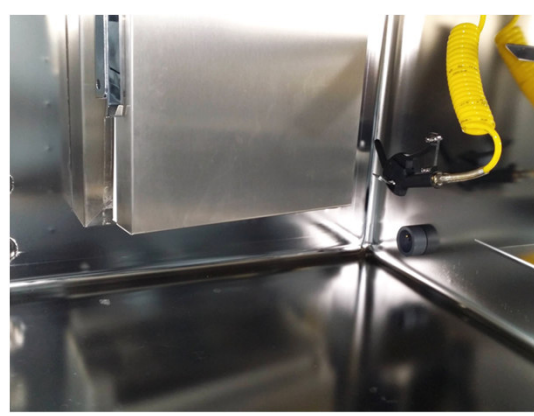




Glovebox Solutions For Battery Applications







Rounded corners for easy cleaning and decontamination



Customised design

More from CHROMSPEC s r.o.



Title:

Advanced Batteries Accumulators and Fuel Cells -26^{th} ABAF

Edited:

Martin Šedina Antonín Šimek Jiří Báňa

Jiří Báňa Tomáš Kazda Petr Bača

Publishing Office:

Marie Sedlaříková Martin Šedina Tomáš Kazda Petr Bača

Deadline:

July 28th 2025

Publisher:

Brno University of Technology

Faculty of Electrical Engineering and Communication Department of Electrical and Electronic Technology

Year:

2025

The autors are fully responsible for the content and language of their contribution